Doctoral theses at NTNU, 2021:18

Netsanet Nigatu Tessema

Dam runup and overtopping from waves generated by landslides

Doctoral thesis

NTNU
Norwegian University of Science and Technology
Thesis for the Degree of Philosophiae Doctor
Faculty of Engineering
Department of Civil and Environmental Engineering

NTNU
Norwegian University of Science and Technology

Netsanet Nigatu Tessema

Dam runup and overtopping from waves generated by landslides

Thesis for the Degree of Philosophiae Doctor

Trondheim, August 2021

Norwegian University of Science and Technology
Faculty of Engineering
Department of Civil and Environmental Engineering

NTNU
Norwegian University of
Science and Technology

NTNU
Norwegian University of Science and Technology

Thesis for the Degree of Philosophiae Doctor

Faculty of Engineering
Department of Civil and Environmental Engineering

ISBN 978-82-471-9902-2 (printed ver.)
ISBN 978-82-471-9614-4 (electronic ver.)
ISSN 1503-8181 (printed ver.)
ISSN 2703-8084 (online ver.)

Doctoral theses at NTNU, 2021:18

Printed by NTNU Grafisk senter

NTNU
Norwegian University of Science and Technology

A Joint Degree Between

Addis Ababa University

Addis Ababa Institute of Technology

School of Civil and Environmental Engineering

and

NTNU

Faculty of Engineering

School of Civil and Environmental Engineering

Dam Runup and Overtopping from Waves Generated by Landslides

By: Netsanet Nigatu Tessema

A PhD. Dissertation Submitted to the School of Graduate Studies of Addis Ababa University and NTNU in Partial Fullfillment for the degree of Doctor of Philosophy in Civil Enginering (Hydraulic Engineering Stream)

Addis Ababa

December, 2020

Abstract

Waves may be generated by the impacts of e.g. landslides, rock falls and snow avalanches with water. Such waves are referred as impulse waves. Landslide generated impulse waves on dammed reservoirs run up the reservoir banks as well as the upstream dam slope. Such waves may overtop and even breach the dam and result in flooding of the downstream area with hazardous consequences. One infamous example of such phenomenon and resulting catastrophe, is an impulse wave that occurred at the Vaiont dam in Italy in 1963, where a concrete dam was overtopped by more than 70 m height. The resulting flood wave destroyed the village Longarone located downstream of the dam and about 2000 people perished. Hence, for reservoirs in landslide prone areas, a means of estimating the hazard associated with an impulse wave overtopping a dam is of importance. Among the studies in the literature conducted for the slide generated waves, the slide impacting the reservoir was simulated with a slide infront of the dam.

The present study illustrates the slide generated wave in a 3D physical model where slides are generated from the side of the bank or aligning perpendicular to the reservoir's longitudinal axis. The generation, propagation and overtopping of subaerial landslide generated impulse waves was investigated in an undistorted hydraulic model based on the Froude similitude. Scale effects due to fluid viscosity and surface tension are considered negligible since still water depth greater than 0.20 m (in model) is used for all tests. A model basin with 4.5 m length, 1.7 m width at the bottom and 2.22 m width at dam crest level, with a total reservoir capacity of 2.5 m^3 is used. Solid blocks are used to simulate the slide falling into a reservoir with five types of block arrangement having different characteristics like slide width, slide length, and slide release height sliding on the ramp inclined at an angle of $\alpha = 50^o$ to a basin. A systematic variation of slide parameters like slide length, slide width, slide volume, slide release height, still water depth, and dam front face angle were made. Dams having an upstream slope of 1: 1.5, 1: 2 and 1: 2.25 were used in the analysis.

The present study aims at presenting equations for the prediction of discharge over the crest, overtopping volume and runup height due to landslide generated waves for the specific cases studied. Calibration of coefficient of discharge values for 1: 1.5 and 1: 2.25 dam were done for calculating the discharge based on the overtopping depth. Overtopping volume prediction equation based on slide parameters, with and without considering relative wave amplitude, has

been presented for both cases. Further, the runup height for overtopping and no overtopping cases has been analysed based on the video recorded. It can be used in the design of freeboard against landslide generated waves for landslide susceptible reservoirs.

Preface

Impulse waves created by slides falling into reservoirs may runup the dam which may cause damages to the dam itself and further to the area downstream. Particular attention has to be given to embankment dams which, if overtopped, may suffer serious damage or even fail completely. Hence it is of importance that the run up height due to such waves is considered in freeboard design of dams in areas susceptible to landslides.

It was against this background, that the NVE (Norwegian Water Resources and Energy Directorate) initiated in collaboration with NTNU (Norwegian University of Science and Technology, Trondheim, Norway) an experimental study program in 2014. The study program was continued in 2015 through 2017 with focus on landslide generated waves falling sideways into a reservoir, as well as the effect of different dam related parameters on the overtopping. The study used a physical model, that was extracted and modified from 1:500 model used by Lindstrøm et al., (2014), to study slide generated waves into fjords. The same slide blocks were used as in the study of Lindstrøm et al. (2014). A considerable database is available from these studies that was made available for the current research. The current research is a continuation of the study program at NTNU ending in 2017.

This thesis is submitted to the Addis Ababa Institute of Technology (AAiT) in Addis Ababa for the partial fulfillment of the requirements for the degree of Philosophiae Doctor (PhD). This work is the result of the collaboration between the School of Civil and Environmental Engineering, AAiT, Ethiopia and Department of Civil and Environmental Engineering, NTNU, Norway. The research was supervised with Asie Kemal Jabir (Dr. Ing) at AAiT and Associate Professor Fjola G. Sigtryggsdottir at NTNU as main supervisors. Professor Leif Lia is registered as a co-supervisor at AAiT and NTNU.

The PhD study can be grouped into three phases: Phase one comprise the course works conducted at AAiT as well as writing of the conference paper. Phase two embraces work carried out at NTNU and comprises the laboratory works, conceptualization and defining research questions, initiating the data analysis, initiating writing of journal papers and structuring of the content. Phase three was carried out both at AAiT and at NTNU and comprises data analysis and writing of journal papers as well as writing the thesis.

This thesis comprises an introduction to the research that has resulted in on conference paper (Paper IV) and three scientific journal papers (Papers I to III) . Two of the scientific journal papers are published (Paper I and II), thereof Paper II was chosen as “the Editor’s Choice Article” in the journal Water.

Acknowledgements

I would like to thank my supervisor Fjola G.Sigtryggsdottir for her dedicated support and guidance throughout my PhD study. She has been always providing encouragement and was always willing and enthusiastic to assist in any way she could throughout the research project. I could not have imagined having a better advisor and mentor for my PhD study. My sincere gratitude goes to my co advisor Professor Leif Lia for inviting to work at the laboratory of NTNU. I thank him for his motivation and immense knowledge whenever I needed him. I like to express my deepest gratitude to my co-supervisor Dr. Ing Asie Kemal Jabir, for believing in me and being optimist all the time. Furthermore, many thanks goes to Wollo University for providing me with a scholarship for my PhD study.

I would like to express my profound gratitude to my families (my mom Tsehay T/Mariam, my dad Nigatu Tessema and siblings for providing me with endless support and encouragement all the way. Biya Desalegn Haile, I thank him for his help in Matlab. I would like to thank my friends in Norway, Kiflom Wassihun and his wife Meazi, Ashenafi S. Gragn and his wife Aryam and Geir Tesaker with his family. I couldn't imagine my stay without them, they made me feel like home..

My husband Ermyas Tamene Haile and my daughter Tnbite Ermyas, I know have been a mess and was not around the last days of submitting this document. Thank you for your patience and your endless support with love.

Table of contents

List of papers

The results of this PhD research are presented in the three Journal papers, Paper I to III, whereas the conference paper referred to below can be taken as a general insight into the problem.

Paper I: Case Study of Dam Overtopping from Waves Generated by Landslides Impinging Perpendicular to a Reservoir's Longitudinal Axis

Netsanet Nigatu, Fjola G. Sigtryggsdottir, Leif Lia, Asie Kemal

Journal of Marine Science and Engineering, 2019,7,221; doi:10.3390/jmse7070221 (Open Access)

Paper II: Physical Model Study on Discharge over a Dam Due to Landslide Generated Waves

Netsanet Nigatu, Fjola G. Sigtryggsdottir, Leif Lia, Asie Kemal

Journal of Water, 2020, 12, 234; (Selected as Editor's Choice paper)

Paper III: Landslide Generated Wave Runup over a Rigid Dam for Freeboard Prediction

Netsanet Nigatu, Fjola G. Sigtryggsdottir, Leif Lia, Asie Kemal

Manuscript submitted to: Journal of Applied Water Engineering and Research

The work in these journal papers and a manuscript are complemented by the following conference paper presented at an international conference.

Paper IV: The Impact of freeboard on embankment dams

Netsanet Nigatu, Leif Lia, Asie Kemal, Fjola G. Sigtryggsdottir

Hydro Africa 2017-International conference on Hydropower and dams

Marrakesh, Morocco

List of Figures

List of Tables

Abbreviations

a (m) = wave amplitude;

a_M (m) = maximum wave amplitude;

b (m) = slide width;

b_b (m) = reservoir bottom width;

B_c (m) = crest width;

C_d (-) = coefficient of discharge;

$d_o\ (m)$ = maximum overtopping depth;

$d_{max}\ (m)$ = maximum overtopping depth;

E (-) = overtopping volume parameter;

f (m) = freeboard;

F *(m)* = Froude number;

g (m/s^2) = gravitational acceleration;

h (m) = still water depth;

h_o(m) = landslide release height;

H (m) = dam height;

H_M (m) = maximum wave height;

L (m) = wave length;

l_b (m) = reservoir length;

l_c (m) = crest length;

l_s (m) = slide length;

M (-) = relative slide mass;

m_s (Kg) = slide mass;

s (m) = slide thickness;

S (-) = relative slide thickness;

t (s) = time;

T (s) = wave period;

T (-) = wave type product;

P (-) = impulse product parameter;

q ($m^3/s/m$) = the mean overtopping unit discharge;

Q_{max} (m^3/s) = maximum discharge;

R (m) = run up height;

R^2 = coefficient of determination;

t (s) = overtopping duration;

$v_s(m/s)$ = slide impact velocity;

W (-) = runup height parameter;

W_S (m^3) = slide volume;

W_W (m^3) = overtopping volume;

α (°) = slide ramp inclination;

Φ (°) = slide front angle;

Φ_S (°) = internal friction angle;

θ (°) = slope of side banks;

β (^{o}) = upstream dam slope angle;

ε (-) = relative wave amplitude;

ρ_s (kg/m^3) = bulk slide density;

ρ_w (kg/m^3) = density of water.

1 Introduction

This doctoral thesis investigates dam runup and overtopping from waves generated by landslides impinging perpendicular to a reservoir's longitudinal axis. This introduction provides in Section 1.1 and 1.2 a general overview of the background of the present study on general terms. In Section 1.3 landslide hazards including at dam reservoirs are shortly reviewed with focus on these hazards in Ethiopia and Norway, but this threat at dam reservoirs motivated the present study. Subsequently, dam safety in national dam safety guidelines and consideration of freeboard as a design measure to prevent overtopping from wave runup are considered in Section 1.4, and related to consequence classification of dams in Section 1.5. Then the scope and objectives of the present research is outlined in Section 1.6, along with research questions. Finally, outline of the thesis is provided in Section 1.7.

1.1 Overview

Dams are large hydraulic structures, which provide society with essential benefits such as water supply, flood control, recreation, hydropower, irrigation etc. With increasing demand on water resulting from world population growth and industrialization, the rate of dam construction and design has substantially increased in recent years. Dams provide not only beneficial but also potentially adverse effects on the living environment. If a dam fails it may cause severe loss of properties and lives, as well as damage to the environment, thus creating a considerable amount of suffering and hardship. Figure 1 describes that the most common cause of failure of earth and rock fill dams is overtopping (31 % as primary cause and 18 % as secondary cause). This is followed by internal erosion within the body of the dam (15 % as primary cause and 13 % as secondary cause) and in the foundation (12 % as primary cause and 5 % as secondary cause) (ICOLD, 1995). Overtopping may happen for different reasons, such as insufficient spillway capacity, blocked spillways, wind and landslide generated waves, settlements etc. An important parameter to prevent overtopping of a dam due to these factors is providing sufficient freeboard, which is defined as the vertical height between the still water level and the dam crest. Freeboard of a dam should preferably be designed against the probability of occurrence of the simultaneous occurrence of these factors.

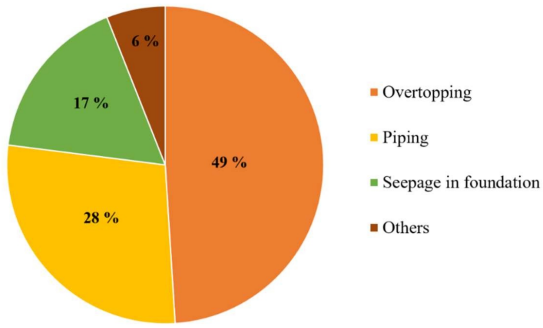

Figure 1: Distribution of failure mechanisms of earth and rockfill dams (statistics from ICOLD (1995)).

Among the potential causes of dam overtopping, landslide generated waves are addressed hereafter, as this is the theme of the present study. Landslide generated waves are typically caused by landslides, rock falls, shore instabilities, snow avalanches or glacier calving in lakes or reservoirs (Heller et al., 2009). The waves generated as such mass wasting plunge into a reservoir propagate across the water body, run up the reservoir banks, as well as the dam slope and overtop the dam if the waves are large enough. These tsunami-like waves are referred to as impulse waves. Dams are vulnerable to these impulse waves which may lead damage to the dams and even catastrophic consequences with flooding of the downstream area. The hazard is intensified in case of embankment dams, which may breach due to the wave overtopping and thereby add to the downstream flooding. Historically, dam overtopping caused by landslide generated waves have resulted in a few major adverse events all over the world. For example, a catastrophic event occurred in Lituya Bay, Alaska, in July 8, 1958, where an 8.3 magnitude earthquake along the fault triggered a major subaerial rockslide into Gilbert Inlet at the head of Lituya Bay on the south coast of Alaska. The rockslide impacted the water at high speed creating a giant nonlinear wave and the highest wave runup of 524 m along the slide axis (Fritz et al., 2009; Miller, 1960). Another extreme event was the Vaiont reservoir catastrophe which occurred in 1963. After the reservoir had been impounded for the first time behind the 262 m high double curved arch dam, the left valley flank became unstable. About 300 million m^3 of subaerial slide, which is twice the reservoir capacity, slid into the reservoir. The displaced reservoir water spilled over the dam crest to a depth of at least 70 m, and swept through the

village of Longarone, which led to about 2,000 casualties. The dam itself survived with almost no damage (Mueller, 1968). One recent event occurred in 2018 at Hidroituango site, Columbia, where three landslides occurred between the 7th and 28th of April, 2018. These landslides blocked the flow of water through the tunnel increasing the reservoir water level which led to extensive flooding downstream. Reports indicated that about 7000 people had been evacuated to mitigate the risk (Dave, 2018) (Figure 2).

Figure 2: A large landslide scar at Hidroituango dam site, Colombia (Dave, 2018).

1.2 Landslide generated impulse waves in reservoirs

The wave generation mechanisms of landslide generated impulse waves can be categorized as subaerial, partially submerged, and submerged slide (Heller, 2007) as seen from Figure 3. The categorization bases on the initial position of a slide relative to the still water surface. The present study investigates only the effect of subaerial landslide generated impulse waves.

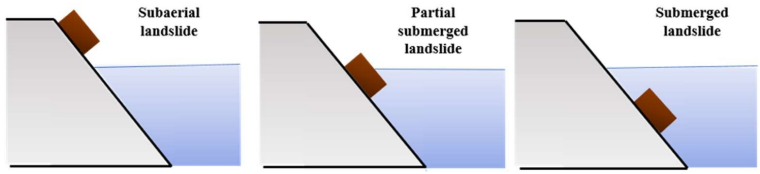

Figure 3: The three types of landslides based on their initial position relative to the still water level (adopted from Heller et al. (2009)).

Considering subaerial slides falling into reservoir, there are three main phases describing the phenomenon (see Figure 4): (Phase 1) slide impact with wave generation; (Phase 2) wave propagation with wave transformation; and (Phase 3) run up of the impulse wave and overtopping of a dam.

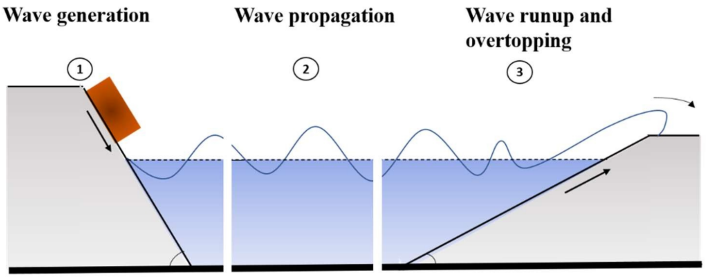

Figure 4: The three phases of an impulse wave for subaerial slide (adopted from Heller et al. (2009)).

The wave generation (phase 1) and wave propagation (phase 2) have been adressed with simple physical experiments and numerical simulation which will be discussed in Chapter 2 on the theoretical background, Section 2.3. However, only few studies consider the last phase, wave runup and overtopping of dam (phase 3) which will be discussed in Chapter 2, Section 2.4.

There have been numerous experimental and numerical studies on landslide generated waves conducted in 2D experimental tests using rectangular prismatic water wave channels from landslides falling from 1a direction in Figure 5. Considering a narrow mountain valleys, which is commonly the case, the shape of a reservoir is usually longer than its width and thus, a potential landslide threat from mountain sides in a direction perpendicular to reservoir's longitudinal axis is common. However, the available studies in the literature (reviewed in Chapter 2) do not directly investigate the 3D effects relating to narrow valleys and a landslide falling into dammed reservoir perpendicular to the reservoir's longitudinal axis. Furthermore, among the studies in the literature only few consider dam overtopping and include formulas for predicting the parameters describing the overtopping like overtopping volume, discharge, overtopping depth and run up height. Hence, this study investigates the problem by conducting

experiments on a 3D physical model with slides falling in the direction assigned as 1b as seen in Figure 5 and by presenting a predictive formulas for those parameters.

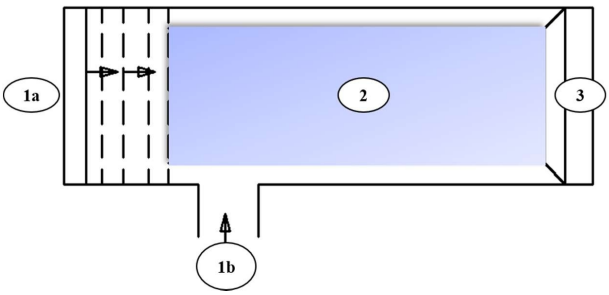

Figure 5: General layout of slide impact into a reservoir: 1a and 1b are slide impact zone, 2 is the wave propagation zone, and 3 is the wave runup and dam overtopping zone (Tessema et al., 2019).

1.3 Landslides

Natural hazards are a multi dimensional and a multi disciplinary events. They are complex and vary greatly in their frequency, speed, duration and the affected area. Landslides and landslide generated ground failures are among the common geoenvironmental hazards in many of the hilly and mountainous terrains of the world. Landslides present a threat to life and livelihood throughout the world, ranging from minor disruption to social and economic catastrophe.

Motivation for the present study are the existing cases of dams in landslide prone regions of Norway, including from rockslides, as well as, existing and planned dams in landslide prone regions of Ethiopia. Thus, landslide hazard is shortly reviewed in this section for these two countries for an overview of the problem considering dams.

1.3.1 Landslides in Ethiopia

Although East Africa is a region where landslide is a widespread phenomenon, the research on this topic is restricted. Steep slopes, high annual rainfall, increasing population pressure and deforestation, earthquakes and extreme rainfall make most areas in East Africa very sensitive to landslides (Glade and Michael J., 2005). Many areas lack quantitative data of landslides

which can be used for undertaking remedial measures and emergency preparedness in case of occurrence.

Landslide hazard is a problem to address in the development of Ethiopia, one of east Africa countries. Such hazards represent a limiting factor for urbanization and infrastructural projects and, generally, for all the activities performed on and at the foot of slopes (Abebe et al., 2010). Ethiopia, having steep slope topography, is currently implementing huge dams and developing infrastructure for hydropower development. The hilly and mountainous terrains of the highlands of Ethiopia, (including areas with altitude over 1500 m a.s.l) which are characterized by variable topographical, geological, hydrological and land use conditions are frequently affected by landslides. The most important causes for landslides in this area are steep slopes, deep weathered soils with high clay content and high annual rainfall. Among the mentioned causes, Ayalew (1999) described the main triggering factor for slope failure as a heavy rainfall, where the rainwater infiltrates and causes an increase in the total weight of the slope material, rising the water table and increasing the pore pressure in fine grained deposits. Landslides may occur in conjunction with other vital natural disasters such as earthquakes, floods and volcanic eruptions. Earthquakes are recurrent events in Ethiopia, especially along the rift system (Ayele, 1995), which is one of the triggering factors for rapid slope failures in the area such as rock falls, rock slides, and debris mud flows (Gouin, 1979). Hence, landslides and landslide-generated slope failures into reservoir need to be given due attention in order to reduce losses from such hazards.

Generally, most of the plateau in the north and west part are noted as active zones of landslide in Ethiopia, where about 300 lives were lost (Ayalew, 1999). Accordingly, the northern Omo River basin, the lower Wabe-Shebele River valley, the Wendo Genet slope, the Blue Nile Gorge, the town of Dessie, the Wundmen area in Weldiya, the Gilgel Gibe River, the Uba Dema village in Sawla, and parts of Tigray are some of the areas where imposing landslide events have been reported in the last decade (Abebe et al., 2010). Broothaerts et al. (2012) studied the landslides that occurred in Gilgel Gibe catchment (based on number of slides, n = 60), and found that 75% of the landslides occurred in debris material which is a mixture of fine earth and rock fragments, resulting from weathering processes and ancient landslides.

Slides can be described based on different factors as slide property, formation and the style of failure. Ayalew (1999) has summarized the 64 landslides that have occurred in Ethiopia based on the depth of sliding and the angle of the slope. It is seen that the critical depth of most of landslides in Northern and Southern Ethioian highlands ranges from 5 m to 15 m and they occurred where the slope angles is between 20^0 to 45^0. Temesgen et al. (2001) has classified the slope angle with landslide event distribution and the maximum landslide events have been observed on the slope angle ranging from 10^0 to 20^0 followed by 30^0 to 40^0 interval. Woldearegay (2013) reviewed the previous studies and concluded that most of the reported debris /earth slides/ flows and rockslides have taken place in areas with slope angles between 15^0 to 45^0.

Although most of the dams in Ethiopia are constructed on reservoirs with steep slopes, slides impacting a reservoir and dam are not extensively studied. In one of the landslide active areas, Gilgel Gibe catchment, landslides falling into reservoir are source of sediment in Gilgel Gibe I hydroelectric power plant (Broothaerts et al., 2012), but further analysis is needed to quantify the amount of sediment load in the reservoir due to these slides. On April 2008, since the start of construction of Tekeze dam, a massive landslide has occurred near the dam site which led to an additional cost of 42 million dollars to build a retaining wall for protecting the slides from falling into the reservoir (Hailemariam Gugsa and Schneider, 2010; International Rivers, 2009).

1.3.2 Landslides in Norway

Landslides as well as large rock slope failures are one of the most serious possible natural hazards in Norway. Here the focus will be on rock slopes. Rock avalanches and related tsunamis have caused serious disasters in the past. Norway experienced three major tsunami disasters due to subaerial rockslides plunging into water in the twentieth century, Loen (in 1905 and 1936) and Tafjord (in 1934). The Loen disaster (in 1936) with 73 casualties occurred when 1×10^6 m^3 of rock mass falls and generates a runup height of 74 m. Tafjord disaster occurred in 1934 when 3×10^6 m^3 rock mass dropped into the fjord. The tsunami generated by the avalanche reached a maximum of 62 m above sea level, and several inhabited villages along the fjord were destroyed and 41 people were killed. During the last hundred years, 174 people

have lost their lives in three such events in a limited region in northern west Norway (Blikra et al., 2006).

Some attention was focused on the stability of Norwegian rock slopes after these destructive rock avalanches and tsunamis. Especially important was the review of Bjerrum et al., (1968) who addressed the general factors of importance for understanding the behaviour of rock slopes in Norway. In order to predict such events, there is obviously a need for a better understanding of rock slope failures.

Large scale rock slope failures in Norway range from the sliding of relatively intact masses of rock to fully disintegrated and fast moving rock avalanches. Rock slope failures that develop into true rock avalanches are the dominating type of event in Norway, mainly due to the high, steep topographic relief of Norwegian fjords and valleys. Blikra et al. (2006) presented some examples of different types of rock slope failures in Norway. Major deformations of valley fill and fjord sediments are commonly related to large volumes of rock. They concluded that the mechanisms for occurrence and triggering of rock slope failures are still uncertain, but seismic ground shaking and creep processes are probably important although, in some areas, effects of glacial unloading during the deglaciation phase cannot be excluded. Extensive studies of Norwegian rock slope failure areas support a subdivision into three principle types: (1) Rockfall areas, (2) rockslide areas, and (3) complex fields (Braathen et al., 2004). This classification was based on structural geometry and style of deformation, slope gradient, and volumes involved.

Romstad et al. (2009) investigated rock slide potential from topographical conditions around lakes in Norway. Of 100 lakes that were identified to have the highest rock slide potential, 46 are hydropower reservoirs with associated dams. Hence, landslides with the potential of generating impulse waves pose a threat for many dams in Norway. Furthermore, these dams are generally built in mountain valleys resulting in narrow reservoirs.

1.4 National Guidelines

Safety of dams is not only determined with their design and construction phase. It is also determined by all actions starting from planning, monitoring, and evaluating as well as identifying the dam safety issues during the operational lifetime of the project. This is done

with guidelines provided in the country where the dam is located. The importance of dam safety has for example been recognized in Norway with governmental supervision of dams for over 100 years. Furthermore, dam safety is currently emphazied in Norway with comprehensive dam safety regulations and guidelines. In some other countries, such as the Eastern Nile Countries, dam safety regulations do not have as long history.

In 2013, ENTRO (Eastern Nile Technical Regional Office) took this task and carried out a comparative analysis of other's countries dam safety guidelines and recommended the most appropriate and suitable guideline to be adopted for Eastern Nile Countries including Ethiopia. In 2014, it released Small Dams Safety Guideline and Reference Dam Safety Guideline for Eastern Nile Countries. The guideline draws concepts and processes from various international guidelines like ICOLD family of Technical and National Committees and also various US Federal Agencies. However, due to the limited number of dams designed and constructed from this guideline, little experience is obtained so far.

In general, freeboard design of a dam should consider reasonable combinations of appropriate components (see Paper III). However, ENTRO guideline considers wind setup and wave runup as a principal design criterion and discusses in brief a calculation procedure for these factors. It is also stated that generally that if the reservoir rim is unstable, additional freeboard should be provided with building a camber. Similar consideration is for example also provided in the Norwegian Dam Safety Guidelines (NVE, 2012).

Accordingly, potential landslides falling into reservoirs should be highlighted for freeboard design and studies have to be done in countries where this hazards is relevant, such as Ethiopian reservoirs and dam, considered by planners, decision-makers, and concerned organizations. The outputs from this study can be used in understanding and quantitatively describing the landslide parameters related to freeboard in landslide prone areas.

1.5 Classification of dams

Different attempts have been made to categorize dams in order to find the optimum focus and use of resources to address dam safety. Fully risk-based concepts like risk analysis and probabilistic dam safety analyses have been used in many countries but the popularity for such methodology has varied greatly during the years. The potential Consequences Classification

(PCC) is a classification system for all dams with a safety risk according to their incremental impacts or consequences as a result of failure. More common today is a methodology based on estimating only the consequences from a potential dam failure. Consequences are listed in groups such as loss of life, infrastructure, economic and social factors and environmental and cultural factors. From these the dams are for example categorized into 3 to 5 classes with a given interval of loss of life, e.g. *level 4* >1000, *level 3* 100-1000, *level 2* 10-100, *level 1* 1-10 and *level 0* no loss. Similarly, dams can be classified by infrastructure and economic factors, such as: *level 4* > 100 mill. USD, *level 3* > 1 mill. USD, *level 2* > 100,000 USD, *level 1* and *level 0* minimal economic loss. Another classification method is to count the number of accommodation units affected. For example, dams in Norway are classified according to their consequence hazard potential into five classes (class 0, 1, 2, 3 and 4). Class 0 is for dams with no failure consequences, while class 4 is the highest consequence class embracing dams of very high consequence. Medium consequences are described with consequence class 2, which is reached if 1-20 accommodation units and/or major infrastructure are affected by a dam break. Conversely, consequence class 3 is reach if 21-150 accommodation units are affected and/or a major infrastructure. Requirements to dam safety are stricter for the higher consequence classes.

Countries which uses the consequence class system normally have different deterministic design criteria for freeboard and crest width for different classes. For example, the Norwegian Water Resources and Energy Directorate (NVE) described freeboard values for class 3 and class 4 dams in Norway should be a minimum of 4.5 m and 6 m respectively (NVE, 2012). The minimum specified freebord also depends on the type of the structure, where criteria are more stringent for embankment structures, which are more likely to fail from overtopping, than for concrete structures that can withstand some overtopping. According to ENTRO guideline, the maximum still water level of the reservoir should be maintained at all times below the top of the impervious core, unless analysis can demonstrate that temporary exceedance of the top of the core does not endanger the dam.

1.6 Scope, objectives and research questions

The main objective of this study is to understand the overall process of landslide generated waves (wave generation, propagation, and overtopping) on embankment dams on narrow

reservoirs. It will particularly contribute to the process of developing a method to calculate total overtopping volume, the runup height and maximum discharge over dams as a result of landslide generated waves. In addition, 3D effects on overtopping process will be investigated. The study is composed of running an experimental study on the existing 3D physical model in hydraulic laboratory of NTNU, comprising a reservoir, dam and a landslide ramp. Geometry of the reservoir is fixed, so is the location and height of the dam as well as the location and inclination of the ramp on which landslide blocks slide into the reservoir. The upstream slope of the dam has inclination that is common on embankment dams. The varying variables are the freeboard of the dam (still water depth in reservoir), upstream dam slope, slide release height and landslide volume. Throughout the study a systematic variation of slide, reservoir still water depth and dam parameters is applied.

The specific objectives of the study are to use the (existing) 3D physical model to do the following:

1. Qualitatively investigate the process of the wave generation and propagation in the narrow reservoir towards a dam.
2. Qualitatively and quantitatively investigate the overtopping of the dam by landslide generated waves.
    2.1. Propose a formula for estimating the total overtopping volume over the dam crest due to impulse waves generated by a landslide impinging perpendicular to the reservoir‘s longitudinal axis.
    2.2. Investigate the distribution of the overtopping wave (volume, discharge, overtopping depth, and overtopping duration) along the dam crest.
    2.3. Investigate the feasibility of employing the steady state weir equation to predict the overtopping discharge over a dam crest due to landslide generated waves.
3. Qualitatively and quantitatively investigate the run up of a landslide generated wave on the dam slopes.
    3.1. Investigate the wave propagation (wave height), and runup pattern along the dam crest.
    3.2. Propose a formula for landslide generated wave runup height based on slide parameters which can be further used in freeboard design against landslide generated waves.
4. Compare the results from the study to the literature as applies.

Throughout the study the following research questions have been considered and are answered in this thesis:

R1. What wave types are generated in the physical model of the present study as the landslides of different volume and geometry impinges the reservoir?

R2. How does the reservoir geometry and the configuration with the landslide impinging perpendicular to the reservoir's longitudinal axis affect the wave propagation and overtopping/run up process? (In other words: How is the reservoir geometry affecting the whole overtopping process?)

R3. Can the total overtopping volume be predicted for a specific landslide/dam/reservoir configuration to obtain rough estimates for the case considered? (In other words: How much water overtops a dam for a specific landslide/dam/reservoir configuration?)

R4. Can the overtopping rate due to landslide generated waves over dams be predicted with modified steady state predictive equation?

R5. Do the landslide parameters: landslide volume and velocity, influence the overtopping volume and overtopping depth?

R6. Do the dam related parameters: upstream face slope and freeboard, influence total overtopping volume, overtopping rate and overtopping depth?

R7. Can one reasonable mitigate the landslide wave hazard through freeboard design considering run up of the landslide generated wave and how much freeboard is needed for a specific landslide configuration?

The study scope is limited to investigating the impact of landslide generated waves on dams by defining the parameters which describe the dam overtopping process for cases of landslides falling perpendicular to reservoir's longitudinal axis. The current study aims at shedding light on this phenomenon through providing predictive equations for the specific case mentioned; however, applications of the results must consider the limitations of the model setup described in the thesis.

1.7 Thesis outline

This thesis is composed of six main chapters. This Chapter 1 provides an overall overview of the topic and why it is important to address internationally, as well as in Ethiopia and Norway with the scope and aim. Chapter 2 presents the theoretical background and literature review of the three phases of landslide generated waves highlighting the wave propagation analysis observed in the experiments. Chapter 3 describes the research methodology and gives an overview of the experimental setup that is presented in the papers (also refer to Paper I, II and III), scale relations and instrumentation. The summary of experimental results is presented in Chapter 4 organized as per the journal papers. Chapter 5 desribes discussions of the results and the limitations of the present study. Also recommendations for further investigations are presented. Finally, the conclusion and answers to the research questions explained in Chapter 1 are adressed in Chapter 6.

2 Theoretical background

This chapter provides an overview of the theoretical background of relevance for the present study. First, basic wave parameters and main wave types are introduced in Section 2.1; followed by an overview on landslide generated impulse waves in Section 2.2. Subsequently, in Section 2.3, the wave generation by landslides (Phase 1 in Figure 4) and propagation (Phase 2 in Figure 4) are reviewed. Finally, in Section 2.4, previous studies on the wave runup on a dam slope and overtopping of the dam crest are considered.

2.1 Water waves

Landslide generated impulse waves belong to the category of impulse waves, i.e. they are principally influenced by the gravitational force in contrast to capillary waves (Heller et al., 2009). Generally, waves can be classified as linear and nonlinear wave based on the value of the basic wave parameters. Figure 6 shows an idealized sine wave in the (x, z) plane with the basic wave parameters, namely the wave amplitude a, wave height H, wave length L, wave period T, wave celerity c, and still water depth h. The ratio of the wave length to still water depth L/h is the criterion for the definition of shallow (L/h >20), intermediate (2< L/h <20) or deep-water waves (L/h <2). Linear waves have the form of a sine wave. If the wave seems small (H/h < 0.03) and flat (H/L < 0.006) it can be categorized under linear wave. The more these values increase the more nonlinear it becomes (Heller et al., 2009).

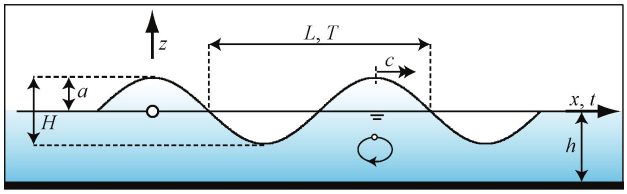

Figure 6: Principal wave parameters (Heller et al., 2009).

2.1.1 Nonlinear wave types

Nonlinear wave types can be categorized into four main groups; Stokes wave, cnoidal wave, solitary wave and bore waves where landslide generated waves may be allocated to one of those groups (Heller et al., 2009). Stokes waves can be categorized in deep water to

intermediate water wave where the wave trough is flatter and longer than the wave peak. Cnoidal waves falls in periodic intermediate or shallow water group which has mainly oscillatory character. Whereas solitary wave is another category of nonlinear shallow water wave (with $L = \infty$) with only a wave peak but no trough. This implies the wave amplitude is equal to the wave height ($a = H$). In theory the wave may propagate over unlimited distances without decay or any change of shape. The last category bore wave is a shallow water wave which has a steep front and a gently sloped back. It is created e.g. during wave breaking near the shore, and also if a solitary wave breaks which occurs if the wave amplitude of a solitary wave above a horizontal bed exceeds 0.78 h.

Generally, four methods are available to classify impulse waves for wave channel experiments, i.e. 2D waves; a) optical wave profile inspection, b) nonlinearity a/H, c) Ursell parameter $U = HL^2/h^3$, and d) wavelet tranform analysis (Heller and Hager, 2011).

Wiegel et al. (1970), Noda (1970), Huber (1980), Fritz et al. (2004) and Heller and Hager, (2011) classified for example the wave types with method (a). Heller and Hager (2011) further presented a classification method that is discussed below after accounting for the different contributions. For detailed account, the paper by Heller and Hager (2011) is referred to.Wiegel et al. (1970) identified the impulse waves generated by a vertically falling box as solitary waves, complex solitary wave or a series of cnoidal waves, and bores. Noda (1970) gave a graphical wave type classification containing oscillatory waves, nonlinear transient waves, solitary waves and bores. Furthermore, Wiegel et al. (1970) and Noda (1970) defined the slide Froude number F as the ratio of the falling box velocity v_s, and the shallow water waves celerity as, $F = v_s/(gh)^{1/2}$. Huber (1980) detected sinusoidal waves, cnoidal waves, solitary waves, and transient waves. Finally, for method (a), Fritz et al. (2004) distinguished between weakly nonlinear oscillatory waves, nonlinear transient waves, solitary like waves, and dissipative transient bores. Zweifel et al. (2006) applied method (b) to describe strongly nonlinear ($0.9 < a/H < 1.0$), moderately nonlinear ($0.6 < a/H < 0.9$), and weakly nonlinear ($0.4 < a/H < 0.6$) waves and classified the impulse waves in oscillatory waves, transient waves, solitary waves, and bores. Method (c) has been applied by Huber (1980) to distinguish the linear wave theory for $U < 15$, cnoidal wave theory for $15 < U < \infty$, and solitary wave theory for $U \infty$.

Panizzo et al. (2005) applied method (c) and (d) for wave basin experiments for the waves propagating on the slide length axis, and presented a preliminary wave classification in 2D. Heller and Spinneken (2015) applied all four approaches described above for the 3D case. The 3D tests involved only Stokes- and cnoidal- like waves like that of the 3D tests of Panizzo et al. (2005b). A general observation is that 3D waves tend more towards the Stokes- like type with increasing distance from source.

2.1.2 Wave type zones

Heller and Hager (2011) defined wave type zones in the near field caused by granular slides directly from the relationship between slide Froude number F ($F = v_s/(gh)^{1/2}$) and the wave type product T, where $T = S^{1/3}Mcos[(6/7)\alpha]$ is the relevant number characterizing a landslide impacting a water body. They observed the previously mentioned four wave types and transient types which are described with four nonlinear wave theories, namely stokes wave, cnoidal wave, solitary wave, and bore wave. The boundaries of the wave type zones identified by Heller and Hager's (2011) observations from the 2D case, are as follows: mainly Stokes-like waves fall in the zone $T < 4/5F^{-7/5}$, mainly bore-like waves in the zone $T > 11F^{-5/2}$, and mainly cnoidal- and solitary-like waves in the intermediate zone $11F^{-5/2} \leq T \leq 4/5F^{-7/5}$.

Heller and Spinneken (2015) further investigated the wave types for the 3D case. They concluded from their 3D test results that the lower boundary ($T < 4/5F^{-7/5}$) defined by Heller and Hager (2011) for 2D waves remains characteristic also for 3D waves, whereas in the intermediate range both Stokes- and cnoidal-like waves were observed.

2.2 Landslide generated impulse waves

Landslide generated waves are caused by landslides, rockfalls, shore instabilities, snow avalanches or glacier calving in oceans, bays, lakes or reservoirs. Based on the slide properties and the bathymetry, a prediction of the generated wave magnitude may be conducted. Heller et al. (2009) described five different prediction methods: a) generally applicable equations developed from model tests; b) prototype specific model tests; c) numerical simulations; d) empirical equations derived from field data; and e) analytical investigations. Heller et al. (2009) and Evers and Frederic M. (2018) discussed the merits and limitations of these methods. Among the mentioned approaches, generally applicable equations developed from model tests

are quickly and easily used at low cost and time. For an existing dam, for example such equations can provide an initial estimate of the wave parameters due to the slide impact to the reservoir. This may help in the prediction of the impact of a creeping slide and in taking decision on further preventive measures which may be needed. In addition, they provide an input to the design of dams against these waves. However, scale effects in too small models cannot be ignored and model effects occur with geometrical variations from the prototype. In order to be able to neglect scale effects, the still water depth in the slide impact zone should be $h \geq 0.2$ m (Heller et al., 2008) and in addition the wave period should be $T \geq 0.35$ s (Hughes, 1993), such that the waves (as gravity waves) are dominated by gravity and not by surface tension forces (as capillary waves) (Heller et al., 2009). In the physical model employed in the present study, still water depth of $h > 0.2$ m, was used.

Generally, the process of subaerial slide falling into a reservoir can be qualitatively grouped into three different phases as seen in Figure 4: (1) slide impact with wave generation; (2) wave propagation; and (3) wave runup and overtopping phases. When a landslide falls and reaches the free surface (phase 1 in Figure 4), a disturbance is generated and an energy exchange between landslide and water takes place. The induced waves quickly leave the generation area and propagate in the reservoir (phase 2 in Figure 4). Depending upon the reservoir configuration (like long narrow reservoir considered in this study), reflection of waves may occur along the reservoir sides to the dam crest. Finally, the propagated wave reaches the dam, runs up the upstream slope and if large enough, overtops the dam (phase 3 in Figure 4), often resulting in great damage to the dam structure or cause flooding to downstream area. The first two phases (phase 1 and 2) grouped as one and the last phase (phase 3) are discussed in Section 2.3 and Section 2.4 respectively, aiming at reviewing the available literatures.

2.3 Impulse wave generation and propagation

This section deals with experimental investigations aimed at analyzing physical phenomena occurring in the impulse wave generation and propagation area, i.e. phase 1 and 2 described above (see also Figure 4). The basic wave features defined in the literature were reviewed in the previous section (Section 2.1). In case of landslide generated waves, features like the wave amplitude and wave height, depend on the landslide characteristics like slide volume, velocity, density, slide front angle, release height and so on.

The first experimental study to be addressed is impulse waves reproduction in a physical model carried out by John Scott Russel (1845). He used a vertical falling box in order to generate solitary waves and this method was named after him as "Scott Russell's wave generator". This wave generator was later employed by Wiegel (1955) to model submarine slide generated waves. The study revealed that the wave amplitude depends on the slide body weight and its initial submergence, whereas the wavelength was mainly dependent on the slide body length. However, no explicit wave parameter prediction was deduced from this study. Furthermore, L.Law and A. Brebner (1968) used a roller with ball bearings inclined at different angles (17.7^0, 21^0 and 25^0) to convey boxes of different lengths, heights and weights into water of various depths to generate waves. In all cases studied, the leading wave was always the most significant and contained more than 90 % of the wave energy in the system. The rate of increase of wave height was greater for an increase in mass than an increase in the velocity of impact. This was further confirmed by Kamphuis and Bowering (1970) who used similar approach to generate waves describing the greatest influence of dimensionless volume and slide Froude number on the wave height. In addition, they reported that the first wave was always the highest in the train. None of these investigators focused on what controlled the characteristics of waves in the near field. Later, Walder et al. (2003) conducted experimental analysis using solid block in a two-dimensional landslide volume and demonstrated that the quantities controlling near field wave properties are landslide volume, submerged time of motion of the landslide and vertical impact speed.

Numerous experimental and numerical studies on landslide generated waves are further available in literature. Many of those were conducted based on prismatic wave channel (2D) (Ataie-Ashtiani and Nik-Khah, 2008; Di Risio and Sammarco, 2008; Kamphuis and Bowering, 1970; Synolakis, 1990; Watts, 1997; Wiegel, 1955; Zweifel et al., 2006) while others are based on wave basin (3D) (Bellotti and Romano, 2017; Briggs et al., 1995; Di Risio and Sammarco, 2008; Evers, 2017; Fritz et al., 2009; Heller and Spinneken, 2015; Heller et al., 2009; Huber et al., 2017; McFall and Fritz, 2016; Panizzo et al., 2005a; Romano et al., 2016). Those studies include landslides modelled with granular material (Evers, 2017; Fritz et al., 2003a, 2003b, 2004, 2009; Heller and Hager, 2010; Huber, 1980, 1982; Zweifel et al., 2006) or block models (Di Risio et al., 2009; Heller and Spinneken, 2013; Kamphuis and Bowering, 1970; Noda, 1970; Sælevik et al., 2009). Ataie-Ashtiani and Nik-Khah (2008) and Zweifel (2010) presented

results comprising both approaches. However, when granular landslides are used, scale effects will be encountered, mainly related to surface tension and fluid viscosity. This was in particular observed by (Heller et al., 2008) when the water depth is lower than 0.20 m.

For generation of waves, the generally applicable equations governing the effects of impulse waves on dams are based only on 2D models. The 2D equations developed by Heller (2007), based on Zweifel (2004) and Fritz (2002), are converted for 3D conditions using a method implicitly contained in Huber and Hager (1997). Heller and Hager (2010) identified the slide impact velocity v_s, the slide thickness s, the slide mass m_s, the still water depth h, and the slide impact angle α as the relevant parameters for impulse wave generation (see Figure 7). Based on these parameters a set of dimensionless quantities (Froude number F, relative slide thickness S, relative slide mass M) are defined and developed the so-called impulse product parameter P for describing the 2D characteristics of landslide generated impulse waves as;

$$\mathbf{P = FS^{1/2}M^{1/4}[cos(6/7\alpha)]^{1/2}} \quad \text{for } 0.17 \leq P \leq 8.13 \tag{1}$$

where S is relative slide thickness; $S = s/h$, M is relative slide mass; $M = m_s/(\rho_w B h^2)$.

Wiegel et al. (1970) and Noda (1970) defined the slide Froude number F as the ratio of the falling box velocity v_s, and the shallow water waves celerity as, $F = v_s/(gh)^{1/2}$.

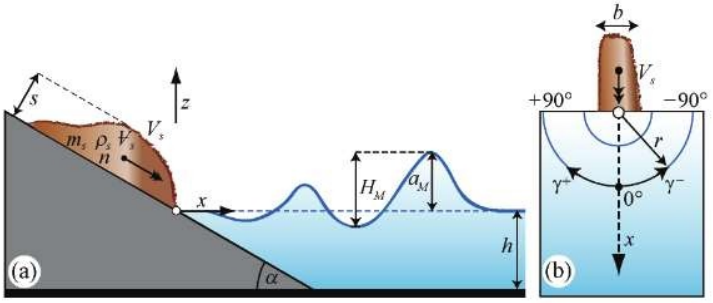

Figure 7: Sketch defining the governing parameters on impulse wave generation and the most important wave parameters in (a) 2D and (b) 3D (Figure from Heller et al., 2009).

With regard to the effects of impulse waves on dams, the maximum wave height H_M and wave amplitude a_M are of particular importance (see Figure 7). Heller Valentin and Hager Willi H. (2010) empirically derived these wave characteristics in the near field as:

$$\boldsymbol{H_M = (5/9)P^{4/5}h} \tag{2}$$

$$a_M = (4/9)P^{4/5}h \tag{3}$$

These equations are for the calculation of impulse waves which propagate confined, longitudinally in a reservoir, following the impact of a slide mass in a longitudinal direction (2D approach) (see Fig. 7a). The 3D case (Fig. 7b) considers that a slide mass can impact at any possible location into the reservoir and propagate radially and freely from the slide impact zone unlike 2D approach.

2.4 Wave runup and overtopping

Once impulse waves are generated by landslides, they propagate and interact with the water body boundaries, such as a reservoir. The interaction can for example be refraction, reflection, and/or runup on reservoir banks as well as dam slopes If the induced wave runup on a dam slope exceeds the dam freeboard, the water will overtop the dam and flood the downstream areas. The last phase of landslide generated waves, phase 3 in Figure 4, wave runup and overtopping of a dam has been investigated with physical model experiments (De Girolamo et al., 2014; Huber et al., 2017; Kobel et al., 2017; Liu et al., 2005; Müller, 1995) and numerical modelling (Bosa and Petti, 2011; Li et al., 2019; Manenti et al., 2019; Manenti S. et al., 2016; Xiao and Lin, 2016). Among the numerical modelling done to study this process, a smoothed particle hydrodynamics (SPH) approach has been used with 2D (Manenti et al., 2019; Manenti S. et al., 2016) and 3D (Vacondio et al., 2013) numerical simulations. In physical as well as in numerical models, solitary waves were applied to simulate the overtopping characteristics of impulse waves on dam structures because this wave type represents the extreme case (Heller and Hager, 2011).

2.4.1 Wave runup

In designing dam freeboard, the runup height is among the parameters that have to be determined. To calculate the runup height of impulse waves experimental studies (De Girolamo et al., 2014; Fuchs, 2013; Gedik et al., 2005; Hall and Watts, 1953; Müller, 1995; Synolakis, 1987; Teng et al., 2000) and analytical investigations (Carrier et al., 2003; Dodd Nicholas, 1998; Hibberd and Peregrine, 1979; Titov and Synolakis, 1998; Ying and Fredric, 2001; Zelt, 1991) have been conducted. The early reports by Hall and Watts (1953) proposed two equations for different beach angle ($\beta < 12^0$ and $\beta > 12^0$). In both cases, the runup height is expressed based on the plane beach angle, the relative wave height and the still water depth. Synolakis (1987) found that nonlinear and linear shallow water equations for a sloping beach is the same. Identical parameters like that of (Hall and Watts, 1953) are used to express the run up height for a gentle slope of only 1: 19.85 (V: H) beach. Müller (1995) investigated the wave runup and overtopping of dams for non-breaking waves on dams having upstream slope of 1:1 and 1:3 (V: H) based on plane beach angle, the relative height, still water depth and the wave length. In order to use this formula, determination of wave length is required. Hence, to overcome this additional step Di Risio (2005) provided a parameter T_S, which is expressed based on still water depth and the wave height, for the prediction of the run up height. A recent study by Fuchs (2013) presented similar equation as that of Hall and Watts, (1953) but for different shore slopes. Teng et al. (2000) investigated the maximum run up of non-breaking solitary waves of both smooth and rough beaches of slope 10^0, 15^0 and 20^0. It is concluded that the runup depends on the roughness and beach slope. Further experiments were conducted by Gedik et al. (2005) on permeable, armored and not armored beaches on a 1:5 sandy beach and suggested an empirical formula for both cases. According to the result, the run-up heights are reduced up to 50 % on armored over non armored shores.

2.4.2 Dam overtopping

In dam overtopping from impulse waves, the overtopping volume and overtopping rate are the other relevant parameters that have to be determined. This helps in hazard assessment and preparedness for the effects to downstream of the dam. However, there are only few studies available on the topic of dam overtopping from impulse waves. The only researches dealing with this issue are those of Müller (1995), Di Risio (2005), Huber et al. (2017), and Kobel et

al. (2017). Müller (1995) and Kobel et al. (2017) used solid, non-erodible dam model, while Huber et al. (2017) used erodible granular dam model

Müller (1995) performed a series of 2D experiments by reproducing the effect of both the dam slope and crest width. He further developed the following three step approach to predict overtopping volume: a) run up height at an inclined plane is computed; b) overtopping volume per unit length dam crest for $f = 0$ is calculated with an empirical equation and, 3) the overtopping volume per unit length dam crest is computed based on the first two steps, including a freeboard consideration. In addition, the formula for the time duration of the overtopping event was proposed for maximum overtopping discharge calculation. In a similar way, Di Risio (2005) performed 2D experiments and an empirical formulation for calculating overtopping volume without computing the runup height values. The most recent study of Kobel et al. (2017) derived empirical formula for overtopping volume, maximum overtopping depth and wave overtopping duration with cases having freeboard. The effects of still water depth, dam height, wave amplitude, dam front face angle and dam crest width is studied. An empirical best-fit approach resulted in easy to apply worst case non-dimensional predictions for overtopping volume V, maximum overtopping flow depth d_o, and overtopping duration t_o. The result shows relative overtopping volume increases significantly with the relative still water depth, moderately with the relative wave amplitude and slightly with the relative maximum wave amplitude. In a similar way to Kobel et al. (2017), Huber et al. (2017) investigated the effect of solitary wave overtopping a granular dam with a 2D laboratory study.

The above mentioned studies involving a dam are based on 2D experiments. Thus the recent published papers (Paper I (Tessema et al., 2019) and Paper II (Tessema et al., 2020)) from the present study, involving a 3D physical model, are a valuable addition to the literature on the topic of dam overtopping from landslide generated waves, and similarly is expected for the manuscript (Paper III) on the wave runup on the dam slope. This contribution is accounted for and discussed in the following chapters.

3 Research and Testing Methodology

This chapter provides a description on the physical model employed in the present study, as well as the instrumentation, the measurements and testing methodology. First, in Section 3.1, the background of the 3D physical model is reviewed and main features described, including the fixed parameters. The experimental setup is outlined in more detail in Section 3.2, followed by a description of the measurement system in Section 3.3, and the test program in Section 3.4. Finally, Section 3.5 accounts for scale relations.

3.1 Introduction to the physical model

In 2008, a physical model was built in the Hydraulic laboratory of NTNU to study the effects of landslide generated tsunami waves in fjords. The topography and bathymetry of the southern part of Storfjorden fjord system in western Norway was simulated in a scale of 1:500 with this physical model. Using the measured data from the scale model, Løvholt et al. (2015) simulated the generated tsunami inundation with a numerical model which provided a good match with the measurements. After the completion of this work, the model was reconstructed to a conceptual scale of 1:190 to study the effect of landslide generated waves on embankment dams. Several test series have been conducted with different model setup on the physical model to study the impacts of landslide generated waves on dam overtopping. The effects of different landslide, reservoir and dam parameters on the embankment dam overtopping has been studied. The executed physical experiments under several experimental scenarios gave insight into the parameters and dam overtopping (Biedermann, 2017; Mortensen et al., 2016; Ponziani and Gardoni, 2017; Sigtryggsdottir, 2017).

The physical model (see Figure 8) simulates a landslide falling into the reservoir, where an impulse wave is generated, propagates and runs up the upstream dam slope or overtops a dam. Unlike the previous studies in literature on the 2D case, i.e. conducted in rectangular prismatic water wave channels with landslides impacting a reservoir along the longitudinal direction, the present study considers the 3D effect relating to narrow valleys and slides impinging perpendicular to a reservoir‘s longitudinal axis. This setup makes the results from the experiments more realistic in a way natural occurrence of slides into reservoir are most likely to occur. The limited studies available considering similar setups motivated this study to

investigate landslides impacting a reservoir in lateral direction in a physical scale model. Table 1 describes all the fixed parameters for the physical model setup used in the present study.

Table 1: Fixed parameters for the physical model setup of the present study (dimensions are given in the conceptual prototype scale of 190).

Parameter	Fixed	Notation
Slide ramp	Location	perpendicular to the reservoir axis
	Inclination	$\alpha = 50^0$
Slide properties	Solid blocks	blocks chained together with minor opening between them
Reservoir	Geometry, like reservoir length and width	l_b= 742.9 m and b_b = 336.3 m
	Slope of side banks	$\theta = 50^0$
Dam	Height	H = 60.8 m
	Crest length	l_c= 421.8 m
	Crest width	B_c = 10.07 m

3.2 Experimental setup

The main structural components of the physical model used in this study are the slide ramp where slide blocks are placed, the basin simulating the reservoir and the dam (Figure 8). Each of these components belonging to the model setup is discussed in this section.

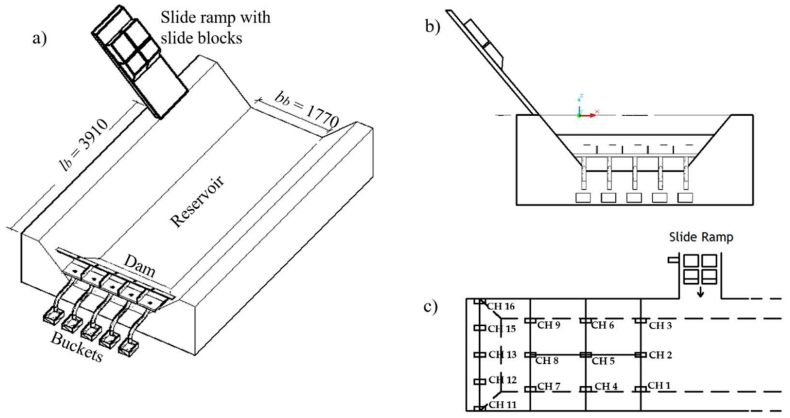

Figure 8: Physical model having three basic components: the slide, the reservoir and the dam; a) Isometric view, b) front view, and c) top view showing the sensors.

3.2.1 The slide

The slide was modelled with blocks placed on a 2 m long slide ramp inclined at a constant angle of α = 50^{o} where it is possible to place blocks of different size and arrangement (see Figure 9).

For each test setup, different slide block arrangements are made as seen in Figure 10 with values provided in Table 2. In each block arrangement the slide blocks are tapered at an angle of $\Phi = 45^{0}$ at the front to have the highest impact (Sælevik et al., 2009). The blocks are attached to each other with chains, the slide body is then attached to a steel panel with a hook. When the hook is removed, the blocks slid into the reservoir generating impulsive waves (see Figure 9).

Figure 9: The slide ramp where 4B are placed to slide into the reservoir.

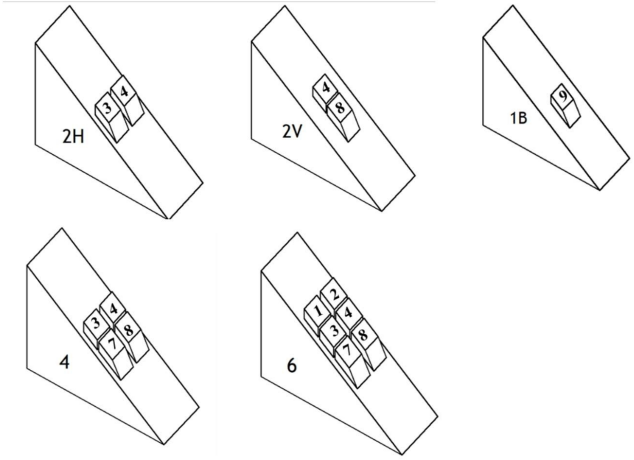

Figure 10: Slide block setup where in each arrangement the block numbers are mentioned (refer Table 2 for their value).

Table 2: Slide block characteristics in the model setup (model scale)

	Block arrangement				
Slide characteristics	**1 block**	**2H blocks**	**2V blocks**	**4 blocks**	**6 blocks**
Slide length (l_s) (m)	0.5	0.5	1.08	1.08	1.66
Slide width (b) (m)	0.45	0.9	0.45	0.9	0.9
Shape ratio (l_s/b)(-)	1.11	0.56	2.4	1.2	1.84
Slide volume (W_s) (m^3)	0.02	0.072	0.074	0.15	0.23

3.2.2 The basin

The reservoir is simulated with a trapezoidal basin having planar slope sidewalls of water-resistant plywood covered with a concrete paste for increasing the roughness. It is 4.5 m long, 1.7 m wide at the bottom and 2.2 m at dam crest level, with a total reservoir capacity of 2.5 m^3. These dimensions in model scale correspond to 860 m long reservoir, 320 m wide at the bottom and 17 Mm^3 in prototype of scale 1: 190 (see Figure 11).

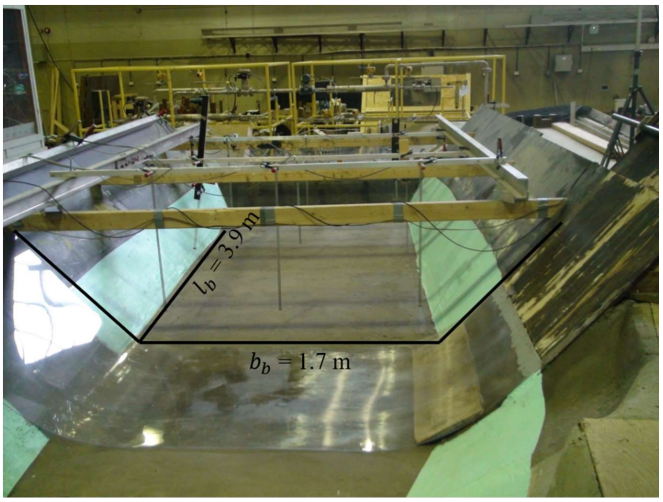

Figure 11: Picture of the trapezoidal basin with its dimensions. View towards the dam.

3.2.3 The dam

Dams having upstream slopes of 1: 1.5, 1: 2 and 1: 2.25 are used for the analysis and represent the upstream slope inclination of embankment dams. The dam crest is divided into five different sections (CH 11 to 16), referred to in the following as dam crest sections, to clearly see the distribution of the overtopping waves along the crest. Five ultrasonic sensors (*mic+35/LU/TC*) are placed in each section to measure the overtopping depth over the dam crest with time (Figure 12a). The corresponding volume of overtopping water for each dam section is collected in five buckets with pipes of 100 mm in diameter (Figure 12b).

Figure 12: Picture of dam crest sections, CH 11 through CH 16 on the left and five buckets collecting overtopping water at each dam section on the right.

3.3 Measurement system

In an experimental study, the reliability and trend of the data should be analysed. For this study, this has been done by repeating the same test 20 times and estimating the repeatability of the results obtained. Furthermore, to check the test repeatability, each test with identical parameters was repeated three times and analyzed. All test data are given as the average of these three individual tests.

Nine wave gauges of type *`DHI wave-meter 102E`*, CH 1 through CH 9, are placed at the top of the trapezoidal basin to measure the wave height propagating along the reservoir. This wave meter working principle is to measure the conductivity between two parallel electrodes which are partly immersed in water (Figure 13). In addition, five ultrasonic sensors (*mic+35/IU/TC*)

placed at the top of each dam section (CH 11 through CH 16) to measure the height of the water that overtopped the dam crest (Figure 13).

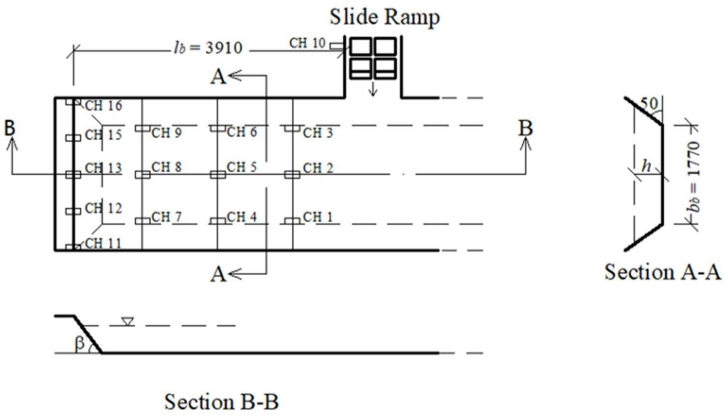

Figure 13: Planar view of sensors placement in the model set up (measurments in mm) (Tessema et al., 2019).

The water that overtopped the dam was collected in five calibrated buckets (Figure 14a) and recorded manually with an ultrasonic sensor as seen in Figure 14b. The calibration procedure for the buckets is described in Appendix A.

Figure 14: a) Five buckets for collecting the overtopping volume; and b) Ultrasonic sensor for measuring overtopping volume (Photo: Netsanet Nigatu, NTNU).

The speed of the landslide is directly influenced by the initial position of the slide relative to the edge of still water level. Increasing the travel distance of the slide to the water increases the value of the landslide speed significantly. The friction of the slope can be back calculated to represent a value of the internal friction angle of about $\Phi_s = 25°$.

Figure 15:a) Voltmeter which records the voltage as the block slides down the ramp, and b) rope which unrolls together with the slide blocks connected with rotational sensor.

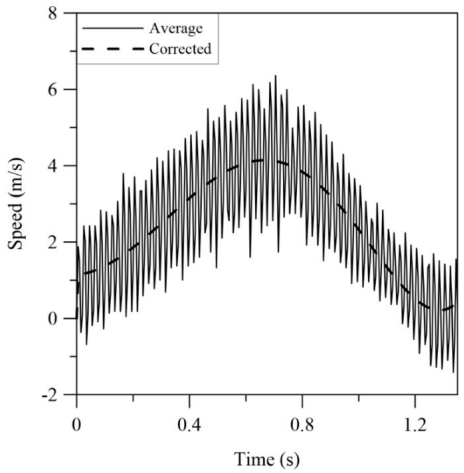

Figure 16: Maximum slide speed extraction with polynomial regression (Test no. 185_2.25s_4.5_2H_200).

To measure the speed of the slide block, a rotational sensor (CH 10) was placed at the side of the slide ramp (Figure 13). It is connected to the rigid sliding blocks through a hook with a rope

which unrolls together with the distance covered by the slide. A voltmeter records the voltage as the block slides down the ramp and the rope unrolls (Figure 15). In order to change the measured voltage into the distance covered by the slide, a calibration factor is required (refer to Appendix A to see how the calibration factor is calculated).

The recording from CH 10 gives a position curve with time which has noises. Hence, a polynomial regression is applied to extract the maximum speed of the slide considering the impact velocity as the maximum one as seen in Figure 16.

A video camera was placed perpendicularly to qualitatively describe the runup and overtopping phenomenon over the dam due to the generated waves. A scale of 2 mm x 2 mm grid was put on the plexiglass where the camera records to have a reference scale in the images. The camera has a maximum resolution of 1920 x 1080 pixels and records up to 30 fps.

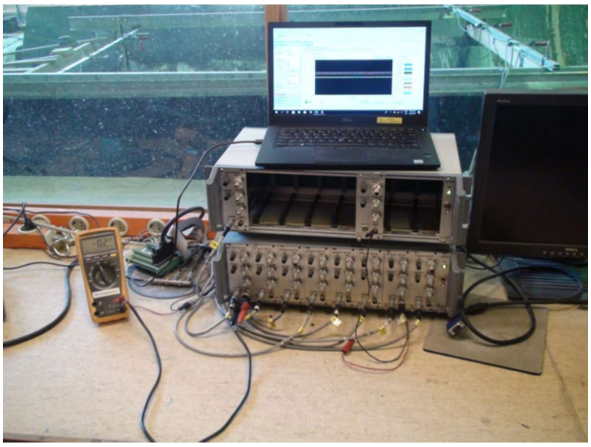

Figure 17: All measurement sensors connected to a computer with `*Agilent Measuring Manager program*`.

The data from the landslide velocity measuring sensor, the wave gauges and the ultrasonic sensors in each dam section are collected in `*Agilent Measuring Manager program*` with a sampling rate of 200 Hz (Fig. 17).

3.4 Test program

Landslide generated waves overtopping on dams was investigated with parameters such as the landslide volume, landslide release height, landslide speed, upstream dam slope and freeboard. These parameters represent the input variables of the study as shown in Table 3.

Table 3: Test program.

Scale	β (V:H)	f (m)	W_S (m^3)	h_0 (m)
Model	1: 2.25	0.024, 0.032	0.072, 0.074, 0.149, 0.225	0.5, 1, 1.5, 2
	1: 2	0.024, 0.032	0.072, 0.074, 0.149, 0.225	0.5, 1, 1.5, 2
	1: 1.5	0.024, 0.032, 0.07	0.02, 0.072, 0.074, 0.149, 0.225	0.5, 1, 1.5, 2
Prototype (1: 190)		4.5, 6, 13	0.14, 0.49, 0.51, 1.02, 1.54 (Mm^3)	95, 190, 285, 380

3.5 Scale relations

The perfect similitude between a hydraulic model and its prototype requires geometric, kinematic and dynamic similarity. For geometrical similarity all ratios of the corresponding linear dimensions (e.g. length) must be identical between the model and the prototype; the kinematic similarity applies to all components of the vectoral motions for all particles at any time (e.g. time) involved in the flow process; in addition, the ratios of all vectoral forces (e.g. gravity) in the two systems must be identical for dynamic similarity (Heller et al., 2008).

Given the free surface flow problem, Froude similitude is considered in the analysis where waves generated by the slide impact are dominated by gravity, not by surface tension forces (Mehaute, 1976). It only considers the inertial and gravity forces whereas the fluid viscosity, the surface tension, and the elastic compression forces are neglected. However, they may cause scale effects if their effects are large. The relevant force ratio for impulse wave generation is the square root of the inertial to the gravity force, which is to be the same on a scale model as on a prototype. The Froude similitude stems from the fact that the gravity acceleration is the same on the model as in the prototype. Table 4 describes the most important similitude ratios to up scale the model data to its prototype.

Table 4: Similitude ratios based on length ratios for the model setup used in this study according to the Froude similitude.

Quantity	**Fundamental dimension**	**Model: Prototype**
Length	[L]	$L_r = 1:190$
Area	$[{L_r}^2]$	$L_r = 1:36.1\ x\ 10^3$
Volume	$[{L_r}^3]$	$L_r = 1:6.86\ x\ 10^6$
Time	$[{L_r}^{1/2}]$	$L_r = 1:13.78$
Velocity	$[{L_r}^{1/2}]$	$L_r = 1:13.78$
Discharge	$[{L_r}^{5/2}]$	$L_r = 1:0.5\ x\ 10^6$

4 Summary of results

In the following sections, the main findings of the research study are presented. The sections are divided by main outcomes of the research and the related journal papers and manuscript, Paper I to III, are identified within each heading. Section 4.1 accounts for results regarding wave type investigation from Paper I. In Section 4.2 wave propagation analysis is discussed, however this is not included in the published journal papers. Results from Paper I summarized in Section 4.3 describe analysis of the total overtopping volume of the landslide generated waves overtopping the dam, while the results of Paper II comprising prediction formulas for the overtopping depth and rate are summarized in Section 4.4. Finally, the research outcome of Paper III on landslide generated wave runup on dams for freeboard predictions are summarized in Section 4.5.

4.1 Wave type observed (Paper I)

Wave classification methods to characterize landslide generated waves and identifing wave types observed in 2D experiments in a wave channel, are available in the literature as previously discussed. The Froude number, F, and the wave product number, T, are important in this respect. In Paper I, these parameters are calculated from all the tests of this study and plotted along with boundaries of the wave type zones identified by Heller and Hager (2011) from granular slides. The datapoints for the smaller landslide volumes (2 blocks) of this study all fall within an intermediate boundary, for which mainly cnoidal-like and solitary-like waves were observed in the 2D case. Most of the datapoints resulting from tests with 4 blocks, also fall within that boundary. Conversely, the largest landslide arrangement (6 blocks) falls into the zone where mainly Stokes-like waves were observed in the 2D tests considered by Heller and Hager (2011) when defining the boundaries. However, the 3D waves generated in this study are more complex than in the 2D case. Considering profiles of recorded waves at the different wave channels in the physical model of this study, Stokes-like waves, rather than any of the other wave types were observed. Furthermore, investigation into selected waves revealed a ratio of wavelength to reservoir depth in the range of intermediate water waves.

4.2 Wave propagation analysis

Two types of impulse wave propagation patterns are commonly investigated in model tests: unidirectional (Di Risio and Sammarco, 2008; Fritz et al., 2004; Zweifel et al., 2006) and omnidirectional (Heller and Spinneken, 2015; Heller et al., 2009; Mohammed and Fritz, 2012; Panizzo et al., 2005a). The former is investigated in a 2D wave flumes whereas the latter is studied in 3D wave basins. In this study, to make qualitative evaluation of the wave propagation and to clearly see the pattern, simulation has been made with *'Matlab Software'* (Figure 18).

The wave propagation process is simulated, i.e. recreated numerically from the experimental data, for the wave guage sensors, CH 1 to CH 9, which are installed at the top of the reservoir to measure the wave height with time. Generally, the generated wave can be classified as impact and reflected waves (as described in Paper III) based on its origin where the first one is generated from the direct impact of the slide and the latter is from the reflections from the underwater movement of the slide or reflections from the basin sides.

When the slide impinges into the reservoir, the water level at CH 3 changes instantly (Figure 18b and c) followed by CH 2 across CH 1 (Figure 18c, d and e) progressively. In the wave generation area, a perturbation is generated and energy exchange between landslide and water takes place. The first wave generated by the direct impact of the slide is called incident wave. The highest incident wave is recorded in CH 1. The induced wave quickly leaves the generation area and propagate in the near field (Figure 18f and g) and overtops the dam in a uniform manner timewise across the five dam sections (referred as impact wave in Figure 19), however the wave depth of first overtopping wave is highest at the left edge and gradually reducing towards the right edge. A reflected wave is generated by the underwater movement of slides or the reflections from the slide basin immediately after the impact wave is gone. The 2nd wave (reflected wave) propagates along CH 6 to CH 9 (Figure 18h and i) and overtops the dam at right section (see eg. Figure 19). The 3rd reflected wave propagate along CH 4 (Figure 18j) and overtops the dam at the left section (see eg. Figure 19). Other minor waves are observed in the video throughout the reservoir basin, until about t = 12 s generated due to the reflection across the reservoir sides.

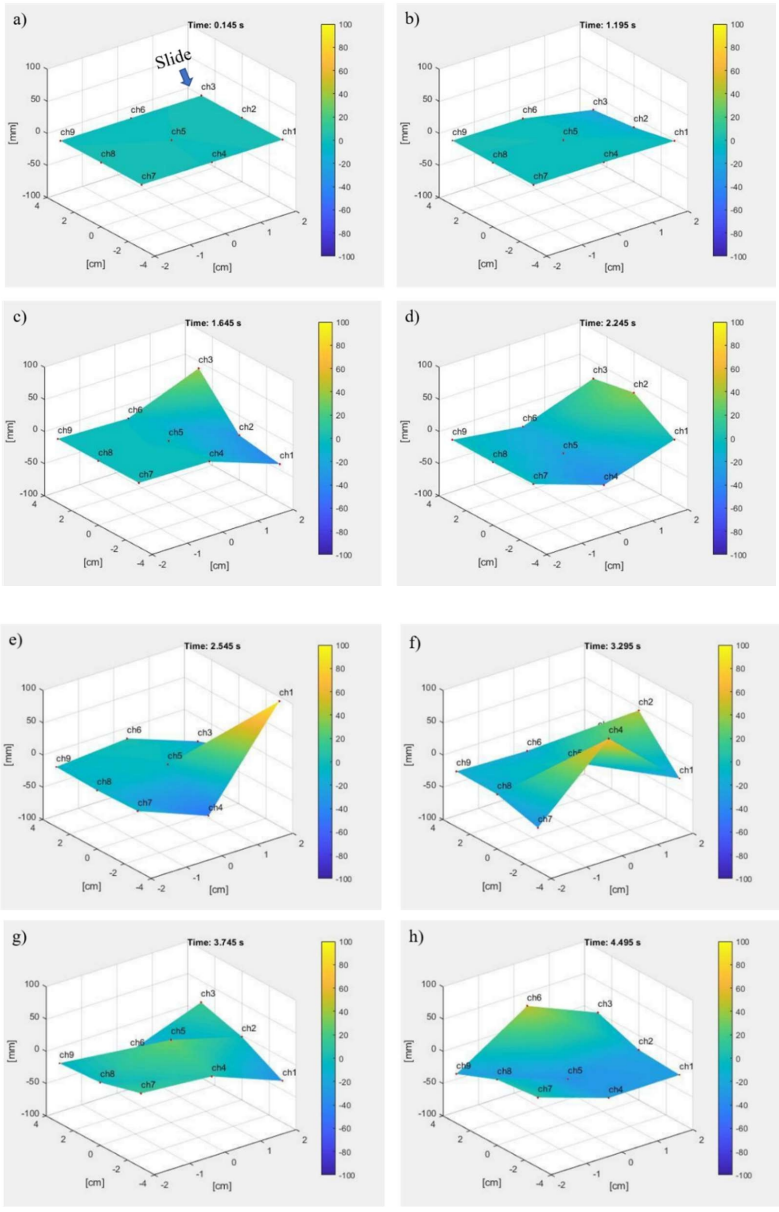

(Fig. 18 continued on next page)

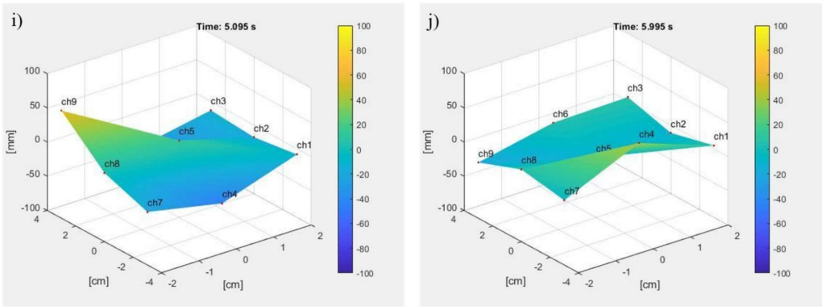

Figure 18: Time series sequence of wave propagation for Test no. 185_2.25s_4.5_2H_200.

In analysing the wave running up the upstream dam slope, it is seen that the wave pattern overtopping the dam is not uniform. This is due to the narrow reservoir (where the reservoir length is more than its width) considered and the slide impact location (i.e. slide impact from the sides of the reservoir), as well as due to reflection of the wave at the reservoir banks.

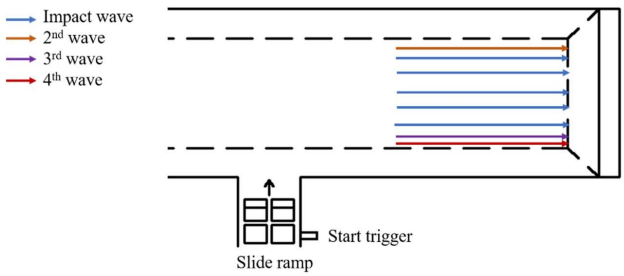

Figure 19: The patterns of wave running up dam slope along the crest. (Schematic figure).

4.3 Overtopping volume Analysis (Paper I)

Paper I: Case study of Dam Overtopping from Waves Generated by Landslides Impinging Perpendicular to a Reservoir's Longitudinal axis (Tessema et al., 2019).

In previous studies by others, impulse waves were investigated leading to a general description to predict overtopping volume based on a reservoir and dam properties in 2D settings. For the specified model setup of the present study, in 3D settings, Paper I provides such information

with systematic variation of slide, basin and dam parameters such as slide volume, slide release height, slide speed, upstream dam face slope angle and wave amplitude for cases with freeboard, $f > 0$. A total of 66 experiments were conducted varying these input parameters.

Based on the experimental results, an extensive regression was performed, and a formula obtained which can be used in predicting the amount of water that will overtop the dam crest for a specific slide event. More specifically, the prediction formula from Paper I can be used for estimating the total volume of water overtopping a dam from impulse waves generated by a landslide impinging perpendicular to the reservoir longitudinal axis. The results can be further used for early risk assessment for similar cases.

The proposed equations from Paper I, given below with Eq. (4) and Eq. (5), are presented with limitations explained in the Paper I considering two different cases, with (Eq. (4)) and without (Eq. (5)) considering the effect of relative amplitude (these equations are expressed as Eq. (4) and Eq. (6) respectively in the Paper I (Tessema et al., 2019)).

$$\frac{W_w}{h^3} = 0.21\left[\left(\frac{W_s}{h^3}\right)\left(\frac{h_0}{h}\right)^{0.43}(\mathrm{F}^2)^{-0.08}\,\varepsilon^{0.04}(\beta/90^0)^{-0.01}\right] = 0.21E_1 \tag{4}$$

The following limitations apply: $2.67 < W_s/h^3 < 9.52$, $1.67 < h_o/h < 6.97$, $1.25 < \mathrm{F} < 2.66$, $0.18 < \varepsilon < 0.73$ and $0.27 < (\beta/90^0) < 0.37$.

$$\frac{W_w}{h^3} = 0.17\left[\left(\frac{W_s}{h^3}\right)\left(\frac{h_0}{h}\right)^{0.42}(\mathrm{F}^2)^{-0.03}\,(\beta/90^0)^{-0.1}\right] = 0.17E_2 \tag{5}$$

In both cases, the relative overtopping volume increases linearly and thus most significantly with the relative slide volume, but moderately with the relative landslide release height. However, the impact of relative wave amplitude, as well as relative upstream dam slope and Froude number is quite small.

The other main finding of this study is that the overtopping process for the 3D case is described with an uneven distribution of the volume of water overtopping the dam crest as seen in Figure 20. During the overtopping process, the highest waves push large volume of water for a specific time, whereas the lower waves may not produce overtopping. In the 3D wave model the overtopping volume distribution is not uniform throughout the crest, having large values at the

edges (flanks) of the dam (Figure 20). A large amount of water is collected at the right and left edges (CH 16 and CH 11, respectively) of the crest, on average about 28 % each of the total volume. Whereas a smaller volume of water overtops the middle section of the dam crest (CH 12, CH 13 and CH 15).

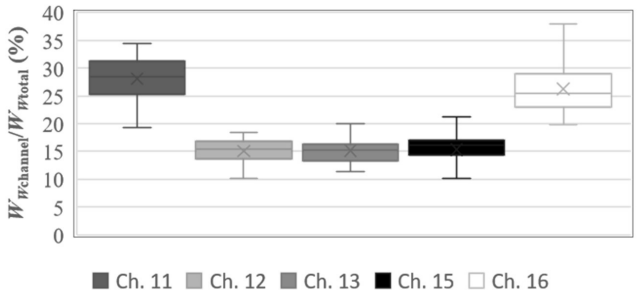

Figure 20: Overtopping volume distribution over the five dam crest sections (from Paper I (Tessema et al., 2019)).

Measured overtopping volumes were compared to the overtopping volume predicted with equations from Kobel et al., (2017), as presented here in Figure 21. As previously discussed, Kobel et al., (2017) presented an empirical equation for predicting overtopping volume for a 2D case. Two approaches are considered for the comparison: Approach 1 considers the largest wave amplitude recorded at wave gauge channels closest to the landslide impingement zone (CH 1, CH 2 and CH 3) whereas Approach 2, considers the wave amplitude recorded at the wave gauges closest to the dam (CH 7, CH 8 and CH 9). The overtopping volume calculated with Kobel's et al., (2017) predictive equation using Approach 1 overestimates the experimental data while Approach 2 generally underestimates the overtopping volume.

The overestimation factor with Approach 1, represented as the ratio between the predicted and measured overtopping, has a mean value of 2.63 with standard deviation of +/- 1.09. For Approach 2, the measured total overtopping volume versus the one predicted by (Kobel et al., 2017) has a mean value of 0.70 and standard deviation of +/- 0.53. The predictive equations presented in the present study (Eqs. (4) and (6)) extracted from the experimental data,

overestimates the experimental data by a factor of 1.13 and 1.18 and standard deviation od +/- 0.5 and 0.48, respectively (Figure 21).

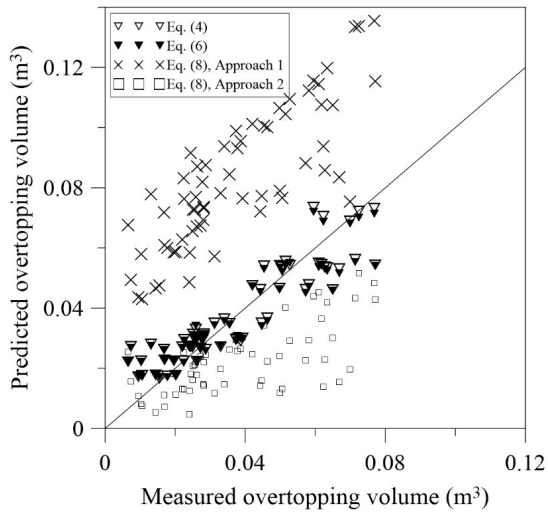

Figure 21: Predicted overtopping volume versus the total overtopping volume measured in the model tests (in m^3) of the present study. The total overtopping volume is predicted by Eqs. (4) and (6) (expressed as Equation (4) and (6) respectively in (Tessema et al., 2019)) of the present study and the overtopping volume from a solitary wave using Kobel et al. (2017)`s Equation (8) using Approach 1 and 2 (Tessema et al., 2019).

4.4 Overtopping discharge analysis (Paper II)

Paper II: Physical model study on overtopping rate over embankment dam due to landslide generated waves (Tessema et al., 2020).

In Paper II of the present study, an analysis was made to investigate whether a steady state weir equation for predicting discharge can be applied for a simple rough estimate in the case of landslide generated wave overtopping a dam. The test program involved experiments with a variation of governing parameters including slide release height, slide volume, still water depth, and upstream dam slope. Based on the results from the experiments, calibration of coefficient of discharge values for each dam section was obtained from a steady state weir equation. This

value ranges from 0.53 to 1.53 and 0.4 to 0.96 for 1: 1.5 and 1: 2.25 upstream dam slopes respectively.

A general two step procedure is presented for predicting the overtopping discharge (see Figure 22); (1) calculate the maximum overtopping depth based on all the required parameters of the slide, reservoir, and dam including slide volume, slide release height, still water depth, dam height, and dam front face angle; (2) calculate the maximum overtopping discharge, Q_{max}, with the proposed formula (Eq. (6)).

$$\frac{Q_{max}}{\sqrt{2g\,B^5}} = x\left[\frac{d_{max}}{B}\right]^y \tag{6}$$

where d_{max} is the maximum overtopping depth (see Eq. (7)), B is length along the dam crest (the weir length). Furthermore, for x and y: $0.06 \leq x \leq 0.09$ and $0.83 \leq y \leq 1.07$ for dams having an upstream slope of 1 to 1.5 and $0.05 \leq x \leq 0.16$ and $0.95 \leq y \leq 1.23$ for dams having an upstream slope of 1 to 2.25. The value of the coefficients x and y is listed in Table 5 of Paper II (Tessema et al., 2020).

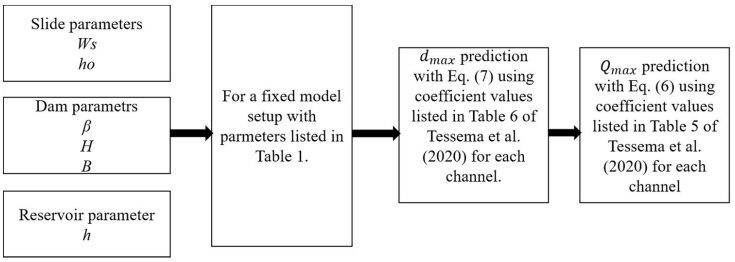

Figure 22: Flow chart showing the proposed calculation procedure for the overtopping discharge.

Based on the presented predictive equation (Eq. (7)) for the relative maximum overtopping depth, the relative slide volume and relative still water depth were found to have a significant effect.

$$\frac{d_{max}}{H} = \mathrm{a}\left[\left(\frac{W_s}{H^3}\right)^{\mathrm{b}}\left(\frac{\beta}{90^0}\right)^{\mathrm{c}}\left(\frac{\mathrm{h}}{H}\right)^{\mathrm{d}}\left(\frac{h_o}{H}\right)^{\mathrm{e}}\right] \tag{7}$$

where the coefficients are listed in Table 6 of Paper II (Tessema et al. ,2020) for each channel with the following limitations of parameters: $2.2 < W_s/H^3 < 6.87$, $0.27 < \beta/90^{\circ} < 0.37$, $0.90 < h/H < 0.94$, $1.56 < h_o/H < 6.25$.

Another factor for calculating the discharge over the dam is found to be the duration of the overtopping. A higher overtopping volume for short duration of overtopping yields a higher discharge over the crest. Hence, higher overtopping discharge values are observed at the edges of the dam crest sections. The overtopping duration will be discussed further in Section 5.2.2.

4.5 Runup height and freeboard prediction (Paper III)

Paper III: Landslide Generated Wave Runup over a Rigid Dam for Freeboard Prediction (Tessema et al., (2020b)).

The freeboard provided for a dam should be evaluated based on the simultaneous occurrence of different factors or events of which landslide induced wave runup is one of them, however, with due consideration of the likelihood of the factors or events. Thus, a large landslide event should not be combined with other natural events of low occurrence probability. For run up height determination, a systematic parametric variability and stepwise regression were performed in Paper III to see the impact of the input variables. The input variables considered for the analysis of runup height, R, were; landslide volume W_s, landslide release height h_o, landslide impact velocity V_s, wave amplitude a, still water depth h, and dam slope angle β.

For the analysis, the experimental data was put into two groups: the first data set was used for the analysis of the runup height where overtopping occurs, whereas the second data set was used for the runup height with no overtopping cases. In the first case the runup height (R) produced due to the generated waves exceeded the freeboard (f) provided for the dam ($R > f$), whereas in the latter the provided freeboard is sufficient for overcoming the generated wave ($f > R$).

For a qualitative analysis of the runup process, a video camera was installed to enable view of the runup on the dam. The video images were analysed and images were extracted with a time frame $t = 0.03$ s to describe the process over the sloping surface and dam crest for overtopping cases (test no. 55_1.5S_4.5_4B_150) and no overtopping cases (test no. 275_1.5S_0.07_1B_200). The generated waves can be classified based on their origin as

impact waves (1st wave), generated from the direct impact of the slide to the reservoir and reflected waves (2nd, 3rd, and 4th) which originates mainly from reflections from the basin sides, and potentially the underwater movement of the slide.

A systematic experimentation and a data analysis was carried out in Paper III to derive a fit equation for the runup height, presented here with Eq. (8), with limitation of parameters listed in Table 4 of Paper III.

$$\frac{R}{h} = \mathbf{0.1}\,(W_S/h^3)^{0.34}\,(tan\,\beta)^{-0.16}\varepsilon^{0.14}(F)^{0.29} = \mathbf{0.11}W; \qquad 1.4 < W < 2.94 \qquad (8)$$

where W is runup height parameter defined as $W = (W_S/h^3)^{0.34}\,(tan\,\beta)^{-0.16}\varepsilon^{0.14}(F)^{0.29}$.

Based on the Eq. (8), the slide volume and Froude number has a dominant effect followed by wave amplitude in run up height determination. In general, a larger volume of slide impacting a reservoir leads to higher runup height value over the dam surface. A slide having high speed which leads to high slide Froude number, F, has higher energy which further generates a high wave which runs up the dam slope.

The predictive equation from this study, Eq. (8), was compared to other predictive formulas in the literature (Fuchs, 2013; Hall and Watts, 1953; Synolakis, 1990). Two approaches are considered here: Approach 1 considers the largest wave amplitude recorded at wave gauge channels closest to the landslide impingement zone (CH 1, CH 2 and CH 3) and assumes it is a solitary wave. Conversely, Approach 2 considers the wave amplitude recorded at the wave gauges closest to the dam (CH 7, CH 8 and CH 9). A comparison is made between the predicted and measured relative runup height, where the predicted relative runup height is calculated with Eq. (8). It demonstrates that the predictive equations from literature over estimates the experimental data in both cases (Approach 1 and Approach 2). In comparison, Approach 1 and Approach 2 over estimates the experimental data by a factor of 3.1 to 7.3 and 1 to 4 respectively. This is discussed further in Chapter 5

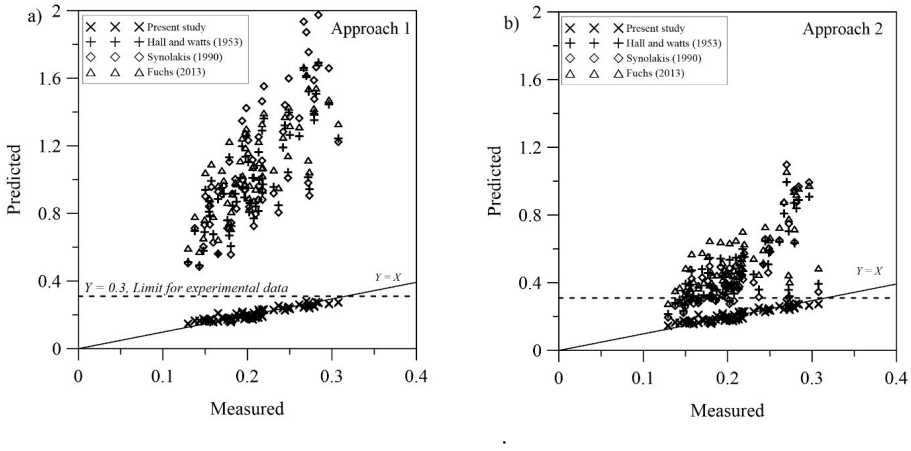

Figure 23: The comparison of measured relative runup height and predicted with the proposed equation of the present study (Eq. (8)) and from literature. (Approach 1 (left) and Approach 2 (right)).

4.6 Parametric study

The parameters that are not clearly discussed in the papers, but deserves a discussion are presented in Appendix D. The discussion in this subsection favors prototype scale over the dimensionless parameters used hitherto, to provide a connection to real world problems through the dimensions. Table 1 is referred to for the dimensions of different parameters in the model and a prototype scale of 1: 190 is used. The relation between the overtopping volume and the slide impact velocity (the release height) as well as the slide volume considering different freeboard of the dam is discussed.

5 Discussion

Four specific research objectives for the PhD study were presented earlier in the Chapter 1 Introduction. To address these objectives and associated subobjectives, the research outcomes from Paper I to III are discussed herein and related to the literature discussed in Chapter 2, or as applies. Discussion related to objective 1 through 4 is presented in Section 5.1 through 5.4, whereas Section 5.5 reviews some parameters that are not clearly discussed in the papers, but are worthy of a discussion. In Section 5.6 limitation of the model setup is discussed and the parametric limitation of the results are summarized in Section 5.7. Finally, recommended further studies are summarized in Section 5.8.

5.1 Wave type, wave generation and propagation (Objective 1)

Research outcome of the study relating to Objective 1 are discussed in this section. The Objective 1 is to qualitatively investigate the process of the wave generation and propagation in the narrow reservoir towards the dam. First the wave type generated in the present study is discussed, then the wave generation and propagation.

5.1.1 Wave type in the physical model (Paper I)

The wave type generated by the landslide as it impinges the reservoir may be influential for the dam, since the wave type, such as Stokes-, solitary-, cnoidal- or bore waves, influences for example the runup height and wave force on a dam (see e.g. Heller and Hager (2011)). Thus, in Paper I it was considered of interest to identify the wave type generated in the 3D physical model employed. Considering profiles of recorded waves at the different wave channels in the physical model of this study, Stokes-like waves, rather than any of the other wave types were observed. However, available wave classification methods to characterize landslide generated waves and identify wave types are developed mainly from observation in 2D experiments in a wave channel. The 3D waves generated in this study are more complex than in the 2D case, and not all the waves fell into the boundary assigned for 2D waves by Heller and Hager (2011), considering datapoints identified by the Froude number, F, and the wave product number, T, given here in Chapter 2. Heller and Spinneken (2015) have noted similar finding for the 3D case (see also Chapter 2). They concluded from their 3D test results that the lower boundary

($T < 4/5F^{-7/5}$) defined by Heller and Hager (2011) remains characteristic also for 3D waves, whereas in the intermediate range both Stokes- and cnoidal-like waves were observed. Research finding from the present study supports this conclusion.

5.1.2 Wave generation and propagation in the physical model

Several past research works have described landslide wave generation and propagation. The wave generation is influenced by parameters relating to both the landslide and reservoir. The results of this study relate to results from other similar studies (Heller, 2007; Heller and Hager, 2014, 2010, 2011; Heller et al., 2009) namely that the stillwater depth in the slide impact zone, the slide volume, slide width, slide thickness, slide grain diameter (for granular slides), slide impact velocity, the density of water, gravitational acceleration, and the distance from the point of impact and the elapsed time influences the wave generation, as describe by the Impulse Product Parameter (P) (see Eq (1)) by Heller and Hager (2010). For the wave generation in the physical model of this study the landslide volume is the most influential, but also the slide impact velocity which is dependent on the slide volume and the release height.

Two-dimensional properties of landslide generated wave generation and propagation have been investigated in flumes (Ataie-Ashtiani and Nik-Khah, 2008; Kamphuis and Bowering, 1970; Synolakis, 1990; Watts, 1997; Wiegel, 1955), while other studies (Bellotti and Romano, 2017; Briggs et al., 1995; Di Risio and Sammarco, 2008; Evers, 2017; Fritz et al., 2009; Heller and Spinneken, 2015; Huber et al., 2017; McFall and Fritz, 2016; Romano et al., 2016; et al., 2009) investigated the three-dimensional effects by considering wide reservoirs (3D water bodies) (Evers, 2017; Heller and Spinneken, 2015; Huber et al., 2017), as well as several geometries such as planar beaches and islands (Bellotti and Romano, 2017; Briggs et al., 1995; McFall and Fritz, 2016; Romano et al., 2016). The two different approaches, prismatic wave channel (2D) and rectangular wave basin (3D), cover the extreme cases of restricted transverse (2D) and completely free radial propagation of the impulse waves above a horizontal waterbed (Heller et al., 2009).

However, the above-mentioned studies do not directly investigate with experiments the 3D effect of the wave propagation relating to narrow valleys and a landslide falling into a narrow reservoir perpendicular to the reservoir's longitudinal axis, i.e. setups as used in the present

study. Study into the wave propagation in the physical model of this study (described in Chapter 4) demonstrates how waves are reflected at the reservoir banks. Even though it is difficult to find in the literature similar setups with such wave reflections considering a reservoir and a dam, Heller et al., (2009) investigated this through a calculation example for a similar case as in the present study, only the reservoir in the calculation example has a slight bend. However, the calculation example does not go as far as consider reflected waves from both sides of the reservoir as observed in the physical model of this study.

Generally, it is seen in the present study that the wave pattern propagating throughout the reservoir and towards the dam is not uniform over the surface and reflections play an important part in the whole process. This results in uneven run-up on the dam and uneven overtopping of the dam crest as further discussed in the following sections on overtopping and runup.

5.2 Dam overtopping from landslide generated waves (Objective 2)

In this subsection, Objective 2, described in Chapter 1 Introduction, is summarized. To address the Objective 2 and its three sub-objectives, the research outcomes from Paper I and II are discussed herein. This includes discussion on formula for defining parameters of the impact of landslide generating wave on dams. These parameters include overtopping volume, discharge, overtopping depth, and runup height. Additionally, the uneven distribution along the dam crest is discussed. The results are compared to the relevant literature as applies, in accordance with Objective 4.

5.2.1 Prediction of the total overtopping volume (Subobjective 2.1, Paper I)

Only a few studies consider dam overtopping with formulas for the overtopping volume based on wave and dam parameters. These studies are mainly those of Huber et al. (2017) in the case of an erodible granular dam model, and Kobel et al. (2017), Di Risio (2005) as well as Müller (1995) in the case of a solid, non-erodible dam model. The resulting formula for the overtopping volume is based on (2D) experimental tests. For example, Kobel et al. (2017) used rectangular prismatic water wave channels with solitary waves propagating directly towards a dam and proposed a prediction formula for the volume of the water overtopping the dam.

The above-mentioned studies do not directly investigate the 3D effect relating to narrow valleys and a landslide falling into a narrow dammed reservoir perpendicular to the reservoir's longitudinal axis as does the present study. Paper I (Tessema et al., 2019) uses the data collected from the 3D physical model of this study and arrives at the predictive equation for the total volume of water overtopping the dam, presented here as Eqs. (4) and (5), through empirical data analysis. The formula derived is dependent on both the landslide and dam parameters. The dam parameters considered, for the upstream slope and freeboard, relate e.g. to those relevant for embankment dams.

The main contribution of this study is the inclusion of 3D effects into the investigation of dam overtopping from landslide generated waves. Thus, it is interesting to compare the results to other studies, even though these base on a 2D approach. Paper I compared the predictive equation for the 3D setup from the present study and this by (Kobel et al., 2017) derived from 2D setups. The comparison is presented in Chapter 4.3 with Figure 21. Thus, the Figure 21 compares results from studies representing the two cases, i.e. a 2D study using solitary waves through Approach 1, versus the present 3D study of landslide impinging perpendicular to the reservoir's longitudinal axis and inducing a more complex wave field (Figure 18). Additionally, the 3D wave effects are considered for the 2D formulation with the Approach 2 described above.

Kobel et al (2017) applied 2D solitary waves in their experiments and state that such waves represent the extreme case. The comparison in Figure 21 confirms this statement by Kobel et al. (2017), considering that the predicted overtopping volume is on average more than twice the experimental results in Approach 1 use of Kobel's et al (2017) equation for the prediction of the overtopping volume. However, Figure 21 also demonstrates that given the relative wave amplitude close to the runup zone as in Approach 2, the use of Kobel et al. (2017)'s equation may underestimate the total overtopping volume for cases of narrow reservoirs.

The comparison in Figure 21 indicates that in a risk assessment for the downstream area, threatened by the water overtopping a dam, the water volumes estimated by the prediction formulas of the present study (see Paper I) may be more appropriate for reservoir and dam cases that can be represented by the physical model of this study. However, the distribution of the overtopping wave along the dam crest should be considered.

5.2.2 Distribution of the overtopping wave along the dam crest (Subobjective 2.2, Paper I and II)

One important feature extracted from the present study of landslides impinging perpendicular to the longitudinal axis of the reservoir is the uneven distribution of the overtopping volume over the dam crest. Eqs. (4) and (5) provide the total volume of water overtopping the dam. However, from a dam safety perspective the distribution of this along the dam crest is of interest. This distribution can be comprehended from Figure 20.

Distribution of the overtopping wave along the dam crest has not been directly included in other dam related studies referred to previously. Still, Heller et al. (2009) discuss the effect of the reservoir shape with two extreme cases. Firstly, a long narrow reservoir and a slide that impacts longitudinally into this reservoir. Secondly, a wide reservoir into which a slide mass can impact at any possible location. In the second case the reservoir geometry is such that the impulse wave can propagate radially and freely from the slide impact zone. In 3D settings the wave parameters depend on the wave propagation angle. Thus, it is possible to consider the distribution of the overtopping wave along the dam crest, e.g. at the inner and outer flanks, by dividing the dam crest in appropriate number of sections for the calculation of wave runup and subsequent overtopping. However, the quality of the prediction would depend on the geometry of the reservoir and may be limited in the case of a landslide impinging perpendicularly to the longitudinal axis in a narrow reservoir as in the present study.

The uneven distribution of the overtopping wave in the physical model of the present study, can further be realized from the overtopping depth distribution given in Figure 24 and a plot of the maximum overtopping duration for each channel along the dam crest in Figure 25.

The maximum overtopping depth was further analyzed in Paper II (Tessema et al., 2020). For the model setup of the present study, a predictive equation for maximum overtopping depth is proposed in Paper II given herein with Eq. (7), based on slide volume, slide release height, still water depth, upstream dam slope angle, and dam height. On the basis of the analysis, both the relative slide volume and relative still water depth was found to have a significant effect on the relative overtopping depth.

A higher overtopping volume for a short duration of the overtopping yields a higher discharge over the crest. The highest overtopping occurs at CH 11 and 16 (see Figure 20), contrariwise, the smallest duration of the maximum overtopping wave is observed at these channels (see Figure 25: Box plot for the maximum overtopping duration for each channel along the dam crest (From Paper II) (model scale).

This indicates the highest maximum discharges at these sections of the dam. Conversely, for CH 13 in the middle of the dam, the duration of the wave is the longest and the overtopping volume lowest along with at CH12 and CH15. Thereby indicating that the maximum discharge will be lowest at CH 13, i.e. mid-way along the dam crest. Paper II (Tessema et al., 2020) further investigates the overtopping discharges as discussed in the next section.

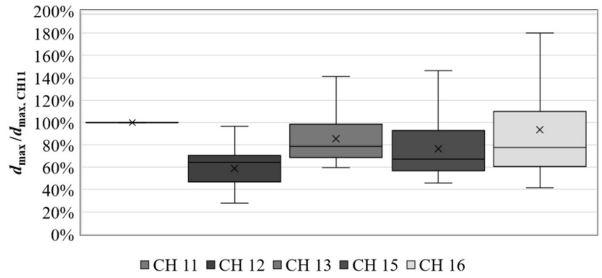

Figure 24: Box plot for overtopping depth distribution of all channels standardized with overtopping depth measured in channel 11 (From Paper II) (model scale).

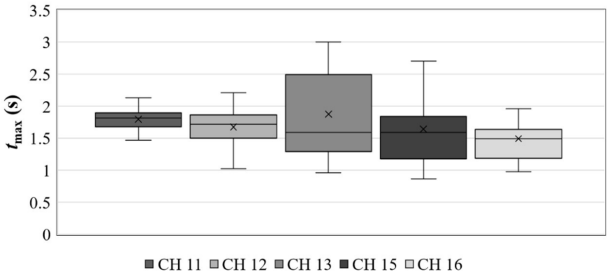

Figure 25: Box plot for the maximum overtopping duration for each channel along the dam crest (From Paper II) (model scale).

5.2.3 Prediction of the maximum overtopping discharge (Subobjective 2.3, Paper II)

Overtopping discharge is required to estimate inundation of the downstream area for risk assessment application, and emergency planning. Some previous experimental studies have considered overtopping discharge from impulse waves, and those are mostly the same studies as those mentioned earlier on the overtopping volume. The earliest is the study by Müller (1995), who provided an equation to predict the average overtopping discharge based on the run up height and overtopping volume, but this equation is limited to cases without freeboard. The most recent study, is again this by Kobel et al. (2017), from which the overtopping discharge can be calculated for cases with freeboard, using the previously discussed predictive equation for overtopping volume, in addition to a predictive equation on the duration also proposed by Kobel et al. (2017). Unlike these previous studies derived from 2D experimental setups in rectangular prismatic water wave channels with landslides impacting a reservoir in longitudinal direction, the present study considers the 3D effect relating to narrow valleys and slides impinging perpendicular to reservoir's longitudinal axis. Due to the uneven distribution of the overtopping wave for the 3D case, as discussed above, the overtopping discharge is considered for each channel along the dam crest.

Research objective 2.3 is to investigate whether it is feasible to employ the steady state weir equation to predict the overtopping discharge over a dam crest due to landslide generated waves. This is addressed in Paper II (Tessema et al., 2020) and predictive method is presented for maximum discharge, see Eq. (6), over dams having upstream slopes of 1: 1.5 and 1: 2.25 as a result of slide generated waves in the physical model of this study. The method requires prediction of the maximum overtopping depth with Eq. (7). Within the framework of this simplified approach, the predictive equation is validated by plotting the experimental discharge with the predicted one, which shows good correlation with 10 % deviation.

The present study simplifies a dynamic phenomenon with the assumption that maximum overtopping discharges of landslide generated waves can be evaluated with a formulation derived for steady state flow on a weir. However, a rapidly varied flow occurs, and inertial effects exist that are neglected with the given approach. The motivation for the simplified approach presented is to provide a simple means for rough estimation and preliminary information for cases relating to the model setup, i.e. relatively narrow mountain reservoirs.

Such estimates and preliminary information can be used in risk assessments and in planning the monitoring of the landslide geohazard with due consideration of interrelations to other hazards (see e.g. Sigtryggsdóttir et al. (2016) and Sigtryggsdóttir and Snæbjörnsson (2019)).

5.3 Run up of a landslide generated wave on the dam slopes (Objective 3)

Landslide generated waves run up on the dam slopes and only overtop the dam if the runup height is larger than the freeboard provided on the dam. The overtopping events represent extreme cases, while run-up events may be more likely to occur from smaller landslides. Thus, prediction of runup by landslide generated impulse waves need to be as accurate as possible to prevent overtopping (see e.g. Evers and Boes (2019)). In this subsection, Objective 3, described in Chapter 1 Introduction, is summarized. To address the Objective 3 and its two sub-objectives, the research outcomes from Paper III are discussed herein. This includes discussion on run up wave pattern and predictive formula for the wave runup height. The results are compared to the relevant literature as applies, in accordance with Objective 4.

5.3.1 Runup pattern along the dam crest (Objective 3.1)

Several studies are available on impulse wave runup on slopes, mainly from solitary waves. Most of the studies are on gentle slopes (Hafsteinsson et al., 2017; Pujara et al., 2015), while others have studied steep slopes (Fuchs, 2013; Hall and Watts, 1953; Synolakis, 1990). However, most of the studies are 2D experimental studies. Again, the contribution of the present study is mainly the introduction of 3D effects. The uneven overtopping pattern has previously been discussed, and similar is observed for the runup pattern.

Generally, it is seen in the present study that the wave pattern propagating throughout the reservoir and running up the slope is not uniform over the surface. The 1st wave (impact wave) runs over the dam uniformly in time throughout the whole section. The second and third waves (referred as reflected wave) comes to the right and then left edge (to the side where the slide impacts) of the dam section. The 4th one comes again to the right edge. Thus, the pattern is the same as for the overtopping cases, except that the freeboard is larger than the wave runup and thus no overtopping occurs. These runup cases were further analyzed in Paper III to arrive at a predictive equation of the runup height for freeboard considerations.

5.3.2 Prediction of landslide generated wave runup on dam slopes (Objective 3.2)

Several studies have concluded with a predictive formula for the wave runup based on experimental results, e.g. Di Risio (2005); Fuchs (2013); Hall and Watts (1953); Synolakis (1987), and Teng et al. (2000). Furthermore, Evers and Boes (2019), compiled an experimental dataset containing 359 runup heights by impulse and solitary waves, and proposed a new prediction equation for steep to vertical slopes. However, these equation base mainly on 2D experimental setups as previously mentioned. Among the studies, all runup height prediction methods are based on reservoir and dam parameters. Thus, again the main contribution of this study relates to the 3D physical model setup and prediction of run up height based on slide, reservoir and dam parameters.

A general equation for runup height prediction is presented based on the slide, wave and dam properties in Paper III, and given herein with Eq. (8). The slide parameters like slide volume W_s, upstream dam slope $tan\,\beta$, and slide Froude number F are the most dominant parameters on the runup height prediction. In general, a larger slide volume impacting a reservoir leads to higher runup height value over the dam surface. A slide having high speed which leads to high slide Froude number has higher energy which further generates a high wave which can runs up the dam slope. Moderate effect of wave amplitude and dam slope angle was observed in runup height prediction. An increase in upstream dam slope decreases the amount of water running up the dam surface by decreasing the wave energy.

A comparison is made in Paper III, and given here in Figure 23, between the runup predicted by the Eq. (8) of the present study representing the 3D case and the predictions basing on the 2D case by Hall and Watts (1953), Synolakis (1990), and Fuchs (2013), versus the measured maximum runup height values. These predictive equations from the literature have been applied to determine the runup height on the opposite shore of slide impact (in direct prolongation of the slide axis). As previously mentioned, two approaches are considered here for the comparison Approach 1 and 2. Thus, the

Figure 23 compares the measured data to predictions from studies representing 2D and 3D cases, i.e. a 2D study using solitary waves through Approach 1, versus the present 3D study of landslide impinging perpendicular to the reservoir's longitudinal axis and inducing a more

complex wave field (Figure 18). Additionally, the 3D wave effects are considered for the 2D formulation with the Approach 2 previously described in Chapter 4.

The demonstrates that the predictive equations from literature overestimates the experimental data in both cases (Approach 1 and Approach 2). This variation can be attributed to the difference between the model setup where all the studies in the literature listed were used in coastal engineering, mainly in 2D wave channels, whereas this study is targeted at defining the runup height over the dam due to the impulse waves generated by landslides in 3D settings.

In previous studies regarding runup height prediction, i.e. those of Hall and Watts (1953), Synolakis (1990), and Fuchs (2013), only wave amplitude and upstream dam slope were used as input parameters for defining run up height, however in the proposed equation from this study the slide parameters are included. Furthermore, the comparison carried out on the runup predictions in

Figure 23 relates to the Approach 1 and Approach 2, discussed before for the use of Kobels's et al (2017) comparison of predictions of overtopping volumes. The main conclusion of the comparison is that the 3D effects can be considerable in estimates of the runup heights and this is difficult to obtain from 2D experimental results. This must be considered in freeboard design of dams threatened by landslide generated waves. The uneven distribution of the landslide generated waves on narrow reservoir with the landslide impinging perpendicular to the reservoir's longitudinal axis should further be acknowledged in freeboard design.

5.4 Comparison to literature (Objective 4)

The research findings from Papers I and III were compared to the results from the literature as stated in objective 4. This has been discussed in the previous sections, Sections 5.2 and 5.3, and is only summarized within this section to give clearer overview of the comparison and the relevance of the 3D approach.

- The main findings of Paper I were to propose predictive equation for the total overtopping volume for the 3D case considered in this study. The experimental data was compared with results using the predictive equations from the present study and by Kobel et al. (2017), which presented an empirical equation for predicting the

overtopping volume for cases of 2D laboratory scale setup. Two approaches were used, where Approach 1 used the maximum wave amplitude measured closest to the landslide impact zone, whereas Approach 2 used the maximum wave amplitude measured closest to the dam. Approach 1 overestimates the measured values considerably on the average, while Approach 2 underestimates this (for details see Paper I). The predicitive equations presented in this study, Eqs. (4) and (5), gives the best prediction although overestimates the experimental data slightly on the average (see Figure 21).

Research outcome from Paper III is of significant in presenting a predictive equation for runup height over the dam due to slide generated waves (Eq. (8)). This equation was compared to the results from the predictive equations found in the literature (Fuchs, 2013; Hall and Watts, 1953; Synolakis, 1990) (Figure 23).

- Figure 23The approaches used for the comparison aligns with this of Approach 1 and 2 described above from Paper I and the use of Kobel's et al. (2017) equation. The predicted value with Hall and Watts (1953), Synolakis (1990) and Fuchs (2013) overestimated the predicted value with the present study and the experimental data considerably with both approaches (Approach 1 and 2) by a factor of 3.1 to 7.3 and 1 to 4 respectively.

The predictive equations from the literature, for the overtopping and the wave runup, are all derived from 2D experimental data, mainly using solitary waves. Approach 1 is conservative and considers that theoretically, the height of a solitary wave (and wave amplitude) does not decrease and the 2D wave may propagate over unlimited distances without any change of shape. Thus, Approach 1 assumes solitary waves. Approach 2 considers that the waves used in this study are not solitary waves, but 3D wave that decays as it propagates towards the dam at different wave propagation angles. Approach 1 is conservative, however can easily be applied, by using methods from the literature to estimate the wave amplitude in the impact zone of the landslide, such as this presented by Heller et al. (2009). Conversely, Approach 2, is more realistic as this accounts for the decay of the wave as it travels from the impact zone (see also methods presented by Heller et al. (2009) for simple estimates of the decay), however at the same time this approach may result in underestimation for the overtopping values of 3D cases as the one of the present study.

5.5 Limitation of the model setup

A major limitation of all studies on landslide induced waves overtopping dams is the lack of relevant field data and cases to calibrate physical and numerical models. This is in addition to potential scale effects in physical models, and the simplifications inherent in all modelling, including arising from potential inaccuracies of the instruments.

The experimental setup used in this study has a fixed reservoir geometry as well as a fixed landslide ramp slope and fixed distance to the slide ramp (see Table 1 and Figure 8), which limit the applicability of the results and must be considered in using the results. Only one type of slide, slide blocks chained together, are used to simulate rockslides. Furthermore, the landslide block arrangement used in the present study must be considered, as well as that the slide blocks used represent subaerial rockslides, i.e. that are released above the water surface. The dam in the model is non-erodible, but the upstream slopes represent those of an embankment dam. A constant dam height, crest length and crest width are used for the study.

5.6 Parameter limitations

Parameters with a dimension may be scaled up to a prototype with the similitude ratios. The parameter limitations in the present study are (model data),

- Still water depth 0.288 m ≤ h ≤ 0.296 m
- Slide length 0.50 m ≤ l_s ≤ 1.66 m
- Slide width 0.45 m ≤ b ≤ 0.90 m
- Slide volume 0.072 ≤ W_s ≤ 0.225 m^3
- Slide weight 15 ≤ M_s ≤ 244.7 kg
- Slide release height 0.50 m ≤ h_o ≤ 2 m
- Slide impact velocity 2.10 ≤ V_s ≤ 4.59 m/s
- Upstream dam slope $24^o \leq \beta \leq 34^o$

Dimensionless parameters are identical between a model and its prototype. The dimensionless parameter limitations are as follows:

- Overtopping volume parameter (with ε) 2.9 ≤ E_1 ≤ 14.8

- Overtopping volume parameter (without ε) $3.7 \leq E_1 \leq 17.8$
- Slide Froude number $1.25 \leq F \leq 2.66$
- Relative wave amplitude $0.18 \leq \varepsilon \leq 0.73$
- Coefficient of discharge $0.40 \leq C_d \leq 1.53$
- Runup height parameter $1.4 \leq W \leq 2.94$

5.7 Recommendation for further research

Comprehensive data for impulse wave overtopping a dam were obtained by physical laboratory modeling with a wide range of basic parameters. In addition to the current findings, the following potential objectives would add to both understanding the general process and improvement of prediction equations:

- Fixed reservoir parameters, dam height and slide ramp inclination and location are considered in this study. Having a varied value of these parameters like different dam height value, slide ramp inclination and location would widen the range of parameter and lead to a more general output from the analysis.
- Impulse waves generated by subaerial slides were considered in this study. However, partially submerged or submerged landslides may generate impulse waves which needs further investigations.
- Slide susceptible reservoirs for example considering Ethiopian dams should be identified for the existing dams and further design analysis should be made.
- The comparison of the present physical test data to results obtained by numerical modelling would be a valuable addition to the research area. Only a specific scale model of a prototype or numerical simulations may provide more precise wave data. A quick numerical hazard assessment would then be favorable in terms of time and cost, as compared to physical experiments which require the physical construction of the topography considered.
- Runup height analysis should be done in a better equipped model setup than was available for this study.

6 Answers to research questions and concluding summary

The present PhD study increases the knowledge of the impact of landslide generated waves on dams. It deals with the 3D case of a dam overtopped by waves generated as a landslide impinges the reservoir perpendicular to its longitudinal axis.

6.1 Answers to research questions

This section provides responses to the identified research questions earlier in the Introduction.

Research question R1: What wave types are generated in the physical model of the present study as the landslides of different sizes imping the reservoir?

The recorded timeseries of landslide generated waves in the present study indicate Stokes-like waves. Furthermore, investigation into selected waves revealed a ratio of wavelength to reservoir depth in the range of intermediate water waves. In addition to investigating the time series, the present study employed wave classification method available in the litterature. The classification medthod bases on wave types observed in 2D experiments, wheras the waves in this study are generated in 3D experimental setup. All datapoints for tests involving landslide comprising 2 blocks and mostly those involving 4 blocks fall in the intermediate zone defined for the 2D case for cnoidal and solitary waves. While the datapoints from tests involving the largest slides, 6 blocks, fall into the zone for Stoke-like waves, similar is observed for a few of the tests with 4 blocks. In conclusion, the answer to the research question is that the waves in all the tests conducted in the present study bear a resemblance to Stokes-like waves.

Research question R2: How is the reservoir geometry affecting the whole overtopping process?

For landslides impinging perpendicular to the longitudinal axis of the reservoir, the impulse wave propagates almost radially and freely in the longitudinal directions of the reservoir away from the slide impact zone with the highest amplitude running along the left reservoir bank resulting in an almost simultaneous but uneven distribution of the first wave when it overtops the dam crest. Subsequent overtopping results from waves that reflect as they encounter the

reservoir banks. The second wave is most pronounced at the left edge of the dam, whereas the third wave is most pronounced at the right edge of the dam. Thus, the effect of the reservoir geometry on the overtopping process can be seen through the uneven distribution of overtopping volume, overtopping depth, overtopping duration and overtopping discharge over the dam crest section. The largest values are observed at the edges of the dam crest sections.

Research question R3: Can the total overtopping volume be predicted for a specific landslide/reservoir/dam configuration to obtain rough estimates for the case considered? (In other words: How much water overtops a dam for a specific landslide/reservoir/dam configuration?)

The total overtopping volume can be predicted for cases relating to the physical model setup of the present study. For a specific landslide configuration, a predictive formula (Eqs. (4) and (5)) for calculating the total overtopping volume over the dam crest is presented in this study based on slide, reservoir and dam parameters. These parameters include slide volume, slide release height, slide Froude number, relative wave amplitude, and upstream dam slope.

Research question 4: Can the overtopping rate due to landslide generated waves over dams be reasonably predicted for rough estimates with modified steady state predictive equation?

The discharge due to landslide generated waves can be predicted, for cases relating to the physical model setup of the present study, by applying an equation of the form used for calculating a steady state discharge over a weir. Hence, the general formula for predicting the discharge over the dam crest at different locations can be expressed in terms of calibrated coefficient of discharge, dam crest width, and maximum overtopping depth. The approach simplifies a dynamic phenomenon in order to provide a simple means for rough estimation and preliminary information to use in risk assessments.

Research question 5: Do the landslide parameters, landslide volume and velocity, influence the overtopping volume, overtopping depth and overtopping rate?

The landslide volume is the most influential parameter on the overtopping volume as well as the overtopping depth and rate. A dimensional analysis and power fit regression resulted in a predictive equation for the relative overtopping volume (Eqs. (4) and (5)), that increases

linearly and most significantly with the relative landslide volume. Similar was found through the same approach to predict the maximum overtopping depth (Eq. (7)), particularly at the left edge of the dam, but less at the right edge due to the uneven distribution of the overtopping wave along the dam crest. The overtopping depth directly influences the overtopping rate.

The landslide release height is also influential, but less so than the landslide volume. The relative increase in the release height and thus the landslide speed, results in a moderate increase in the total overtopping volume. Similar relaionships was observed for the overtopping depth and overtopping rate.

Research question 6: Do the dam related parameters, upstream face slope and freeboard, influence overtopping volume, overtopping depth and overtopping rate?

The dam related parameter influences the overtopping volume, overtopping depth and overtopping rate.

The dam upstream face slope angle slightly influences the total overtopping volume in that a steeper slope results in somewhat less overtopping volume. Similarly, the dam upstream face slope angle has an impact on the maximum overtopping depth. The milder the upstream dam slope the higher the overtopping depth becomes. Furthermore, the dam slope angle has an impact on maximum overtopping rate in a way that coefficient of discharge values varies for different slope angle. The steeper the dam slope angle, the higher coefficient of discharge is observed indicating higher maximum discharge values, however here the overtopping depth is influential also and this is lower for the steeper slopes.

The freeboard of the dam influences the total overtopping volume, the overtopping depth and the overtopping rate. The total overtopping volume is somewhat smaller for larger freeboard. The dimensional analysis for predictive equation of the overtopping depth (Eq. (7)) demonstrates that the freeboard is one of the most influential parameter. Hence, larger freeboard yields smaller overtopping depth and further lower overtopping discharge over the dam crest as a result of landslide generated waves.

Research question 7: Can (be reasonable mitigated) the landslide wave hazard through freeboard design and how much freeboard is needed for a specific landslide configuration?

Dams vulnerable to landslides should preferably be designed against landslide wave hazard. This can be addressed by designing the freeboard against these waves, runup height by landslide generated waves should be accounted. However, it depends on the size of the landslide whether the mitigation through freeboard can be considered reasonable due to the associated cost. In such cases the measures taken should depend on the likelihood of the threat and the type of landslide (fast or slow). Monitoring may be the first choice of mitigation from cost perspective. The monitoring must define danger and alarm levels that trigger a predefined emergency preparedness plan, including evacuation of the downstream area.

6.2 Concluding summary

The aim of the research work forming the basis for the thesis has been to shed light on the problem of dam overtopping and runup from waves generated by landslides impinging perpendicular to a reservoir's longitudinal axis. Extensive experimental model studies and analysis were carried out as part of this doctoral study. The study identified the governing parameters to include the slide volume, landslide release height, landslide speed, slide Froude number, still water depth, and upstream slope of the dam. These variables were used to predict parameters used to describe the overtopping process of a dam i.e. overtopping volume, overtopping discharge, overtopping depth and runup height.

The following main findings result from the above descriptions:

- The landslide generated waves in all tests conducted bear a resemblance to Stokes-like waves (Tessema et al., 2019). To investigate this further, 66 data points have been plotted, with the boundaries provided from Heller and Hager (2011) observed for 2D case using granular slides. The boundaries for 2D classification method do not apply for the smaller landslides of this study, which fall in an intermediate range of cnoidal and solitary waves. However, the results support previous 3D studies from the literature (Heller and Spinneken, 2015) that have reported Stokes-like waves, as well as cnoidal waves, in the intermediate range.

- The reservoir geometry influences the wave propagation and results in wave reflection. The 3D wave propagation and reflections result in uneven water surface across the reservoir and uneven distribution of the wave running up and overtopping the dam.
- Based on the fundamental governing variables, an empirical data analysis has been conducted to arrive at equations (Eqs. (4) and (5)) predicting the total volume of water overtopping the dam (Tessema et al., 2019). The result from the analysis highlights the dominant effect of the slide volume followed by the still water depth and landslide release height whereas the effect of the upstream dam slope is small.
- For the total overtopping volume, the experimental data was compared to results using prediction formula derived for the 2D case by Kobel et al. (2017) in Paper I (Tessema et al., 2019). The comparison confirmed that the statement by (Kobel et al., 2017) their approach with a 2D solitary wave represents the extreme case, resulted in an average overestimation of the measured value by more than factor of two, i.e. when assuming a solitary wave.
- For the 3D case studied here with landslides impinging along reservoir‘s longitudinal axis, the overtopping of a dam is not uniform over the crest. On average a slightly higher volume is collected at the left side, i.e., opposite to the landslide impact zone whereas a smaller volume of water overtops the middle section of the dam crest (Tessema et al., 2019).
- An empirical equation (Eq. (7)) was presented for predicting the maximum overtopping depth based on slide volume, slide release height, still water depth, dam height, and upstream dam slope in Paper II (Tessema et al., 2020). The result highlights the dominant effect of relative slide volume and relative still water depth, which directly relates to the freeboard on the dam. Furthermore, the results bring forth the uneven distribution of the wave overtopping the dam for this 3D case with different regression coefficient for different parts (channels) of the dam crest.
- A two-step calculation procedure is presented for the overtopping discharge based on the maximum overtopping depth values with calibrated coefficients listed in Paper II (Tessema et al., 2020) (see Eq. (6)). Unlike previous studies, the maximum overtopping discharge value can be directly estimated based on the overtopping depth (can be predicted with Eq. (7)).

- A predictive equation (Eq. (8)) is presented for the runup height over the dam in Paper III. The result highlights the dominant effect of slide volume, upstream dam slope and slide Froude number, whereas the effect of wave amplitude is found to be small.
- A comparison is made between the measured runup height with the predicted one using the proposed equation from this study (Eq. (8)) and literature in Paper III. It shows that the value predicted with equations in the literature overestimates the measured value and the predicted value presented in this study.

The above-mentioned research outcome are further intended at facilitating risk assessment, emergency preparedness as well as freeboard design for reservoir and dam cases relating to the physical model setup of this study, i.e. with the landslide impinging into a narrow reservoir perpendicular to the reservoir's longitudinal axis. The most important feature extracted regarding the overtopping process for the 3D case in general is the variation in time and space resulting in uneven distributions of the volumes of water overtopping the dam cest. This observation was made possible by the 3D model setup and is of value for dam safety considerations for dams on reservoirs in regions of landslide hazards.

References

Abebe, B., Dramis, F., Fubelli, G., Umer, M., and Asrat, A. (2010). Landslides in the Ethiopian highlands and the Rift margins. Journal of African Earth Sciences *56*, 131–138.

Ataie-Ashtiani, B., and Nik-Khah, A. (2008). Impulsive waves caused by subaerial landslides. Environ Fluid Mech *8*, 263–280.

Ayalew, L. (1999). The effect of seasonal rainfall on landslides in the highlands of Ethiopia. Bull Eng Geol Env *58*, 9–19.

Ayele, A. (1995). Earthquake Catalogue of the Horn of Africa for the Period 1960-1993 (Seismological Department).

Bellotti, G., and Romano, A. (2017). Wavenumber-frequency analysis of landslide-generated tsunamis at a conical island. Part II: EOF and modal analysis. Coastal Engineering *128*, 84–91.

Biedermann, J. (2017). Overtopping of embankment dams from landslide generated waves.

Bjerrum, L., Jørstad, F.A., and Jørstad, F.A. (1968). Stability of rock slopes in Norway (Oslo: Norges geotekniske institutt).

Blikra, L.H., Longva, O., Braathen, A., Anda, E., Dehls, J.F., and Stalsberg, K. (2006). Rock slope failures in Norwegian fjord areas: Examples, spatial distribution and temporal pattern. In Landslides from Massive Rock Slope Failure, S.G. Evans, G.S. Mugnozza, A. Strom, and R.L. Hermanns, eds. (Dordrecht: Springer Netherlands), pp. 475–496.

Bosa, S., and Petti, M. (2011). Shallow water numerical model of the wave generated by the Vajont landslide. Environmental Modelling & Software *26*, 406–418.

Braathen, A., Blikra, L.H., Berg, S.S., and Karlsen, F. (2004). Rock-slope failures in Norway; type, geometry, deformation mechanisms and stability. Norwegian Journal of Geology *84*, 67–88.

Briggs, M.J., Synolakis, C.E., Harkins, G.S., and Green, D.R. (1995). Laboratory experiments of tsunami runup on a circular island. Pure and Applied Geophysics *144*, 569–593.

Broothaerts, N., Kissi, E., Poesen, J., Van Rompaey, A., Getahun, K., Van Ranst, E., and Diels, J. (2012). Spatial patterns, causes and consequences of landslides in the Gilgel Gibe catchment, SW Ethiopia. CATENA *97*, 127–136.

Carrier, G.F., Wu, T.T., and Yeh, H. (2003). Tsunami run-up and draw-down on a plane beach. Journal of Fluid Mechanics *475*, 79–99.

Dave, P. (2018). Hidroituango: another landslide crisis at a hydroelectric dam - The Landslide Blog - AGU Blogosphere.

De Girolamo, P., Di Risio, M., Romano, A., and Molfetta, M.G. (2014). Landslide Tsunami: Physical Modeling for the Implementation of Tsunami Early Warning Systems in the Mediterranean Sea. Procedia Engineering *70*, 429–438.

Di Risio, M. (2005). Landslide generated impulsive waves: Generation, propagation and interaction with plane slopes - An experimental and analytical study.

Di Risio, M., and Sammarco, P. (2008). Analytical Modeling of Landslide-Generated Waves. Journal of Waterway, Port, Coastal, and Ocean Engineering *134*, 53–60.

Di Risio, M., De Girolamo, P., Bellotti, G., Panizzo, A., Aristodemo, F., Molfetta, M.G., and Petrillo, A.F. (2009). Landslide-generated tsunamis runup at the coast of a conical island: New physical model experiments. Journal of Geophysical Research: Oceans *114*.

Dodd Nicholas (1998). Numerical Model of Wave Run-Up, Overtopping, and Regeneration. Journal of Waterway, Port, Coastal, and Ocean Engineering *124*, 73–81.

Enet, F., and Grilli, S.T. (2007). Experimental Study of Tsunami Generation by Three-Dimensional Rigid Underwater Landslides. p.

Evers, F. (2017). Spatial Propagation of Landslide Generated Impulse Waves. Doctoral Thesis. ETH Zurich.

Evers, F., and Boes, R.M. (2019). Impulse Wave Runup on Steep to Vertical Slopes. Journal of Marine Science and Engineering *7*, 8.

Fritz, H. (2002). PIV applied to landslide generated impulse waves. pp. 305–320.

Fritz, H.M., Hager, W.H., and Minor, H.-E. (2003a). Landslide generated impulse waves. 2. Hydrodynamic impact craters. Exp Fluids *35*, 520–532.

Fritz, H.M., Hager, W.H., and Minor, H.E. (2003b). Landslide generated impulse waves.1. instataneous flow fields. Experiments in Fluids *35*, 505–519.

Fritz, H.M., Hager, W.H., and Minor, H.-E. (2004). Near Field Characteristics of Landslide Generated Impulse Waves. Journal of Waterway, Port, Coastal, and Ocean Engineering *130*, 287–302.

Fritz, H.M., Mohammed, F., and Yoo, J. (2009). Lituya Bay Landslide Impact Generated Mega-Tsunami 50th Anniversary. In Tsunami Science Four Years after the 2004 Indian Ocean Tsunami: Part II: Observation and Data Analysis, P.R. Cummins, K. Satake, and L.S.L. Kong, eds. (Basel: Birkhäuser Basel), pp. 153–175.

Fuchs, H. (2013). Solitary impulse wave run-up and overland flow. Doctoral Thesis. ETH Zurich.

Gedik, N., Irtem, E., and Kabdasli, S. (2005). Laboratory investigation on tsunami run-up. Ocean Engineering *32*, 513–528.

Glade, T., and Michael J., C. (2005). The Nature of Landslide Hazard Impact -.

Gouin, P. (1979). Earthquake history of Ethiopia and the horn of Africa.

Hafsteinsson, H.J., Evers, F.M., and Hager, W.H. (2017). Solitary wave run-up: wave breaking and bore propagation. Journal of Hydraulic Research *55*, 787–798.

Hailemariam Gugsa, T., and Schneider, J.F. (2010). Rock Mass Classification of Karstic Terrain in the Reservoir Slopes of Tekeze Hydropower Project. p. 831.

Hall and Watts (1953). Laboratory investigation of the vertical rise of solitary waves on impermeable slopes.

Heller, V. (2007). Landslide generated impulse waves - Prediction of near field characteristics. ETH/VAW 177.

Heller, V., and Hager, W. (2014). A Universal Parameter to Predict Subaerial Landslide Tsunamis? Journal of Marine Science and Engineering *2*, 400–412.

Heller, V., and Hager, W.H. (2010). Impulse Product Parameter in Landslide Generated Impulse Waves. Journal of Waterway, Port, Coastal, and Ocean Engineering *136*, 145–155.

Heller, V., and Hager, W.H. (2011). Wave types of landslide generated impulse waves. Ocean Engineering *38*, 630–640.

Heller, V., and Spinneken, J. (2013). Improved landslide-tsunami prediction: Effects of block model parameters and slide model. Journal of Geophysical Research: Oceans *118*, 1489–1507.

Heller, V., and Spinneken, J. (2015). On the effect of the water body geometry on landslide–tsunamis: Physical insight from laboratory tests and 2D to 3D wave parameter transformation. Coastal Engineering *104*, 113–134.

Heller, V., Hager, W.H., and Minor, H.-E. (2008). Scale effects in subaerial landslide generated impulse waves. Exp Fluids *44*, 691–703.

Heller, V., Hager, W.H., and Minor, H.-E. (2009). Landslide Generated Impulse Waves in Reservoirs: Basics and Computation (ETH Zürich).

Hibberd, S., and Peregrine, D.H. (1979). Surf and run-up on a beach: a uniform bore. Journal of Fluid Mechanics *95*, 323–345.

Hiller, P.H., Lia, L., and Aberle, J. (2018). Field and model tests of riprap on steep slopes exposed to overtopping. Journal of Applied Water Engineering and Research *0*, 1–15.

Huber, A. (1980). Schwallwellen in Seen als Folge von Felsstürzen.

Huber, A. (1982). Impulse waves in Swiss lakes as a result of rock avalanches and bank slides, Experimental results for the prediction of the characteristic numbers of these waves. Trans. 14th Int. Congress Large Dams *3*, 455–476.

Huber, A., and Hager, W.H. (1997). Forecasting impulse waves in reservoirs. Proc. 19th Congrès Des Grands Barrages 993–1005.

Huber, L.E., Evers, F.M., and Hager, W.H. (2017). Solitary wave overtopping at granular dams. Journal of Hydraulic Research *55*, 799–812.

Hungr, O. (2007). Dynamics of Rapid Landslides. In Progress in Landslide Science, K. Sassa, H. Fukuoka, F. Wang, and G. Wang, eds. (Berlin, Heidelberg: Springer), pp. 47–57.

ICOLD (1995). Dam failures statistical analysis. In International Commision on Large Dams (ICOLD), p. Bulletin 99.

International Rivers (2009). Tekeze Dam, Ethiopia.

John, S.R. (1845). Report on Waves: Made to the Meetings of the British Association in 1842-43.

Kamphuis, J.W., and Bowering, R.J. (1970). Impulse waves generated by landslides. Coastal Engineering Proceedings *1*.

Kobel, J., Evers, F.M., and Hager, W.H. (2017). Impulse Wave Overtopping at Rigid Dam Structures. Journal of Hydraulic Engineering *143*, 04017002.

Li, G., Chen, G., Li, P., and Jing, H. (2019). Efficient and Accurate 3-D Numerical Modelling of Landslide Tsunami. Water *11*, 2033.

Lindstrøm, E.K., Pedersen, G.K., Jensen, A., and Glimsdal, S. (2014). Experiments on slide generated waves in a 1:500 scale fjord model. Coastal Engineering *92*, 12–23.

Liu, P.L.-F., Wu, T.-R., Raichlen, F., Synolakis, C.E., and Borrero, J.C. (2005). Runup and rundown generated by three-dimensional sliding masses. Journal of Fluid Mechanics *536*, 107–144.

L.Law, and A. Brebner (1968). Proceedings of the third Australasian Conference on Hydraulics and Fluid Mechanics, Sydney, 25-29 November, 1968. (Sydney, Australia: Sydney : Institution of Engineers, Australia), p.

Løvholt, F., Glimsdal, S., Lynett, P., and Pedersen, G. (2015). Simulating tsunami propagation in fjords with long-wave models. Natural Hazards and Earth System Sciences *15*, 657–669.

Manenti, S., Amicarelli, A., and Todeschini, S. (2018). WCSPH with Limiting Viscosity for Modeling Landslide Hazard at the Slopes of Artificial Reservoir. Water *10*, 515.

Manenti, S., Wang, D., Domínguez, J.M., Li, S., Amicarelli, A., and Albano, R. (2019). SPH Modeling of Water-Related Natural Hazards. Water *11*, 1875.

Manenti S., Pierobon E., Gallati M., Sibilla S., D'Alpaos L., Macchi E., and Todeschini S. (2016). Vajont Disaster: Smoothed Particle Hydrodynamics Modeling of the Postevent 2D Experiments. Journal of Hydraulic Engineering *142*, 05015007.

McFall, B.C., and Fritz, H.M. (2016). Physical modelling of tsunamis generated by three-dimensional deformable granular landslides on planar and conical island slopes. Proc. Math. Phys. Eng. Sci. *472*, 20160052.

van der Meer, J., Pullen, T., Allsop, W., Bruce, T., Schüttrumpf, H., and Kortenhaus, A. (2009). Prediction of Overtopping. In Handbook of Coastal and Ocean Engineering, pp. 341–382.

Mehaute, B.L. (1976). An Introduction to Hydrodynamics and Water Waves (Berlin Heidelberg: Springer-Verlag).

Miller, D.J. (1960). Giant Waves in Lituya Bay Alaska. Geological Survey Professional Paper 48.

Mohammed, F., and Fritz, H.M. (2012). Physical modeling of tsunamis generated by three-dimensional deformable granular landslides: Landslide generated tsunamis. Journal of Geophysical Research: Oceans *117*, n/a-n/a.

Mortensen, R., Lia, L., Hammeren, R., Glimsdal, S., Harbitz, C.B., and Belete, K. wassihun (2016). Overtopping of rockfill dams from landslide generated waves. (Turkey: Trcold), p.

Mueller, L. (1968). New considerations of the Vaiont slide. Rock Mechanics & Engineering Geology.

Müller, D.R. (1995). Auflaufen und Überschwappen von Impulswellen an Talsperren (ETH Zürich).

Noda, E. (1970). Water waves generated by landslides. Journal of the Waterways, Harbors and Coastal Engineering Division *96*, 835–855.

NVE (2012). Veileder for fyllingsdammer.

Øvregård, E., and Lia, L. (2018). Skred i magasin - overtopping av fyllingsdam fra skredgenererte bølger i magasin (NVE).

Panizzo, A., de Girolamo, P., and Petaccia, A. (2005a). Forecasting impulse waves generated by subaerial landslides. Journal of Geophysical Research (Oceans) *110*, C12025.

Panizzo, A., de Girolamo, P., di Risio, M., Maistri, A., and Petaccia, A. (2005b). Great landslide events in Italian artificial reservoirs. Natural Hazards and Earth System Sciences *5*, 733–740.

ponziani, L., and Gardoni, M. (2017). Landslide generated waves in dam reservoirs - Experimental investigation on a physical hydraulic model. Masters thesis. NTNU.

Pujara, N., Liu, P.L.-F., and Yeh, H. (2015). The swash of solitary waves on a plane beach: flow evolution, bed shear stress and run-up. Journal of Fluid Mechanics *779*, 556–597.

Pullen, T., Allsop, N.W.H., Bruce, T., Kortenhaus, A., Schüttrumpf, H., and van der Meer, J.W. (2007). EurOtop wave overtopping of sea defences and related structures: assessment manual. Die Küste.

Romano, A., Di Risio, M., Bellotti, G., Molfetta, M.G., Damiani, L., and De Girolamo, P. (2016). Tsunamis generated by landslides at the coast of conical islands: experimental benchmark dataset for mathematical model validation. Landslides *13*, 1379–1393.

Romstad, B., Harbitz, C.B., and Domaas, U. (2009). A GIS method for assessment of rock slide tsunami hazard in Norwegian lakes and reservoirs. Natural Hazards and Earth System Sciences *9*, 353–364.

Sælevik, G., Jensen, A., and Pedersen, G. (2009). Experimental investigation of impact generated tsunami; related to a potential rock slide, Western Norway. Coastal Engineering *56*, 897–906.

Sigtryggsdottir, F.G. (2017). Landslides into Reservoirs. Overtopping of Embankmnet Dams (NTNU).

Sigtryggsdóttir, F.G., and Snæbjörnsson, J.T. (2019). Geological challenges and geohazard monitoring of a mega engineering hydropower project in Iceland. Engineering Geology *259*, 105152.

Sigtryggsdóttir, F.G., Snæbjörnsson, J.T., Grande, L., and Sigbjörnsson, R. (2016). Interrelations in multi-source geohazard monitoring for safety management of infrastructure systems. Structure and Infrastructure Engineering *12*, 327–355.

Slingerland, R.L., and Voight, B. (1979). Occurrences, Properties, and Predictive Models of Landslide-Generated Water Waves. In Developments in Geotechnical Engineering, B. Voight, ed. (Elsevier), pp. 317–394.

Synolakis, C. (1990). Generation of Long Waves in Laboratory. Journal of Waterway Port Coastal and Ocean Engineering-Asce -ASCE *116*.

Synolakis, C.E. (1987). The runup of solitary waves. Journal of Fluid Mechanics *185*, 523–545.

Temesgen, B., Mohammed, M.U., and Korme, T. (2001). Natural hazard assessment using GIS and remote sensing methods, with particular reference to the landslides in the Wondogenet Area, Ethiopia. Physics and Chemistry of the Earth, Part C: Solar, Terrestrial & Planetary Science *26*, 665–675.

Teng, M.H., Feng, K., and Liao, T.I. (2000). Experimental study on long wave run-up on plane beaches. (International Society of Offshore and Polar Engineers), p.

Tessema, N.N., Sigtryggsdóttir, F.G., Lia, L., and Jabir, A.K. (2019). Case Study of Dam Overtopping from Waves Generated by Landslides Impinging Perpendicular to a Reservoir's Longitudinal Axis. JMSE *7*, 221.

Tessema, N.N., Sigtryggsdóttir, F.G., Lia, L., and Jabir, A.K. (2020). Physical Model Study on Discharge over a Dam Due to Landslide Generated Waves. Water *12*, 234.

Titov, V.V., and Synolakis, C.E. (1998). Numerical Modeling of Tidal Wave Runup. Journal of Waterway, Port, Coastal, and Ocean Engineering *124*, 157–171.

USBR (1981). Freeboard criteria and guidelines for computing freeboard allowances for storage dams (Denver, Colorado. : U.S. Dept. of the Interior, Bureau of Reclamation).

Vacondio, R., Mignosa, P., and Pagani, S. (2013). 3D SPH numerical simulation of the wave generated by the Vajont rockslide. Advances in Water Resources *59*, 146–156.

Walder, J.S., Watts, P., Sorensen, O.E., and Janssen, K. (2003). Tsunamis generated by subaerial mass flows. Journal of Geophysical Research: Solid Earth *108*.

Watts, P. (1997). Water waves generated by underwater landslides. phd. California Institute of Technology.

Watts, P. (2000). Tsunami Features of Solid Block Underwater Landslides. Journal of Waterway, Port, Coastal, and Ocean Engineering *126*, 144–152.

Wiegel, R.L. (1955). Laboratory studies of gravity waves generated by the movement of a submerged body. Transactions, American Geophysical Union *36*, 759.

Wiegel, R.L., Noda, E.K., Kuba, E.M., Gee, D.M., and Tornberg, G.F. (1970). Water Waves Generated by Landslides in Reservoirs. Journal of the Waterways, Harbors and Coastal Engineering Division *96*, 307–333.

Woldearegay, K. (2013). Review of the occurrences and influencing factors of landslides in the highlands of Ethiopia: With implications for infrastructural development. Momona Ethiopian Journal of Science *5*, 3-31–31.

Xiao, H., and Lin, P. (2016). Numerical Simulation of Dam Overtopping Events Caused by the Landslide Generated Impulse Waves in Mountainous Reservoirs. 4.

Yarde, A.J., Banyard, L.S., and WHAIIsop, N. (1996). Reservoir dams: wave conditions, wave overtopping and slab protection.

Ying, L., and Fredric, R. (2001). Solitary wave runup on plane slopes. Journal of Waterway, Port, Coastal, and Ocean Engineering *127*, 33–44.

Zelt, J.A. (1991). The run-up of nonbreaking and breaking solitary waves. Coastal Engineering *15*, 205–246.

Zweifel, A. (2010). Impulswellen: Effekte der Rutschdichte und der Wassertiefe (GRIN Verlag).

Zweifel, A., Willi H., H., and Hans-Erwin, M. (2006). Plane Impulse Waves in Reservoirs. Journal of Waterway, Port, Coastal, and Ocean Engineering *132*.

MarcelloDi Risio, GiorgioBellotti, AndreaPanizzo, and PaoloDe Girolamo (2009). Three-dimensional experiments on landslide generated waves at a sloping coast - Dimensions. Coastal Engineering *56*, 659–671.

Paper I

Dam overtopping from waves generated by landslides impinging perpendicular to a reservoir's longitudinal axis

Netsanet Nigatu, Fjola G. Sigtryggsdottir, Leif Lia, Asie Kemal

Journal of Marine Science and Engineering, 2019,7,221; doi:10.3390/jmse7070221 (Open Access)

Journal of
Marine Science and Engineering

MDPI

Article

Case Study of Dam Overtopping from Waves Generated by Landslides Impinging Perpendicular to a Reservoir's Longitudinal Axis

Netsanet Nigatu Tessema [1,*], Fjóla G. Sigtryggsdóttir [2], Leif Lia [2] and Asie Kemal Jabir [1]

[1] School of Civil and Environmental Engineering, Addis Ababa Institute of Technology, P. O. Box 385, Addis Ababa 1000, Ethiopia
[2] Department of Civil and Environmental Engineering, Norwegian University of Science and Technology, 7491 Trondheim, Norway
* Correspondence: Netsanet.nigatu@aait.edu.et; Tel.: +251-913-77-15-74

Received: 29 May 2019; Accepted: 25 June 2019; Published: 15 July 2019

Abstract: Landslide-generated impulse waves in dammed reservoirs run up the reservoir banks as well as the upstream dam slope. If large enough, the waves may overtop and even breach the dam and cause flooding of the downstream area with hazardous consequences. Hence, for reservoirs in landslide-prone areas, it is important to provide a means to estimate the potential size of an event triggered by landslides along the reservoir banks. This research deals with landslide-generated waves and the overtopping process over the dam crest in a three-dimensional (3D) physical model test, presenting a case study. The model set-up describes the landslide impacting the reservoir in a perpendicular manner, which is often the case in natural settings. Based on the experimental results, dimensionless empirical relations are derived between the overtopping volume and the governing parameters, namely the slide volume, slide release height, slide impact velocity, still-water depth, and upstream dam face slope. Predictive relations for the overtopping volume are presented as applicable for cases relating to the specific model set-up. Measured overtopping volumes are further compared to a two-dimensional (2D) case reported in the literature. An important feature regarding the overtopping process for the 3D case is the variation in time and space, resulting in an uneven distribution of the volume of water overtopping the dam crest. This observation is made possible by the 3D model set-up, and is of value for dam safety considerations as well as for foundation-related issues, including erosion and scouring.

Keywords: landslide-generated wave; dam overtopping; physical model; overtopping volume; impulse wave

1. Introduction

Dam sites suitable for impounding of a reservoir are often found in mountainous regions or highlands, often in narrow valleys or canyons (see Figure 1). Mountain slopes are generally susceptible for landslides, including rockslides. There are infamous cases of a landslide impinging reservoirs, in turn generating impulse waves overtopping the dam with catastrophic consequences downstream. This includes the Vajont dam tragedy in 1963 where nearly 2000 fatalities occurred [1]. The general process describing such events has been grouped into three phases [2]: (1) slide impact with wave generation; (2) wave propagation with wave transformation; and (3) run-up of the impulse wave and overtopping of a dam (see Figure 2). However, a dam is not overtopped if the wave run-up height is lower than the freeboard f, the elevation difference between the dam crest, and the reservoir still-water level, when the landslide impinges. Still, mountainous slopes surrounding a dam reservoir poses a threat to dam safety. Consequently, a mean of estimating the associated hazard from landslide waves

overtopping a dam is of importance. In such an evaluation, the reservoir settings, such as the geology and topography, are important. The shape of a reservoir in a narrow mountain valley is usually longer than its width (see Figure 1), and thus with a potential landslide threat from the mountain slopes along the length of the reservoir. In other words, a potential landslide may fall from these mountain slopes, i.e., approximately perpendicular to the reservoir's longitudinal axis (see e.g., Figure 2b).

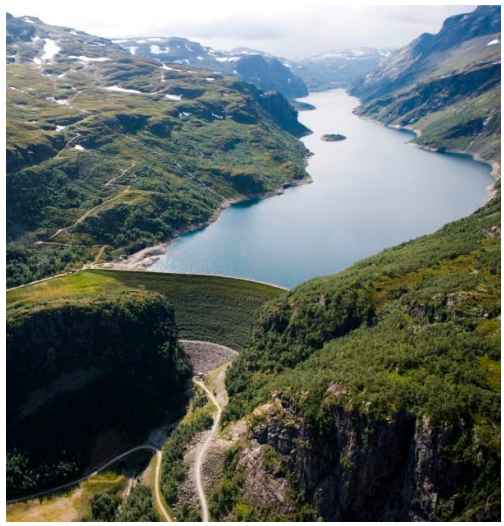

Figure 1. Mountain reservoir in Aurland Municipally Norway (Photo from E-CO Energi / Aerosport, with permission, 2019).

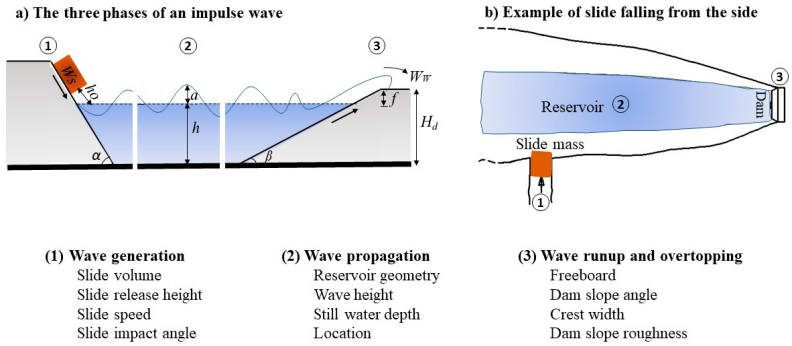

Figure 2. The three phases of landslide-generated waves with the relevant parameters for this study: (1) slide impact with wave generation; (2) wave propagation; and (3) wave run-up and overtopping of a dam; (**a**) a section showing the three phases based on Heller et al. [2]; (**b**) an example plan view of a reservoir.

Numerous experimental and numerical studies on landslide-generated waves (Phase 1 in Figure 2) are available. Many of those were conducted in flumes to investigate two-dimensional (2D) properties [3–7], while other studies [8–17] investigated the three-dimensional (3D) effects of landslide-generated tsunamis by considering wide reservoirs (3D water bodies) [11,16,17], as well as several geometries such as planar beaches and islands [8,12–14]. Those studies include landslides

modeled with granular and cobble material, and investigation into the effect of different landslide parameters such as landslide geometry and energy, on the wave generated. One recent relevant study is that of Evers [16], who investigated, for example, the effect of slide impact velocity, slide mass, slide impact angle, slide width, and still-water depth in 2D and 3D models. Evers [16] found that for the same slide mass (volume) the wave generation is influenced by the landslide geometry, with a wider landslide generating larger waves. Furthermore, he found that the initial wave amplitude and shape are influenced by the slide impact angle. These findings are mentioned here since in the current study the geometry of the slide is not directly considered in the formulations provided, and the slide impact angle is constant.

Only a few studies consider dam overtopping (Phase 3 in Figure 2) and include formulas for the overtopping volume based on wave and dam parameters. These studies are mainly those of Huber et al. [17] in the case of an erodible granular dam model, and Kobel et al. [18] as well as Müller [19] in the case of a solid, non-erodible dam model. The resulting formula for the overtopping volume is based on (2D) experimental tests. Kobel et al. [18] used rectangular prismatic water wave channels with solitary waves propagating directly towards a dam (set-up similar to shown in Figure 3b), thereby simulating waves generated by a landslide impinging from one end of the reservoir directly towards the dam. Kobel et al. [18] point out that the solitary wave type represents an extreme case.

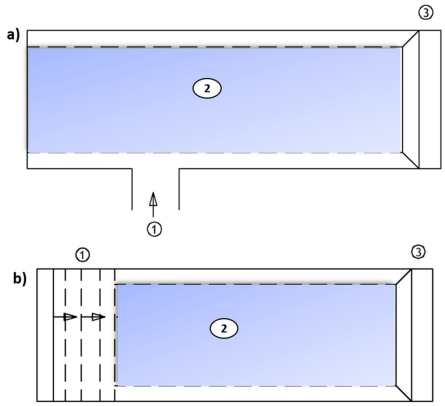

Figure 3. General layout of slide impact into a reservoir: 1 is the slide impact zone, 2 is the wave propagation zone and 3 the wave run-up and dam overtopping zone for (**a**) slide impacting from the side of a gorge; (**b**) solitary wave generated moving directly towards the dam's upstream face.

Depending on the geometry of a particular reservoir, the wave parameters can be computed with a 3D or 2D approach (e.g., [11,16]) and fed into a 2D run-up equation, such as provided by Kobel et al. [18], to obtain an estimate of the volume of water overtopping a dam. Heller et al. [2] discuss the effect of the reservoir shape with two extreme cases. The first case considers a long reservoir and a slide that impacts longitudinally into this reservoir. The second case considers that a slide mass can impact at any possible location into the reservoir and the slide width is less than the reservoir width. In the second case the reservoir geometry is such that the impulse wave can propagate radially and freely from the slide impact zone. In 3D settings the wave parameters depend on the wave propagation angle. The distribution of the overtopping wave along the dam crest, e.g., at the inner and outer flanks (see e.g., [2]), can be considered by dividing the dam crest in appropriate number of sections for the calculation of wave run-up and subsequent overtopping. However, the quality of the prediction would depend on the geometry of the reservoir and may be limited in the case of a very narrow reservoir as in the present study.

The above-mentioned studies do not directly investigate the 3D effect relating to narrow valleys and a landslide falling into a narrow dammed reservoir perpendicular to the reservoir's longitudinal axis, i.e., setups related to this shown in Figure 3a. Thus, further studies are required to investigate directly dammed reservoirs in narrow valleys with mountain slopes prone to landslide impinging perpendicular to the longitudinal axis of the reservoir (Figure 3a). The current study aims at shedding light on the mentioned 3D effect; however, application of the results must consider the limitations of the model set-up of this case study, as later described.

The current study continues an experimental study program initiated in 2014 with focus on landslide-generated waves resulting from lateral slides into a narrow reservoir, as well as the effect of different dam related parameters on wave overtopping. The study uses a 3D physical model that was extracted and modified from a model used by Lindstrøm et al. [20], to study rockslide generated waves into fjords. The same slide blocks are used as in Lindstrøm et al. [20], i.e., essentially modeling rockslides. Other researchers have studied landslide-generated impulse waves using granular deformable slides, e.g., Fritz et al. [21,22] used a 2D physical model and Mohammed and Fritz [23] used a 3D tsunami wave basin. Furthermore, there are studies available, e.g., Ataie-Ashtiani and Nik-Khah [7], Zweifel [24] and Heller and Spinneken [25], comparing the waves generated by granular and block slides. The findings of Zweifel [24] and Ataie-Ashtiani and Nik-Khah [7] was that rigid blocks (as in the present study), result in more extreme waves compared to granular slides. However, Heller and Spinneken [25] revealed that block slides can generate not only larger waves in a wave channel, but also identical or smaller waves than granular slides, depending on certain parameters or features. The identified influential parameters in this regard were the ratio of the slide width to the channel width, the slide front angle and the slope transition from the inclined landslide ramp used in the tests to the horizontal channel bottom. They explain the discrepancy from the previous studies that these parameters were not varied, and their effect thus not recognized.

The main objective of this article is to use the experimental data from the 3D laboratory scale test set-up to propose a formula for estimating the total volume of water overtopping a dam from impulse waves generated by a landslide impinging perpendicular to the reservoir longitudinal axis as shown in Figure 3a. An important part of this objective is to investigate the distribution of the overtopping volume along the dam crest, a feature that can, as described above, only be obtained indirectly through 2D modeling of previous studies essentially using experimental setups relating to that shown in Figure 3b. The experimental set-up of the present study has a fixed reservoir geometry as well as a fixed landslide ramp slope and location, which must be considered in the application of the results. The formula derived is dependent on both the landslide and dam parameters. The dam parameters considered, for the upstream slope and freeboard, relate e.g., to those relevant for embankment dams. However, the dam model used is non-erodible as in the case of Kobel et al. [18]. Considering this, an important further objective of this study is to compare, the overtopping volume measured in this study to predictions based on the formula of Kobel et al. [18].

In the following, the experimental set-up, instrumentation, and test program is outlined, followed by a description of the wave propagation and overtopping process. The experimental data is analyzed to obtain a formula for predicting the overtopping volume based on the landslide and dam parameters. The formula is obtained with data regression analysis resulting from test runs with systematic variation of slide, basin, and dam parameters such as the slide volume, slide release height, slide speed, wave amplitude and upstream dam face slope for cases with freeboard $f > 0$. Following this, the distribution of the overtopping along the dam crest is extracted. Finally, the measured overtopping volumes are compared to results using the prediction formula proposed by Kobel et al. [18]. The analysis chapter is supported with discussions on the limitations of the study and the results. Finally, the main conclusions are stated.

2. Methodology

2.1. Experimental Set-up

The main structural components of the physical model were: (i) a slide ramp on which slide blocks are released; (ii) the basin representing the reservoir; and (iii) an embankment dam (non-erodible) (Figure 4).

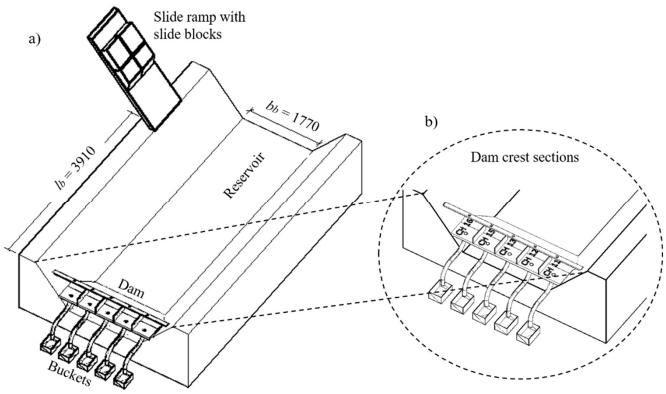

Figure 4. (**a**) Experimental set-up with the main components; slide, reservoir, dam and (**b**) ultrasonic sensors used for measuring the run-up height and buckets for collecting the overtopping water. The wave gauges, which were installed in the reservoir, are not shown on this figure.

The slide was modeled with blocks (see Figure 5) placed on a 2 m long slide ramp inclined at a constant angle of $\alpha = 50°$, where it was possible to place rectangular blocks of different sizes and arrangements. This model represents a reservoir in a narrow valley formed by steep rock mountain slopes. Furthermore, the slide ramp was modeled as a natural extension of the sides of the model reservoir. The inclination of the slide ramp mainly affects the slide speed, along with the friction between the ramp and the blocks. The friction resistance was represented with a friction angle of about 25°. In this study, the slide speed was varied by using different slide release heights. The shapes and sizes of the blocks used in the experiments are shown in Figure 5. Different slide block arrangements were made for each test set-up. For each arrangement the blocks, impinging the water first, were tapered at an angle of 45° at the front to simulate a slide that has a smaller front and a larger body [26]. The slide blocks were attached to each other with chains, the sliding body was then attached to a steel panel with a hook. When the hook was removed, the blocks slid into the reservoir generating impulsive waves.

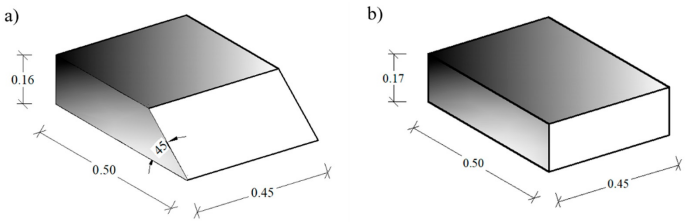

Figure 5. Rigid blocks used to model the landslide (measurement in m): (**a**) trapezoidal solid; (**b**) rectangular solid.

The reservoir was modeled with a fixed trapezoidal basin with sidewalls of water-resistant plywood covered with concrete paste to increase the roughness. It was 4.5 m long, 1.7 m wide at the bottom and 2.2 m at dam crest level, with a total reservoir capacity of 2.5 m^3. The model dam was placed at one end of the reservoir with a constant height of H_d = 0.32 m. The model was conceptual and a scale of 1:190 has been selected relative to prototype, considering that this results in a moderate height of the prototype dam (60.8 m) and a range of landslide volumes from the blocks, representing medium sized slides (0.2 to 1 million m^3) to large slides (1 to 5 million m^3). At this scale (1:190) the model represents an 860 m long reservoir, 320 m wide at the bottom with a reservoir capacity of 17 Mm^3.

Dams with upstream slopes of 1:1.5, 1:2 and 1:2.25 were used for the analysis representing embankment dams. The dam crest was divided into five different sections (labeled Channels (CH) 11 to 16 in Figure 4b) to measure the distribution of the overtopping volumes along the crest. The corresponding overtopping volume for each dam section was collected in five buckets with pipes of 100 mm diameter (see Figure 4b).

2.2. Instrumentation

Nine wave gauges of type '*DHI wave-meter 102E*' were placed at the surface of the trapezoidal basin to measure the wave height at different locations. The principle of this wave meter is to measure the conductivity between two parallel electrodes partly immersed in water. In addition, there were five ultrasonic sensors *(mic+35/IU/TC)* placed at the top of each dam section to measure the height of the water that overtopped the dam crest (see Figure 6). The water that overtopped the dam was collected in five calibrated buckets and recorded manually with an ultrasonic sensor. The initial level of each bucket was measured before the test and the water level rise after the test. The measurement was multiplied by a calibration factor to obtain the overtopping volume.

To measure the speed of the slide block, a rotational sensor (CH 10) was placed at the side of the slide ramp. It was connected to the rigid sliding blocks through a hook with a rope which unrolled together with the distance covered by the slide. A voltmeter recorded the voltage as the block slid down the ramp and the rope unrolled. A calibration factor was required to change the measured voltage into the distance covered by the slide. Then a time variable distance was used to extract the slide impact velocity considering the impact velocity is the maximum.

The data from the wave gauges, ultrasonic sensors and rotational sensors were collected in '*Agilent Measuring Manager program*' with a sampling rate of 200 Hz.

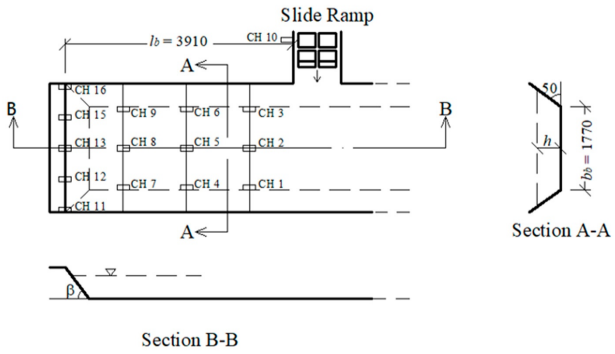

Figure 6. Planar view of sensors placement in the model set-up (measurements in mm).

2.3. Test Program

The overtopping of the dam by landslide-generated waves was investigated with parameters such as the landslide volume W_S, landslide release height h_O, landslide speed v_S, upstream dam slope

β and freeboard f. These parameters represent the input variables of the study provided as shown in Table 1. Four different types of block arrangements (2H, 2V, 4 and 6) with different length, width, and volume were used in the model as shown in Table 2 (Figure 7).

Table 1. Test program.

Scale	β (V:H)	f (m)	W_S (m^3)	h_O (m)
Model (1:190)	1: 2.25	0.024, 0.032	0.072, 0.074, 0.149, 0.225	0.5, 1, 1.5, 2
	1: 2	0.024, 0.032	0.072, 0.074, 0.149, 0.225	0.5, 1, 1.5, 2
	1: 1.5	0.024, 0.032	0.072, 0.074, 0.149, 0.225	0.5, 1, 1.5, 2
Prototype	-	4.5, 6	0.49, 0.51, 1.02, 1.54 (Mm^3)	95, 190, 285, 380

Table 2. Slide block characteristics in the model set-up.

Slide Characteristics	Block Arrangement			
	2H Blocks	2V Blocks	4 Blocks	6 Blocks
Slide length l_S (m)	0.50	1.08	1.08	1.66
Slide width b (m)	0.90	0.45	0.90	0.90
Shape ratio l_S/b (-)	0.56	2.40	1.20	1.84
Slide volume W_S (m^3)	0.072	0.074	0.149	0.225

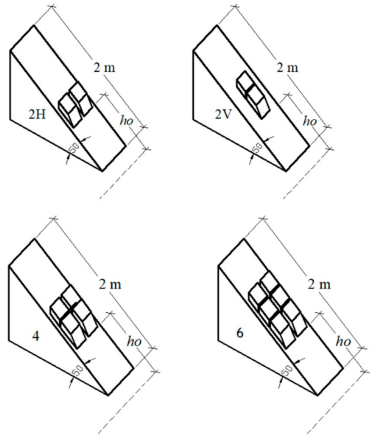

Figure 7. Arrangement of block configurations used in the tests with slide release height h_o parallel to the ramp slope and measured from the still-water level.

A constant dam height H_d = 0.32 m, crest width b_c = 0.053 m and length l_c = 2.2 m were used for the whole test series. However, three different upstream dam slopes were considered, i.e., β = 24° (1:2.25), 27° (1:2) and 34° (1:1.5) (see Figure 8). Additionally, two different freeboards were used: f = 0.024 m (still-water depth: h = 0.296 m) and 0.032 m (h = 0.288 m). Considering a scale of 1:190, the freeboard values correspond to 4.5 m and 6 m, respectively, associated with dams in Norway of high and very high consequences for the downstream area should the dam breach.

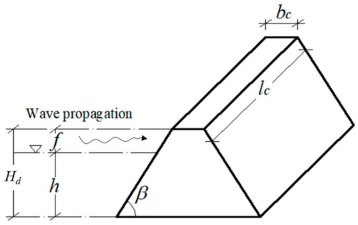

Figure 8. Definition sketch of a dam with the governing parameters.

66 experiments were conducted with varying slide, reservoir, and dam parameters. To check the test repeatability, each test with identical parameters was repeated three times and analyzed, hence a total of 198 tests have been conducted. All test data are given as the average of these three individual tests.

3. Wave Types, Propagation, and Overtopping Process

3.1. Wave Types and Propagation

Heller et al. [2] observed four transient impulse wave types for their 2D experiments in a wave channel: Stokes-like waves, cnoidal-like waves, solitary-like waves, bore-like waves, and all landslide-generated impulse waves may be allocated to one of these types. Each wave type (see Figure 9) has its own characteristics. The wave type influences for example the run-up height and wave force on the dam (see e.g., Heller and Hager [27]). Figure 10 provides an example of the wave profiles from all nine wave gauges on the reservoir, recorded during one of the 3D tests of this study (Test no. 185_2.25s_4.5_2H_200). The 3D waves generated in this study are more complex than in the 2D case; however, compared to the profiles of Figure 9, the recorded waves from all the tests conducted are Stokes-like waves, rather than any of the other wave types. Furthermore, investigation into selected waves revealed a ratio of wavelength to reservoir depth in the range of intermediate water waves.

A classification method to characterize landslide-generated waves is of interest and available in the literature. Heller et al. [2] identified the wave type product, $T = S^{1/3}M\cos[(6/7)\alpha]$, as a relevant number in this regard, where M is the relative slide mass ($M = m_s/\left(\rho_w bh^2\right)$, with m_s as the slide mass and ρ_w as the density of water) and S is the relative slide thickness ($S = s/h$, with s as the slide thickness). Previously, Wiegel et al. [3] and Noda [28] defined the slide Froude number F as the ratio of the falling box velocity v_s, and the shallow water waves celerity ($F = v_S/\sqrt{gh}$) and used F to identify the wave types produced by a falling block. Considering these numbers, Heller and Hager [27] defined wave type zones from the relationship between F and T for the 2D case. The boundaries of these wave type zones are plotted in Figure 11, where the axes show T versus F. Heller and Hager [27] observed for the 2D case mainly Stokes-like waves in the zone $T < 4/5F^{-7/5}$, mainly bore-like waves in the zone $T > 11F^{-5/2}$, and mainly cnoidal- and solitary-like waves in the intermediate zone $11F^{-5/2} \leq T \leq 4/5F^{-7/5}$. It is important to note that Heller and Hager [27] conducted granular slide tests, which may lead to different wave types under identical dimensionless parameters when compared to rigid slides such as in the present study. Heller and Spinneken [11] further investigated the wave types for the 3D case. They concluded from their 3D test results that the lower boundary ($T < 4/5F^{-7/5}$) remains characteristic also for 3D waves, whereas in the intermediate range both Stokes- and cnoidal-like waves were observed. Similar findings can be concluded from the 66 data points from the current 3D study plotted in Figure 11 and identified by the number of blocks used in the tests. The waves in all the tests conducted in the present study bear a resemblance to Stokes-like waves. This also applies to tests, involving 6-block as well as some of the 4-block tests that are plotted in Figure 11 in the intermediate zone defined for the 2D case for cnoidal- or solidary-like waves.

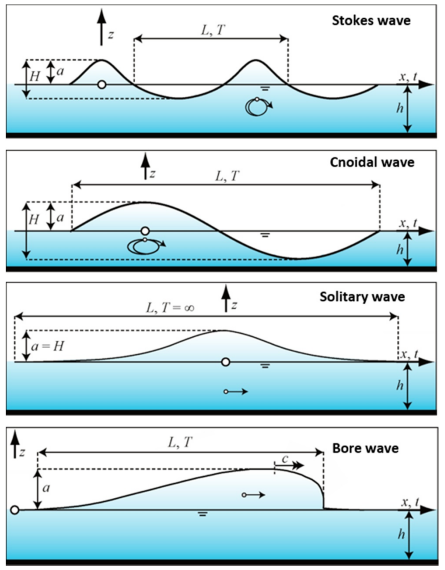

Figure 9. Idealized impulse wave types with the most important wave parameters (from Heller et al. [2], with permission from ETH, 2019).

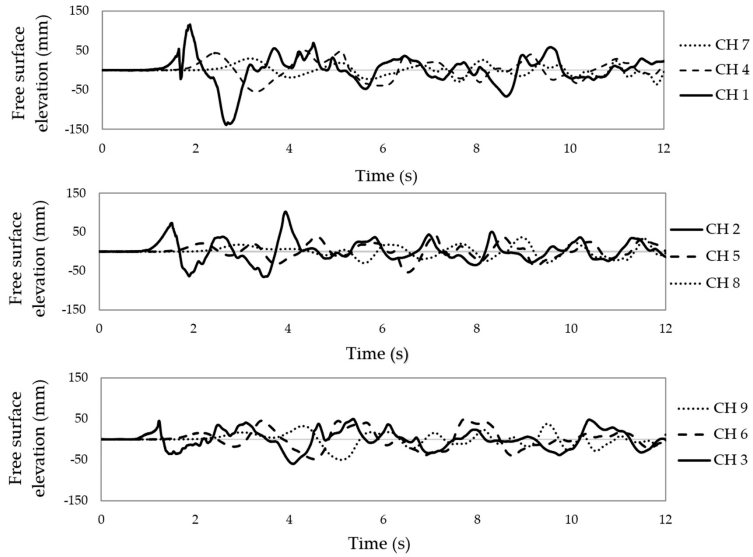

Figure 10. Wave profiles measured with the wave gauge sensors (see Figure 6 for the locations of the sensors) (Test no. 185_2.25s_4.5_2H_200).

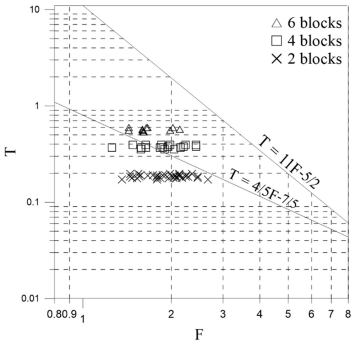

Figure 11. Plot of the wave type product T versus the Froude number F for the 3D tests conducted in the present study. All waves observed were Stokes-like. The boundaries provided are from Heller and Hager [27] observed for the 2D case using granular slides.

3.2. *Wave Overtopping Process*

Impulse waves induced by landslides impacting into reservoirs propagate and create wave run-up on the dam and shorelines. If the induced wave run-up exceeds the dam freeboard f the water overtops the dam and floods the downstream area. Kobel et al. [18] give a detailed description of the overtopping process for the 2D case and investigate the effect of the upstream slope, the freeboard and the dam width. Here, considering a 3D model, the focus is on variation in time and space of the overtopping waves, and thus the overtopping volume. During the overtopping process, the highest waves force a large volume of water over the crest in a short period of time, whereas the smaller waves may not produce any overtopping. The variation of the overtopping process in both time and space can be understood from Figure 12 presenting the time series obtained from all the sensors at the channels along the dam crest.

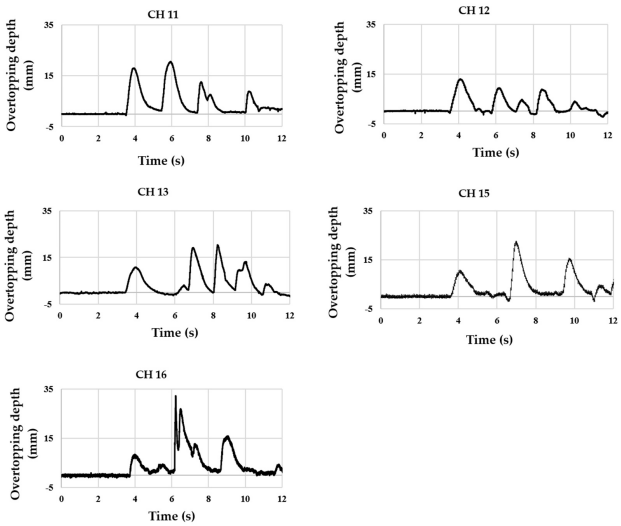

Figure 12. Overtopping depth (mm) versus time (s) over the five dam crest sections (see Figure 6 for the locations of the sensors) (Test no. 185_2.25s_4.5_2H_200).

4. Experimental Results

The experimental results are presented in this section. First, equations for the overtopping volume are derived for the experimental results. Furthermore, the uneven distribution of the overtopping volume is addressed.

4.1. Overtopping Volume

Once impulse waves are generated by landslides, they propagate and if large enough, overtop the dam thereby creating a certain volume of overtopping water. In this section, the relationship between the dimensionless parameters for the overtopping process will be assessed using an approach relating to e.g., that of Kobel et al. [18] and a predictive equation will be presented for the overtopping volume.

A dimensional analysis was conducted between the overtopping volume and the independent variables considering different landslide, reservoir, and dam geometries. Hence, the overtopping volume over the dam crest due to landslide-generated waves can be expressed as a function of:

$$W_w = f(W_s,\ h_o, g, v_s, h, \rho_w, a, l_b,\ b_b, \beta) \tag{1}$$

where W_w (m^3) = overtopping volume, W_s (m^3) = landslide volume, h_o (m) = landslide release height, g (m/s^2) = gravitational acceleration, v_s (m/s) = slide impact velocity, h (m) = still-water depth, a (m) = wave amplitude, l_b (m) = reservoir length, b_b (m) = reservoir width and β (^{o}) = dam front face angle,.

In the model experiments a constant reservoir length, l_b and reservoir width, b_b were used; hence their effect is considered constant.

Applying Buckingham's π theorem, by selecting the repeating variables as; h, ρ_w and v_s, a relationship between dimensionless parameters is obtained:

$$\frac{W_w}{h^3} = f\left(\frac{W_s}{h^3}, \frac{h_o}{h}, \frac{v_s}{\sqrt{gh}}, \frac{a}{h}, \beta/90^o\right) \tag{2}$$

where the wave amplitude a is measured from the zero level to the maximum crest point. Equation (2) can be rewritten:

$$\frac{W_w}{h^3} = f\left(\frac{W_s}{h^3}, \frac{h_o}{h}, \mathrm{F}, \varepsilon, \beta/90^o\right) \tag{3}$$

where $\varepsilon = a/h$ is the relative wave amplitude.

Conducting a power fit regression, a predictive equation is found for the relative overtopping volume:

$$\frac{W_w}{h^3} = 0.21\left[\left(\frac{W_s}{h^3}\right)\left(\frac{h_0}{h}\right)^{0.43}\left(\mathrm{F}^2\right)^{-0.08}\varepsilon^{0.04}\left(\beta/90^0\right)^{-0.01}\right] = 0.21E_1 \tag{4}$$

The following limitations apply: $2.67 < W_s/h^3 < 9.52$, $1.67 < h_0/h < 6.97$, $1.25 < \mathrm{F} < 2.66$, $0.18 < \varepsilon < 0.73$ and $0.27 < \left(\beta/90^0\right) < 0.37$.

E_1 is the overtopping volume parameter considering the relative wave amplitude described as:

$$E_1 = \left[\left(\frac{W_s}{h^3}\right)\left(\frac{h_0}{h}\right)^{0.43}\left(\mathrm{F}^2\right)^{-0.08}\varepsilon^{0.04}\left(\beta/90^0\right)^{-0.01}\right];\ 2.9 < E_1 < 14.8 \tag{5}$$

Equation (4) includes a parameter relating to the wave crest; however, it also includes the relative slide volume which is influential for the wave amplitude as well as the landslide speed through F. However, the impact of ε, as well as $\beta/90^0$ and F, is quite small, indicating that these parameters can be neglected in the analysis of the overtopping volume W_w. The model set-up had a fixed distance from the dam to the slide impact zone. Thus, for this case a more direct relationship with the slide volume is possible by neglecting the wave parameter ε. Rearranging the parameters in Equation (4), for a direct

relationship between W_w and the other parameters on the right-hand side of the equation, results in a relationship for W_s, to the power of 1. Thus, the relationship between W_w and W_s is linear. For cases that can be related to the model set-up, and where no information about the wave properties are available, removal of the wave related parameter is advantageous for a clearer extraction of the relationship between overtopping volume and slide parameters. This further simplifies the process of roughly estimating the overtopping volume related to a known potential slide into a reservoir. Hence, in this study, an additional analysis was made for a predictive equation of overtopping volume excluding wave properties, such as ε. Accordingly, the overtopping volume prediction formula becomes

$$\frac{W_w}{h^3} = 0.17\left[\left(\frac{W_s}{h^3}\right)\left(\frac{h_0}{h}\right)^{0.42}\left(\mathrm{F}^2\right)^{-0.03}\left(\beta/90^0\right)^{-0.1}\right] = 0.17E_2 \quad (6)$$

The following limitations apply: $2.67 < W_s/h^3 < 9.52$, $1.67 < h_o/h < 6.97$, $1.25 < \mathrm{F} < 2.66$ and $0.27 < \left(\beta/90^0\right) < 0.37$

E_2 is the overtopping volume parameter without considering ε described as:

$$E_2 = \left[\left(\frac{W_s}{h^3}\right)\left(\frac{h_0}{h}\right)^{0.42}\left(\mathrm{F}^2\right)^{-0.03}\left(\beta/90^0\right)^{-0.1}\right];\ 3.7 < E_2 < 17.8 \quad (7)$$

Based on the analysis the relative overtopping volume W_W/h^3 increases linearly and thus most significantly with the relative slide volume W_S/h^3, but moderately with the relative landslide release height h_o/h. Furthermore, the impacts of F and $\beta/90^0$ are again quite small. The exponents for F and $\beta/90^0$ in Equation (6) are so small that they may be ignored in the analysis of the overtopping volume. When excluding these parameters, the exponent of the remaining parameters, W_s/h^3 and h_o/h, remains the same for W_s/h^3, but only slightly reduces for h_o/h from 0.42 to 0.40. Furthermore, the constant in front of E_2 increases from 0.17 to 0.19. However, in the present study Equation (6) is considered for further analysis.

Figure 13 shows the correlation between measured relative overtopping volume W_W/h^3 and the overtopping volume parameters, E_1 and E_2, each with $R^2 = 0.80$. To investigate and compare Equation (4) including, and Equation (6) excluding the relative wave amplitude, an analysis was performed for the value of overtopping volume comparing the power regression fits (expressed by $R^2 = 0.80$) between the measured values from the tests and the results from Equations (4) and (6), respectively. Figure 14 reveals large prediction errors for smaller measured overtopping volumes $W_W < 0.01$ m^3 for both cases.

4.2. *Overtopping Volume Distribution*

Overtopping of a dam due to landslide-generated impulse waves is not uniform over the crest, for the case studied here with the landslide impinging along the reservoir's longitudinal axis (Figures 3a and 4). The water overtops the left edge first, and then the right edge and lastly the whole dam crest length. Figure 15 presents the distribution of the overtopping volume along the dam crest showing that a large amount of water is collected at the right and left edges (CH 16 and CH 11, respectively) of the crest, on average about 28% each. On average a slightly higher volume is collected at the left side, i.e., opposite the landslide impact zone. Contrariwise, a smaller volume of water overtops the middle section of the dam crest (CH 12, CH 13 and CH15) (Figure 15). This uneven distribution of the overtopping wave and volume along the crest of the dam is due to the 3D modeling allowing reflected waves from the edges of the reservoir.

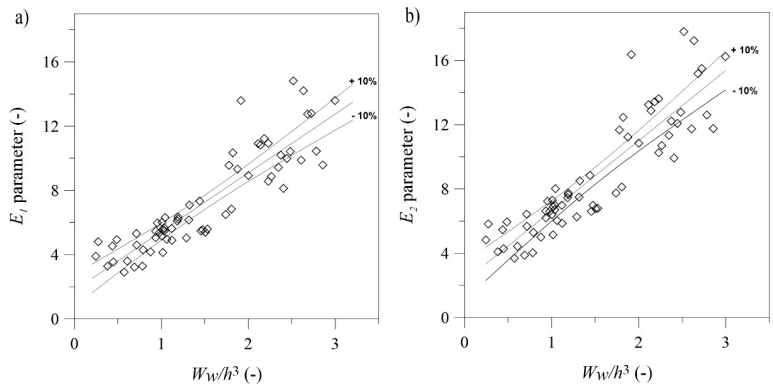

Figure 13. Relative maximum overtopping volume W_W/h^3 versus the wave overtopping volume parameter E_1 and E_2 with and without relative wave amplitude, respectively, as well as with 10% deviation (dashed line): (**a**) E_1 according to Equation (5) (R^2 = 0.80) and (**b**) E_2 according to Equation (7) (R^2 = 0.80).

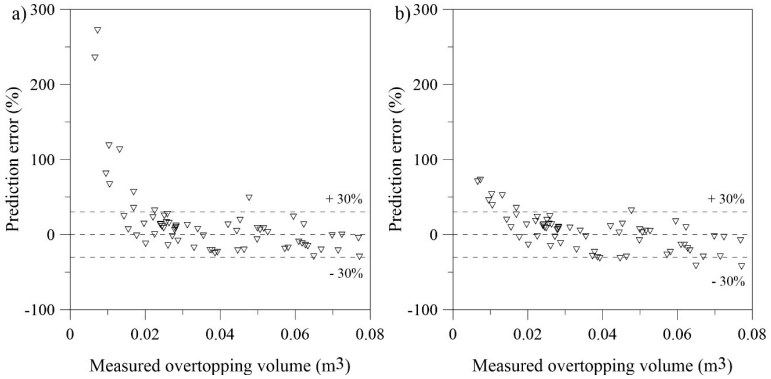

Figure 14. Prediction error for the measured overtopping volume: (**a**) predicted with Equation (4); (**b**) predicted with Equation (6).

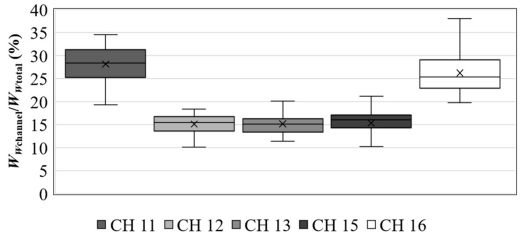

Figure 15. Overtopping volume distribution over the five dam crest sections (see Figure 6). The width of each channel is one fifth of the total dam crest length l_c.

5. Discussion

5.1. Comparison with Other Studies

Other studies include research dealing with dam overtopping due to impulse waves. For example, Müller [19] performed a series of 2D experiments considering the effect of the dam slope and crest width. He proposed an empirical equation for the overtopping volume per unit width, based on the run-up height. Recently Kobel et al. [18] studied dam overtopping due to solitary waves in a 2D laboratory scale set-up, relating to the case in Figure 3b, and presented an empirical equation for predicting the overtopping volume as

$$\frac{W_w}{b_b h^2} = 1.35\left[\varepsilon\left(\frac{h}{H_d}\right)^{(2/\varepsilon)(\beta/90^0)^{0.25}}\left(\frac{a_w}{b_c}\right)^{0.12}\right]^{0.7} \quad (8)$$

where a_w is the effective wave amplitude defined as $a_w = h + a - H_d$.

It is of interest to compare results from Equation (8) to the measurements of the present study and Equations (4) and (6). Here, two approaches are considered. Approach 1 considers the largest wave amplitude recorded at wave gauge channels closest to the landslide impingement zone (CH 1, CH 2 and CH 3) and assumes that this is a solitary wave. Conversely, Approach 2 considers the wave amplitude recorded at the wave gauges closest to the dam (CH 7, CH 8 and CH 9) and calculates the overtopping volume of a single wave overtopping the dam crest for three sections, the dam inner flank and the outer flanks on each side.

Approach 1 considers that theoretically, the height of a solitary wave (and wave amplitude) as used by Kobel et al. [18] does not decrease and the 2D wave may propagate over unlimited distances without any change of shape. Hence, the parameters of this study are inserted into Equation (8) by assuming that a solitary wave, as in Kobel et al. [18], is generated by the landslide where it impinges the reservoir and that this wave overtops the dam. Thus, the maximum relative wave amplitude recorded in the wave generation zone is used in the calculations. This is a conservative approach, considering the model set-up and the 2D solitary wave type used by Kobel et al. [18]. The ranges of relative amplitudes ε used here by this approach are 0.18 to 0.73 which fall reasonably within the range 0.10 to 0.70 investigated by Kobel et al. [18]. To obtain the overtopping volume, the right-hand side of Equation (8) is multiplied be $b_b h^2$. The mean bottom channel width is used here as b_b.

Approach 2 considers that the waves generated in this study are not 2D solitary waves, but a 3D wave that decays as it propagates towards the dam at different wave propagation angles. Approach 2 provides the overtopping volume at the dam for a single wave. The ranges of ε used in the calculations by this approach are 0.10 to 0.34, which falls within the range 0.10 to 0.70 investigated by Kobel et al. [18] for the use of Equation (8). It should be noted that lower relative wave amplitudes are recorded in some of the tests at CH 7 to 9, but that no overtopping occurs at the respective dam crest sections for $\varepsilon < 0.08$ and $\varepsilon < 0.11$ in case of freeboards of 0.024 and 0.032 m, respectively.

In Figure 16 a comparison is made between predicted and measured overtopping volumes, where the predicted overtopping volume is calculated according to Equations (4) and (6) (deduced for the case in Figure 3a) as well as Equation (8) (deduced for the case in Figure 3b) for Approach 1 and 2. The measured overtopping volume is obtained from the model tests of the present study. Figure 16 demonstrates that as expected, the predictive equation of Kobel et al. [18], using a 2D solitary wave approach (Approach 1) overestimates the experimental data. On average the overestimation is more than twice the measured value. The overestimation factor, represented as the ratio between the predicted and measured overtopping, has a mean value of 2.63 with standard deviation of +/−1.09. In comparison, Equations (4) and (6) extracted from the experimental data, on average, also slightly overestimate the experimental data by a factor of 1.13 and 1.18, respectively, and standard deviations of +/−0.5 and 0.48, respectively.

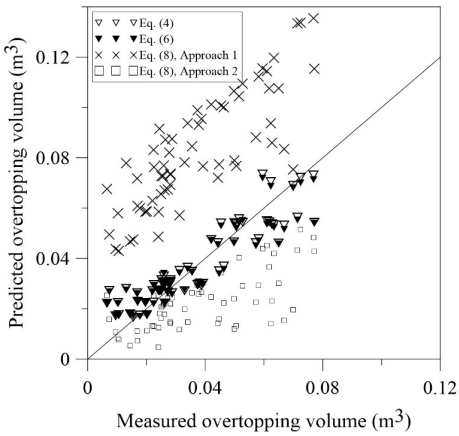

Figure 16. Predicted overtopping volume versus the total overtopping volume measured in the model tests (in m^3) of the present study. The total overtopping volume is predicted by Equations (4) and (6) of the present study and the overtopping volume from a solitary wave using Kobel et al. [18]'s Equation (8) using Approach 1 and 2.

The two Approaches 1 and 2 for the application of Kobel et al. [18]'s Equation (8) are compared in Figure 16. The overtopping volume calculated using Approach 1 overestimates the experimental data while Approach 2 generally underestimates the overtopping volume. For Approach 2, the measured total overtopping volume versus the one predicted by Equation (8), has a mean value of 0.70 with a standard deviation of +/−0.53. The tests that involve large landslide volumes of 4 or 6 blocks, and the highest release height in each case, all result in more than one wave overtopping the dam in the case study. Thus, for these tests the overtopping volume from Approach 2 considering only a single wave largely underestimates the measured total overtopping volume.

5.2. 3D Effects

Figure 16 compares results from studies representing the two cases illustrated in Figure 3, i.e., a 2D study using solitary waves through Approach 1, versus the present 3D study of landslide impinging perpendicular to the reservoir's longitudinal axis and inducing a more complex wave field (Figure 10). Additionally, the 3D wave effects are considered for the 2D formulation with the Approach 2 described above. Figure 16 confirms the statement by Kobel et al. [18] that 2D solitary wave represents the extreme case, considering that the predicted overtopping volume is on average more than twice the experimental results in Approach 1 applying Equation (8). However, Figure 16 also demonstrates that given the relative wave amplitude close to the run-up zone as in Approach 2, the use of Kobel et al. [18]'s, Equation (8) may underestimate the total overtopping volume in cases of narrow reservoirs. Thus, in a risk assessment for the downstream area, threatened by the water overtopping a dam, the water volumes estimated by Equations (4) and (6) are more appropriate for cases as those illustrated in Figures 2a and 3a, but only if these cases can be represented by the physical model of this study (Figures 4 and 6). Approach 1 for the application of Equation (8) by Kobel et al. [18] is appropriate for cases as shown in Figure 3b in case of solitary waves, but is likely to give extreme values, and thus be on the safe side for the cases shown in Figure 3a. Conversely, the 3D Approach 2 to the application of Equation (8) is likely to underestimate the overtopping volume for reservoirs relating to this case study, particularly involving large landslides. Thus, for Approach 2, Equation (8) must be applied cautiously to cases of narrow reservoirs and large landslides because of the potential number of waves

overtopping the dam. Combined application of Approaches 1 and 2 for predictions by Equation (8) could be considered, but may give a wide range of potential overtopping volumes.

One important feature extracted from the present study of landslides impinging perpendicular to the longitudinal axis of the reservoir (Figure 3a) is the uneven distribution of the overtopping volume over the dam crest (Figure 15). Equations (4) and (6) provide the total volume of water overtopping the dam. However, from a dam safety perspective the distribution of this along the dam crest is of interest. This distribution can be estimated from Figure 15.

5.3. Limitations and Potential Practical Application

A major limitation of all studies on landslide induced waves overtopping dams is the lack of relevant field data to calibrate physical and numerical models. This is in addition to potential scale effects in physical models, and the simplifications inherent in all modeling, including arising from potential inaccuracies of the instruments. The results from the present study, and other similar ones, should only be used as an aid in risk assessment, assessment of mitigation measures and in decision making that is influenced by dam safety. Furthermore, when applying Equations (4) and (6) the limitations inherent in the fixed model set-up of the present study must be considered. This includes the fixed reservoir geometry, the fixed slope of the landslide ramp, as well as the fixed distance to the landslide ramp. Additionally, the formulation considers only the landslide volume but not the landslide geometry (see Figure 7 and Table 2), but for two slides of the same volume but a different geometry, the wider slide will produce a larger wave and somewhat a larger overtopping volume. Thus, when applying the formulas, the landslide block arrangement (Figure 7) used in the present study must be considered. Furthermore, the slide blocks used represent subaerial rockslides, i.e., those released above the water surface. The results from this study are likely to give extreme values for cases where the landslide extends into the reservoir.

Geological investigations in reservoir areas may identify a potential landslide or rockslide. From the ranges of estimates of the slide size and location in relation to the dam, the equations from this study can be selected for cases that can be represented by Figure 3a and the model set-up (Figures 4 and 6). Assuming the case of Figure 3a, estimation of the necessary parameters to insert into Equation (6) should be attainable, and the same applies to the dam related parameters. However, the estimation must consider the limitations of the fixed reservoir geometry and landslide location stated above. Furthermore, for cases represented by Figure 3a but with very different landslide location from the model set-up (Figures 4 and 6) the results of this study should be used cautiously, with full recognition of the fixed reservoir and landslide set-up. Conversely, the formulation by Kobel et al. [18] requires evaluation of 3D wave parameters (similar to Approach 2) and can then be applied to the more general case, but with caution, at least in the case of a narrow reservoir and a large landslide impinging perpendicular to the reservoir's longitudinal axis. However, the extreme case can be realized with Approach 1 for the use of Kobel et al. [18]'s Equation (8). In any case, the estimated total volume of water overtopping the dam can subsequently be used to realize the potential size of the event threatening the downstream area. However, a time factor is required for calculations of potential flooding of the downstream area (see e.g., Kobel et al. [18]), i.e., resulting in overtopping discharge values. This will be dealt with in a separate article.

The information on the uneven distribution of the overtopping volume may be of importance in assessments for both dam and foundation-related issues, including erosion and scouring. Furthermore, the assessments mentioned can help in decision making regarding the execution of a project in landslide-prone regions, as well as mitigation measures such as monitoring of the landslide, or restricted operation for example through requirements on a minimum freeboard.

6. Conclusions

The research presented deals with the 3D case of a dam overtopped by waves generated as a landslide impinges the reservoir perpendicular to its longitudinal axis (Figure 3a). The governing

parameters include the slide volume, landslide release height, landslide speed, slide Froude number, still-water depth, and upstream slope of the dam. In line with the main objective of the paper, an empirical data analysis has been conducted to arrive at Equations (4) and (6) predicting the total volume of water overtopping the dam, based on the fundamental governing variables. The result from the analysis highlights the dominant effect of the slide volume followed by the still-water depth and landslide release height whereas the effect of the upstream dam slope is small. Limitations for the trend equations are stated enabling rough predictions, also in cases where information on some of the parameters may be absent. Furthermore, limitations on the applicability relating to the fixed geometry of the set-up are highlighted.

In line with one of the main objectives of the paper, the experimental data was compared to results using prediction formula derived for the 2D case by Kobel et al. [18]. The comparison confirmed the statement by Kobel et al. [18] that their approach with a 2D solitary wave represents the extreme case, which for the case considered here through Approach 1, resulted in an average overestimation of the measured value by more than a factor of two. However, if the 3D decay of a single wave is considered, as in Approach 2, the prediction by Kobel et al. [18] 's equation generally underestimates the experimental data and may result in an undesirable underestimation in cases where the wave is generated by a large rock slide into a narrow reservoir. In these cases, it is important to estimate the potential number of waves overtopping the dam.

Equations (4) and (6) can, with consideration of the stated limitations, be used for predicting the total volume of water that will overtop a specific dam due to landslide-generated waves with given landslide and dam properties. However, in such an estimation it is of high importance to note the limitation of Equations (4) and (6) arising from the fixed model set-up, i.e., geometry of the basin, location of the landslide ramp, and that the landslide geometry is not considered. Still, the equations can then be used to realize roughly the size of the event threatening the downstream area due to potential landslide-generated waves. The results should only be used to support risk assessment, assessment of mitigation measures, and decision making that is influenced by dam safety.

The overtopping process was described by figures and a quantitative data analysis. One important feature extracted regarding the overtopping process for the 3D case is the variation in time and space (Figure 12) resulting in uneven distributions of the volumes of water overtopping the dam crest (Figure 15). This observation was made possible by the 3D model set-up and is of value for dam safety considerations as well as for foundation-related issues, including erosion and scouring.

Author Contributions: Conceptualization, N.N.T., F.G.S. and L.L.; Formal analysis, N.N.T.; Investigation, N.N.T.; Project administration and Supervision, F.G.S.; Writing, N.N.T.; Writing, review and editing, F.G.S.; Review and editing L.L. and A.K.J.

Funding: Norwegian Water Resources and Energy Directorate (NVE) Project 80051.

Acknowledgments: The support and cooperation of the Norwegian Water Resources and Energy Directorate (NVE) and Grethe Holm Midttømme in the associated study and research program at NTNU is gratefully acknowledged. The contribution of Kiflom W. Belete in the early model development and to technical issues is appreciated. The important contribution of Jochen Aberle in the development of the model, particularly in reducing model effects, is acknowledged. Furthermore, the contribution of Geir Tesaker and Joël Biedermann in the laboratory, and of Ermyas Tamene Haile in the 3D drawing of the model set-up is acknowledged. The first author would like to acknowledge the support from Addis Ababa University, School of Civil and Environmental Engineering, as well as from NTNU, Department of Civil and Environmental Engineering.

Conflicts of Interest: The authors declare no conflict of interest.

Notation

a (m)	wave amplitude;
a_w (m)	effective wave amplitude;
b (m)	slide width;
b_b (m)	reservoir width;
b_c (m)	dam crest width;
E (-)	overtopping volume parameter;
F (-)	Froude number;
f (m)	freeboard;
g (m/s^2)	gravitational acceleration;
h (m)	still-water depth;
h_o (m)	landslide release height;
H (m)	wave height;
H_d (m)	dam height;
l_b (m)	reservoir length;
l_c (m)	crest length;
l_s (m)	slide length;
M (-)	relative slide mass;
m_s (kg)	slide mass;
s (m)	slide thickness;
S (-)	relative slide thickness;
T (-)	wave type product;
v_s (m/s)	landslide speed;
W_S (m^3)	slide volume;
W_W (m^3)	overtopping volume;
α (^{o})	slide ramp angle;
β (^{o})	dam front face angle;
ε (-)	relative wave amplitude;
ρ_w (kg/m^3)	density of water;

References

1. Steven, N.W.; Simon, D. The 1963 landslide and flood at Vaiont reservoir Italy. A tsunami ball simulation. *Ital. J. Geosci.* **2011**, *130*, 16–26.
2. Heller, V.; Hager, W.H.; Minor, H.-E. *Landslide Generated Impulse Waves in Reservoirs: Basics and Computation*; VAW-Mitteilung 211; ETH: Zürich, Switzerland, 2009.
3. Wiegel, R.L. Laboratory studies of gravity waves generated by the movement of a submerged body. *Trans. Am. Geophys. Union* **1955**, *36*, 759–774. [CrossRef]
4. Kamphuis, J.W.; Bowering, R.J. Impulse waves generated by landslides. *Coast. Eng. Proc.* **1970**, *1*, 35. [CrossRef]
5. Watts, P. Water Waves Generated by Underwater Landslides. Ph.D. Thesis, California Institute of Technology, Pasadena, CA, USA, 1997.
6. Synolakis, C. Generation of long waves in laboratory. *J. Waterw. Port Coast. Ocean Eng.* **1990**, *116*, 252–266. [CrossRef]
7. Ataie-Ashtiani, B.; Nik-Khah, A. Impulsive waves caused by subaerial landslides. *Environ. Fluid Mech.* **2008**, *8*, 263–280. [CrossRef]
8. Briggs, M.J.; Synolakis, C.E.; Harkins, G.S.; Green, D.R. Laboratory experiments of tsunami runup on a circular island. *Pure Appl. Geophys.* **1995**, *144*, 569–593. [CrossRef]
9. Fritz, H.M.; Mohammed, F.; Yoo, J. Lituya Bay landslide impact generated mega-tsunami 50th anniversary. In *Tsunami Science Four Years after the 2004 Indian Ocean Tsunami: Part II: Observation and Data Analysis*; Cummins, P.R., Satake, K., Kong, L.S.L., Eds.; Pageoph Topical Volumes; Birkhäuser: Basel, Switzerland, 2009; pp. 153–175.
10. Di Risio, M.; Sammarco, P. Analytical modeling of landslide-generated waves. *J. Waterw. Port Coast. Ocean Eng.* **2008**, *134*, 53–60. [CrossRef]

11. Heller, V.; Spinneken, J. On the effect of the water body geometry on landslide–tsunamis: Physical insight from laboratory tests and 2D to 3D wave parameter transformation. *Coast. Eng.* **2015**, *104*, 113–134. [CrossRef]
12. Romano, A.; Di Risio, M.; Bellotti, G.; Molfetta, M.G.; Damiani, L.; De Girolamo, P. Tsunamis generated by landslides at the coast of conical islands: Experimental benchmark dataset for mathematical model validation. *Landslides* **2016**, *13*, 1379–1393. [CrossRef]
13. McFall, B.C.; Fritz, H.M. Physical modelling of tsunamis generated by three-dimensional deformable granular landslides on planar and conical island slopes. *Proc. R. Soc. A Math. Phys. Eng. Sci.* **2016**, *472*, 20160052. [CrossRef] [PubMed]
14. Bellotti, G.; Romano, A. Wavenumber-frequency analysis of landslide-generated tsunamis at a conical island. Part II: EOF and modal analysis. *Coast. Eng.* **2017**, *128*, 84–91. [CrossRef]
15. Di Risio, M.; Bellotti, G.; Panizzo, A.; De Girolamo, P. Three-dimensional experiments on landslide generated waves at a sloping coast. *Coast. Eng.* **2009**, *56*, 659–671. [CrossRef]
16. Evers, F. *Spatial Propagation of Landslide Generated Impulse Waves*; VAW-Mitteilung 244; ETH: Zürich, Switzerland, 2017.
17. Huber, L.E.; Evers, F.M.; Hager, W.H. Solitary wave overtopping at granular dams. *J. Hydraul. Res.* **2017**, *55*, 799–812. [CrossRef]
18. Kobel, J.; Evers, F.M.; Hager, W.H. Impulse wave overtopping at rigid dam structures. *J. Hydraul. Eng.* **2017**, *143*, 04017002. [CrossRef]
19. Müller, D.R. *Auflaufen und Überschwappen von Impulswellen an Talsperren*; VAW-Mitteilung 137; ETH: Zürich, Switzerland, 1995.
20. Lindstrøm, E.K.; Pedersen, G.K.; Jensen, A.; Glimsdal, S. Experiments on slide generated waves in a 1:500 scale fjord model. *Coast. Eng.* **2014**, *92*, 12–23. [CrossRef]
21. Fritz, H.M.; Hager, W.H.; Minor, H.-E. Landslide generated impulse waves. 1. Instantaneous flow fields. *Exp. Fluids* **2003**, *35*, 505–519. [CrossRef]
22. Fritz, H.M.; Hager, W.H.; Minor, H.-E. Landslide generated impulse waves. 2. Hydrodynamic impact craters. *Exp. Fluids* **2003**, *35*, 520–532. [CrossRef]
23. Mohammed, F.; Fritz, H.M. Physical modeling of tsunamis generated by three-dimensional deformable granular landslides: Landslide generated tsunamis. *J. Geophys. Res. Oceans* **2012**, *117*, C11015. [CrossRef]
24. Zweifel, A. *Impulswellen: Effekte der Rutschdichte und der Wassertiefe*; VAW-Mitteilung 186; ETH: Zürich, Switzerland, 2010.
25. Heller, V.; Spinneken, J. Improved landslide-tsunami prediction: Effects of block model parameters and slide model. *J. Geophys. Res. Oceans* **2013**, *118*, 1489–1507. [CrossRef]
26. Sælevik, G.; Jensen, A.; Pedersen, G. Experimental investigation of impact generated tsunami; related to a potential rock slide, Western Norway. *Coast. Eng.* **2009**, *56*, 897–906. [CrossRef]
27. Heller, V.; Hager, W.H. Wave types of landslide generated impulse waves. *Ocean Eng.* **2011**, *38*, 630–640. [CrossRef]
28. Noda, E. Water waves generated by landslides. *J. Waterw. Harb. Coast. Eng. Div.* **1970**, *96*, 835–855.

Paper II

Physical Model Study on Discharge Over a Dam Due to Landslide Generated Waves

Netsanet Nigatu, Leif Lia, Asie Kemal, Fjola G. Sigtryggsdottir

Water,2020,12,234; doi.org/10.3390/w12010234 (Open Access)

---

water

MDPI

Article

Physical Model Study on Discharge over a Dam Due to Landslide Generated Waves

Netsanet Nigatu Tessema [1,*], Fjóla G. Sigtryggsdóttir [2], Leif Lia [2] and Asie Kemal Jabir [1]

[1] School of Civil and Environmental Engineering, Addis Ababa Institute of Technology, Addis Ababa 1000, Ethiopia; asie.kemal@aait.edu.et

[2] Department of Civil and Environmental Engineering, Norwegian University of Science and Technology, 7491 Trondheim, Norway; fjola.g.sigtryggsdottir@ntnu.no (F.G.S.); leif.lia@ntnu.no (L.L.)

* Correspondence: Netsanet.nigatu@aait.edu.et; Tel.: +251-913-77-15-74

Received: 6 November 2019; Accepted: 26 December 2019; Published: 15 January 2020

Abstract: Impulse waves generated by landslides falling into reservoirs may lead to overtopping of a dam and, in turn, to flooding of the downstream area. In the case of an embankment dam, the overtopping may lead to erosion of the downstream slope, ultimately resulting in breaching and complete failure with consequent further hazardous release of water to the downstream area. This research deals with the overtopping process of a dam due to landslide generated waves in a three-dimensional (3D) physical scale model setup. Experiments have been conducted with varying the slide, reservoir, and dam parameters. The primary focus is on investigating the feasibility of employing the steady state weir equation in order to predict the overtopping discharge over a dam crest due to landslide generated waves. Calibration and validation of the coefficient of discharge values for the different dam section are conducted for the specified model setup. Accordingly, a two-step calculation procedure is presented for predicting the overtopping discharge based on the maximum overtopping depth values. Hence, for the fixed setup, which includes a constant slope angle of the landslide surface, a predictive equation for maximum overtopping depth is proposed, based on slide volume, slide release height, still water depth, upstream dam slope angle, and dam height. The relative slide volume and relative still water depth both seem to have a significant effect on the relative overtopping depth.

Keywords: physical model; dam overtopping; impulse waves; discharge

1. Introduction

Dams constructed in alpine regions face the risk of slides, of large volumes and high impact velocities, falling into the dam's reservoir. As a slide plunges into a reservoir, it creates a series of gravity waves, that is, impulsive waves. If the generated impulse wave is large enough, it propagates over the reservoir and overtops the dam. Historically, such events have in some cases had catastrophic consequences. One extreme event was the Vajont reservoir catastrophe (1963), where about 300 Mm^3 (it is estimated to be 270 Mm^3 in other literatures [1,2]) of soil and rock slid into the reservoir and spilled over the dam crest with an 80 m high wave, sweeping through the village of Longarone, which led to the death of 1909 people [3]. Further, a well-known example is Lituya Bay, Alaska, where an earthquake caused a subaerial rock slide into Gilbert Inlet on 8 July 1958, yielding a maximum run up height of 524 m [4]. Considering dams, such events can generally be described by three different phases (see Figure 1); wave generation, propagation, and run up and overtopping. These phases have been studied in the past using mathematical theories, physical model experiments, and numerical simulations.

Numerous physical model studies have, for example, been conducted to study the wave generation and propagation with a two-dimensional (2D) prismatic wave channel [4–12] and 3D wave

basin [3,13–18]. The wave propagation process can be expressed with the wave types generated by the slide impact. Four types of waves were observed based on the slide Froude number F and the dimensionless slide thickness S [12]. Among the wave types, the propagation of the leading wave crest closely followed the theoretical approximations of solitary waves. Further classifications have been applied, such as using the wavelet analysis (i.e., with landslide volume and slide velocity) [3] and a diagram based on slide parameters and still water depth [8] for 3D and 2D models, respectively.

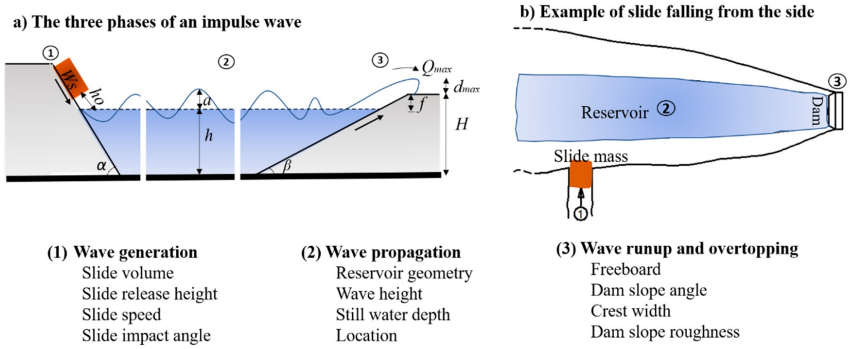

Figure 1. The three phases of landslide generated waves with the governing parameters: (1) slide impact with wave generation; (2) wave propagation; and (3) wave run up and overtopping of a dam. (**a**) A section showing the three phases based on Heller at al. [14]; (**b**) an example plan view of a reservoir.

The overtopping process (phase three) of a dam as a result of landslide-generated impulse waves has been investigated with physical model experiments [15,19–23] and numerical modelling [1,16,24–26]. Among the numerical modelling done to study this process, a smoothed particle hydrodynamics (SPH) approach has been used with 2D [24,25] and 3D [27] numerical simulations. Xiao and Lin [16] applied a coupled solid fluid numerical model based on Reynolds-averaged Navier–Stokes (RANS) to simulate the dam overtopping event of landslide-generated waves in an idealized reservoir. A comparison between the experimental and numerical results showed a reasonable agreement. In physical as well as numerical models, solitary type of waves have been applied to simulate the overtopping characteristics of impulse waves on dam structures [8].

The third phase can be described with the overtopping volume and overtopping discharge over the dam crest. There have been studies to predict these parameters in the literature, where the earliest study by Müller [15] provided an equation to predict the average overtopping discharge based on the run up height and overtopping volume, but this equation is limited to cases without freeboard. The most recent study by Kobel et al. [19] used a rigid dam in a 2D physical model experiment to derive predictive equations for the overtopping volume and duration. The overtopping discharge can be calculated from these parameters for cases with freeboard. In a similar way, Huber et al. [20] investigated the effect of a solitary wave overtopping a granular dam with a 2D laboratory study. A predictive equation for overtopping volume and duration was proposed based on Kobel et al. [19] equations, adding a dam shape parameter given that there is a significance difference in the two setups. The aforementioned studies describe a way of predicting the overtopping discharge with a two-step approach, basing on a 2D experimental setup where slides impact the longitudinal direction of the reservoir. A recent paper by Tessema et al. [21] studied the case of landslides impacting a reservoir from a lateral direction (see Figure 1b) with a 1:190 laboratory scale model for a typical dam of 60 m height. A new empirical equation for the dam overtopping volume as a function of the slide volume, slide release height, slide impact velocity, still water depth, and upstream dam slope was derived for the case studied. The present study further investigates this specific case and gives a general method

for predicting overtopping discharge over a dam as a result of slide-generated waves. Unlike the previous studies conducted in rectangular prismatic water wave channels with landslides impacting a reservoir along the longitudinal direction, the present study considers the 3D effect relating to narrow valleys and slides impinging perpendicular to a reservoir's longitudinal axis (see Figure 1b).

In 2008, a physical model was built in the hydraulic laboratory of NTNU (Norwegian University of Science and Technology, Trondheim, Norway) to study the effects of landslide-generated tsunami waves in fjords. The topography and bathymetry of the southern part of the Storfjorden fjord system in western Norway was simulated, about 40 m from the slide. Using the measured data from the scale model, the tsunami inundation was simulated in a numerical model, providing a good match with the measurements [28]. Later, the model was reconstructed to study the effect of landslide-generated waves on embankment dams. Several test series have been done for different model setups on the physical model to study the impacts of landslide-generated waves on dam overtopping. The effects of different slide, reservoir, and dam parameters on the embankment dam overtopping has been studied. The executed physical experiments under several experimental scenarios gave insight into the parameters and dam overtopping [29–31]. The main conclusions from these experiments are that the overtopping height and volume are mainly a result of landslide size, velocity, dam geometry, and freeboard [32,33]. The current study is a part of this research study.

Despite the fact that a slide-generated wave overtopping process is dynamic, analyses were made in this study for discharge prediction with a formulation derived for steady state discharge calculation over a weir. This approach favors the main objective of this study, namely to provide a simple means of roughly estimating the discharge over a dam crest as a result of landslide-generated waves. However, any application of the results must consider that the dynamic behavior of the overtopping process is not accounted for. Furthermore, limitations of the model setup having the fixed parameters listed in Table 1 must be kept in mind, including that only one type of landslide is considered, that is, rock slides modelled with the solid blocks. A general two step procedure is presented for predicting the overtopping discharge; (1) calculate maximum overtopping depth based on all the required parameters of the slide, reservoir, and dam including slide volume, slide release height, still water depth, dam height, and dam front face angle; (2) calculate the overtopping discharge with the proposed formula. In a 3D setting related to narrow valleys, the distribution of waves along the dam crest (inner and outer edges) is not uniform where the generated wave propagates at different angles. This is considered by dividing the dam crest in a number of sections for discharge calculations. The coefficient of discharge values of each section for the fixed dam setup are calibrated and validated with the experimental data. This study provides such information, which may be of use in risk assessment as well as for the design of embankment dam riprap on the crest and on the downstream slope, see, for example, Hiller et al. [34], for new and existing dams in landslide prone areas.

Table 1. Fixed parameters for the model setup (prototype scale).

Parameter	Fixed	Notation
Slide ramp	Location	perpendicular to the reservoir axis
	Inclination	$\alpha = 50°$
Slide Properties	Solid blocks	blocks chained together with minor opening between them
Reservoir	Geometry, like reservoir length, and width	l_b= 742.9 m and b_b = 336.3 m
	Slope of side banks	$\theta = 50°$
Dam	Height	H = 60.8 m
	Crest length	l_c = 421.8 m
	Crest width	B_c = 10.07 m

This study is organized as follows. The physical model and the governing parameters are described in Section 2. In Section 3, an analysis is conducted on the experimental data to calibrate and validate the coefficient of discharge values for discharge prediction. In addition, the overtopping depth prediction

formula is presented based on slide volume, slide release height, still water depth, dam height, and dam face front angle in Section 3. Finally, the discussion and conclusion are summarized in Sections 4 and 5, respectively.

2. Physical Model

2.1. Experimental Setup

The experiments were carried out on a 1:190 scale physical model in the hydraulic laboratory of NTNU. The basin sides have planar slope sidewalls of water resistant plywood covered with a concrete paste for increasing the roughness. It is 4.5 m in length, 1.7 m in width at the bottom, and 2.22 m in width at dam crest level, with a total reservoir capacity of 2.5 m^3 corresponding to 860 m in length, 320 m in width at the bottom, and 420 m width at dam crest level, with a total reservoir capacity of 17 Mm^3 in the prototype, respectively. The experimental setup and instrumentation can be seen in Figure 2, with fixed parameters described in Table 1. Five ultrasonic sensors (*mic+35/LU/TC*) were used to measure the overtopping depth over the dam crest.

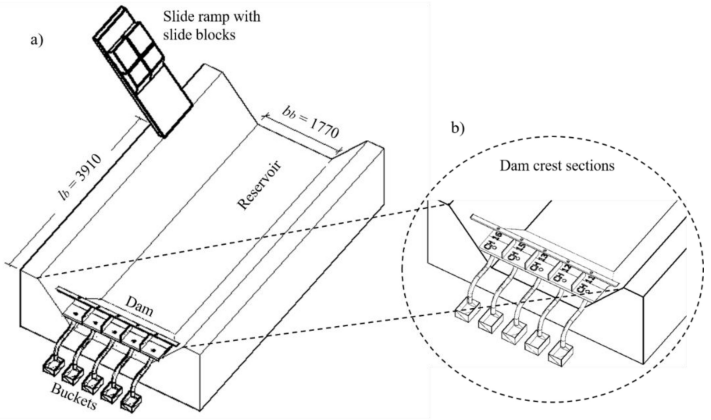

Figure 2. (**a**) Experimental setup with the main components; slide, reservoir, dam, and (**b**) ultrasonic sensors used for measuring the overtopping depth and buckets for collecting the overtopping water (all measurements are in mm).

Dams having upstream slopes of 1 to 1.5 and 1 to 2.25 were used for the analysis. The dam crest was divided into five different sections (CH 11, CH 12, CH 13, CH 15, and CH 16), referred to in the following as dam crest sections, to clearly see the distribution of the overtopping waves along the crest. Five ultrasonic sensors were placed in each section to measure the overtopping depth with time. The corresponding volume of overtopping water for each dam section was collected in five buckets with pipes of 100 mm in diameter. The data from the landslide velocity measuring sensor, wave gauges, and five ultrasonic sensors in each dam section were collected in Agilent Measuring Manager program with a sampling rate of 200 Hz.

Different landslide, reservoir, and dam parameters such as landslide volume W_S, landslide release height h_o, freeboard f, and upstream dam slope β were considered as input parameters for the study (see Figure 3). From the analysis, it was observed that the maximum overtopping depth (d_{max}) over the dam crest was the most dominant parameter that describes the overtopping discharge.

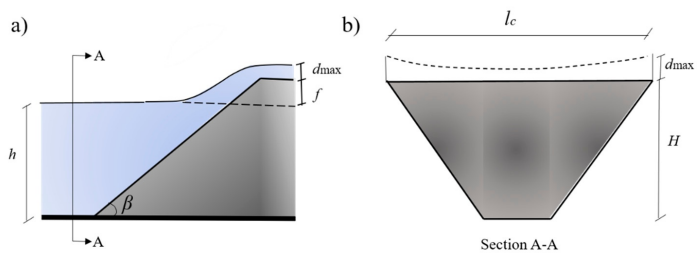

Figure 3. Definition sketch of the overtopping process with the input parameters for overtopping discharge over the dam crest: (**a**) side view, and (**b**) cross sectional view.

2.2. *Test Programme*

A total of 44 experiments were conducted and each experiment with identical parameters was repeated three times to check the repeatability, which means a total of 132 model runs were done. All test data were given as an average of the three individual tests.

Given the free surface flow problem, Froude similitude was considered in the analysis where gravity waves generated by the slide impact are dominated by gravity, not by surface tension forces [35]. Hence, the still water depth in the slide impact zone that is, $h > 0.2$ m, was used to neglect the possible scale effects [36].

The slide was simulated with box blocks connected in chain for different slide arrangements with a length between 0.5 m and 1.66 m and width between 0.45 m and 0.90 m. Four different types of block arrangements (2H, 2V, 4, and 6) (Table 2) were used in the model to simulate the subaerial slide falling into a reservoir. For each block arrangement, different blocks are used, as shown in Figure 4.

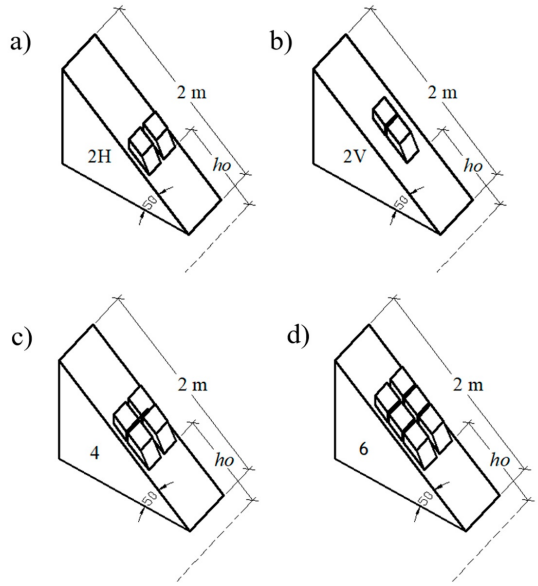

Figure 4. Arrangement of block configurations used in the tests with h_o parallel to the ramp slope and measured from the still water level: (**a**) 2H; (**b**) 2V; (**c**) 4 blocks and (**d**) 6 blocks arrangement.

Table 2. Slide characteristics in the model setup for different block setups (model scale).

Slide characteristics	Block Arrangement			
	2H	**2V**	**4 Blocks**	**6 Blocks**
Slide length l_S (m)	0.5	1.08	1.08	1.66
Slide width b (m)	0.9	0.45	0.9	0.9
Shape ratio l_S/b (-)	0.56	2.4	1.2	1.84
Slide volume W_S $\left(\mathrm{m}^3\right)$	0.072	0.074	0.15	0.23

The most common way to categorize dams is estimating the consequence from the potential dam failure. For different consequence classes of dams, different deterministic requirements are assigned, that is, freeboard and crest width. In this study, freeboard values, f (Table 3), associated to high (f = 4.5 m) and very high (f = 6 m) consequence class dams in Norway are selected.

Table 3. Consequence class with freeboard values and the corresponding still water depth used in the experimental setup for a fixed dam height H = 60.8 m (prototype scale).

Consequence Class	f (m)	Still Water Depth (h) (m)
High	4.56	56.24
Very high	6.08	54.72

A summary of variable parameters is listed in Table 4.

Table 4. Summary of input slide and dam parameters used in the experiments (prototype scale).

β (V:H)	f (m)	Block Arrangement	W_S (m^3)	h_o (m)
1:2.25	4.56	2H	493,848	380
		2V	507,566	285
	6.08	4 blocks	1,021,991	190
		6 blocks	1,543,275	95
1:1.5	4.56	2H	493,848	380
		2V	507,566	285
	6.08	4 blocks	1,021,991	190
		6 blocks	1,543,275	95

3. Data Analysis

The data analysis aims at a rough estimation of the overtopping discharge applying the theory of steady state overtopping discharge formula over a weir. For this purpose, the following analyses of the experimental data were performed. First, the volume of water for each wave was determined using a plot between the overtopping depth and time for each dam crest section. Second, using the steady state flow formula, a calibration is carried out to derive a coefficient of discharge values, C_d, for the different dam slopes and for each dam crest sections. Lastly, a predictive equation is given for d_{max} based on different slide, basin, and dam properties for each channel. This predictive equation gives an estimation of the maximum overtopping depth, which can be used as the overtopping height in the discharge calculation formula derived through the second analysis performed. Thus, the results from these two separate analyses of the experimental data constitute part of a methodology later demonstrated in Section 4.

The simultaneous use of the terms overtopping depth and height for the same physical parameter appear in the literature, that is, overtopping height for steady state equations and depth for landslide-generated wave predictive equation.

3.1. Overtopping Process

In most of the experiments, three major waves were observed during the impact of landslide-generated waves. Each overtopping wave gives a certain overtopping volume of water with a specific duration. In this section, the volume of water for each wave is determined using a plot between the overtopping height and time.

The total volume of water over the dam crest for each section is collected in a bucket and measured for each test. The overtopping distribution over the dam crest is not uniform, where a large amount of water is collected at the right and left flanks of the dam (CH 11 and CH 16) (see Figure 5). This is because of the 3D narrow reservoir used in this study, where wave reflections from the reservoir banks are expected.

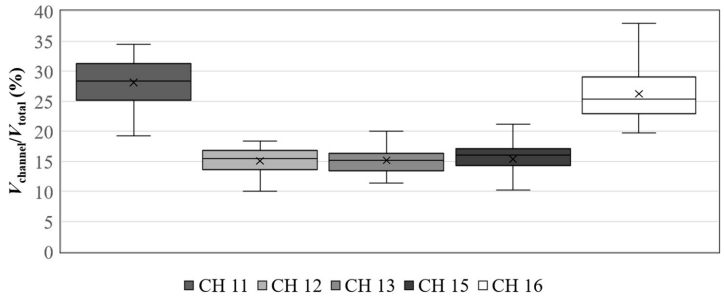

Figure 5. Overtopping volume distribution over the five dam crest sections (see Figure 2b for the position of sensors).

3.2. Discharge

3.2.1. General

Different methods are available to predict the discharge of oscillatory waves at sea defense structures. For example, Van der Meer [37] and Pullen et al. [38] provided empirical wave overtopping discharge formulas for bermed and straight impermeable levee slopes based on a wide range of small and large scale laboratory experimental data. The principal formula used for wave overtopping is as follows:

$$\frac{q}{\sqrt{g H_{mo}^3}} = a exp\left[-\frac{bR_c}{H_{mo}}\right], \quad (1)$$

where q (m^3/s/m) = the mean overtopping discharge per meter; H_{mo} (m) = the overtopping height; R_C (m) = freeboard; and a and b are coefficients that are functions of wave height, slope angle, breaker parameter, and the influence factors.

Yarde et al. [39] used this approach to derive empirical equations for overtopping discharge due to wind-generated waves on inland reservoirs. The relationship between dimensionless overtopping discharge was described as exponential with that of the dimensionless freeboard.

Even if this approach applies for wind-generated waves, it is not applicable to cases with landslide-generated waves overtopping the dam, because of the fact that the wave is subjected to shoaling effects including the wave breaking before it reaches the dam. The wave generated by a landslide impacting into the reservoir propagates undisturbed from the source to the dam structure.

A steady state discharge prediction formula over a dam, which is also described as the weir equation, is expressed as follows:

$$Q_{max,weir} = C_d \times \sqrt{2g} \times B \times {H_{max}}^{3/2}, \quad (2)$$

where $Q_{max,weir}$ (m^3/s) = maximum discharge over a weir, C_d (-) = the discharge coefficient dependent on weir shape, B (m) = length of the weir, H_{max} (m) = maximum overtopping height above dam crest, and g (m/s^2) = acceleration due to gravity.

Here, a simplified approach for calculating the discharge due to landslide-generated waves is selected by applying an equation used for calculating a steady state discharge over a weir, Equation (2). Hence, the general formula for predicting the discharge over the dam crest as a result of landslide-generated waves can be expressed as follows:

$$Q_{max} = C_d \times \sqrt{2g} \times B \times {d_{max}}^y, \quad (3)$$

where Q_{max} (m^3/s) = maximum discharge, C_d (-) = calibrated coefficient of discharge, d_{max} (m)= maximum overtopping depth, and y = calibrated coefficient for each dam section.

Rearranging Equation (3) into the dimensionless form gives the following:

$$\frac{Q_{max}}{\sqrt{2g\,B^5}} = x\left[\frac{d_{max}}{B}\right]^y, \quad (4)$$

where x is calibrated coefficients for each dam section.

The prediction method for d_{max} based on slide, reservoir, and dam parameters is presented in Section 3.3. It is expressed in terms of W_S, h_o, h, H, and β (Equation (8)). The proposed dimensionless equation, Equation (4), in this study is similar to that of Equation (1), which is presented for sea defense structures. The effect of f is considered in calculating d_{max} (Equation (8)), by applying h. For a fixed H considered in this study, h and f are inter-related and can be used alternatively.

3.2.2. Coefficient of Discharge

In order to calculate Q_{max} over the dam crest with Equation (3), C_d has to be calibrated for each channel across the dam. To do so, back calculation was applied with the results from the experiments, where discharge is calculated first and then used for calibrating coefficient of discharge values, which will be discussed in this section.

Each wave (wave 1, wave 2, and wave 3 are considered here) is characterized with the overtopping height and the initial and final time of occurrence, as seen in Figure 6.

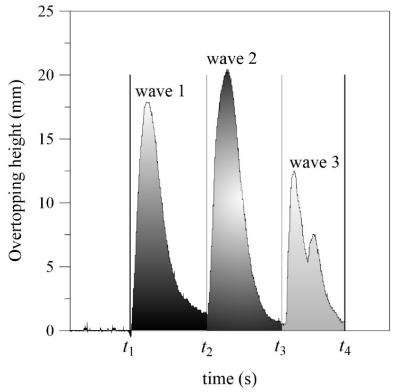

Figure 6. Overtopping height (mm) vs. time (s) plot for Q_{max} calculation considering the three maximum waves recorded in channel (CH) 11.

The discharge for each wave, as seen in Figure 6, can be calculated by dividing the overtopping volume for each wave with its time of occurrence (initial and final time) as follows:

$$Q_1 = \left(\frac{V_1}{t_2 - t_1}\right), Q_2 = \left(\frac{V_2}{t_3 - t_2}\right), Q_3 = \left(\frac{V_3}{t_4 - t_3}\right) \ldots\ldots\ldots, Q_n = \left(\frac{V_n}{t_f - t_i}\right), \quad (5)$$

where Q_1, Q_2, Q_3, and Q_n (m^3/s) = maximum discharge; V_1, V_2, V_3, and V_n (m^3) = overtopping volume for the 1st, 2nd, 3rd, and nth wave, respectively; and t_1, t_2 … $.t_n$ (s) = starting and ending time of occurrence for each wave.

For simplifying the calculation, the overtopping volumes for wave 4, wave 5, and so on are considered negligible. Hence, the maximum of the calculated discharge for the three waves (wave 1, wave 2, and wave 3) is adopted as the maximum discharge for the entire test.

$$Q_{max} = max[Q_1, Q_2, Q_3] \quad (6)$$

The experimental data output from the model setup is put into two groups. The first data set is used to calibrate C_d values, while the other is used for validating the predicted equation for calculating maximum discharge. Hence, for each experiment, the relative maximum discharge is plotted against the relative maximum overtopping height (refer to Equation (4)) for each of the five sections of the dam (CH 11, CH 12, CH 13, CH 15, and CH 16) (Figures 7 and 8). Hence, a relationship is obtained from the plots and the power fit equation seems to define their relationship with statistically good correlation (Figures 7 and 8). This aids in predicting Q_{max} over the dam crest as a result of landslide-generated waves for a specific value of maximum overtopping height. However, calibration of the coefficient of discharge values is done with the steady state equation (Equation (3)), with B with an exponent of 1.

C_d values for dams with an upstream slope of 1 to 1.5 are higher than those with an upstream slope of 1 to 2.25 (Figure 9). This indicates that the value is dependent on the upstream dam slope angle; a milder slope results in lower C_d values. Owing to the effect of the wave reflections in the reservoir, higher values of the coefficient of discharge are observed at the side of the dam (at the same side of point of slide impact).

3.2.3. Method Validation

The predicted equation results in C_d values in the range of (0.53 to 1.53) for an upstream dam slope pf 1 to 1.5 and (0.40 to 0.96) for an upstream dam slope of 1 to 2.25. The largest value is found at the channel left edge (CH 16) of the dam for the slide impact from the right side of the reservoir.

The validity of the proposed equation can be investigated by applying the measured d_{max} for each test of the data set and calculating the respective Q_{max} with the proposed equation. The predicted maximum discharge is plotted to the calculated maximum discharge (from measured volume) in Figure 10 for upstream dam slopes of 1 to 1.5 and 1 to 2.25 with 10% deviation.

The predicted equation for calculating the maximum overtopping discharge seems to fit reasonably for channels 11–13 (found at the left side of the dam). On the contrary, however, the correspondence between the prediction and the measurement was found to be low for channel 15 and 16 (right side of the dam). This is because of the reflection waves in the narrow reservoir having the largest influence of disturbing the flow on the right side of the dam crest.

Hence, a general predictive equation for the overtopping discharge over the dam crest is proposed in the dimensionless form, with the coefficients stated in Table 5 as follows:

$$\frac{Q_{max}}{\sqrt{2g\,B^5}} = x\left[\frac{d_{max}}{B}\right]^y, \quad (7)$$

where $0.06 \le x \le 0.09$ and $0.83 \le y \le 1.07$ for dams having an upstream slope of 1 to 1.5 and $0.05 \le x \le 0.16$ and $0.95 \le y \le 1.23$ for dams having an upstream slope of 1 to 2.25.

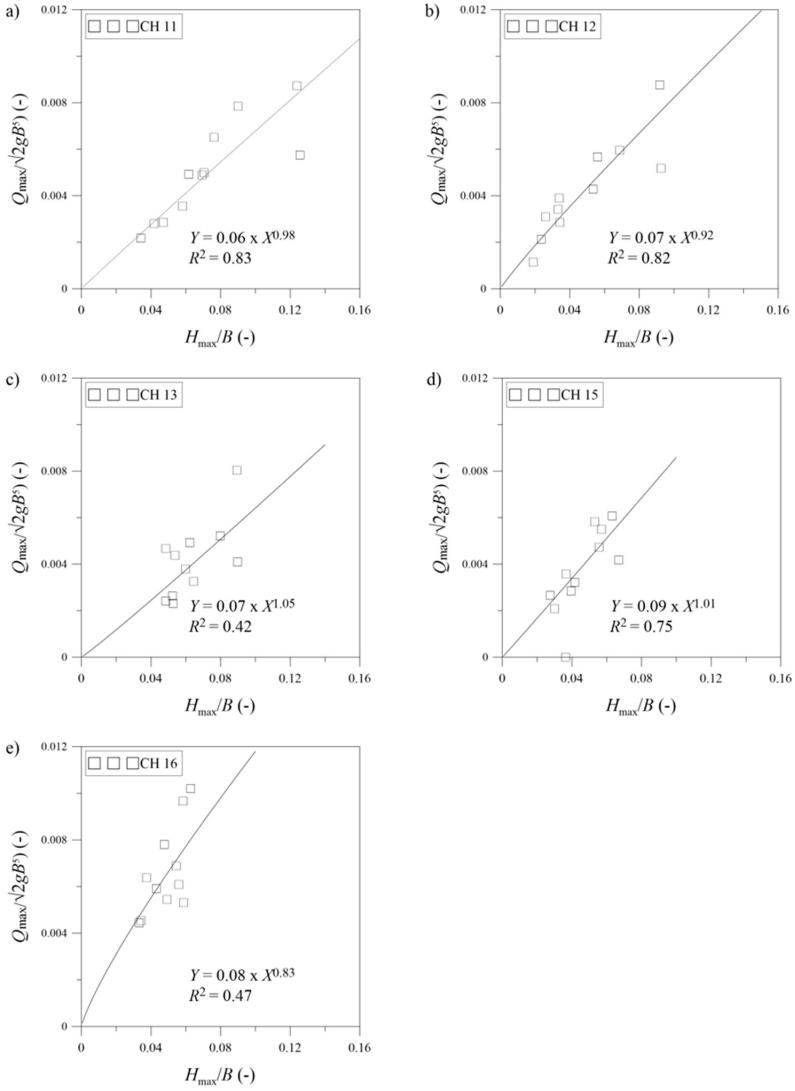

Figure 7. Plot between dimensionless measured maximum overtopping depth and calculated maximum discharge for CH 11, 12, 13, 15, and 16, respectively, for an upstream dam slope of 1 to 1.5 for C_d calibration.

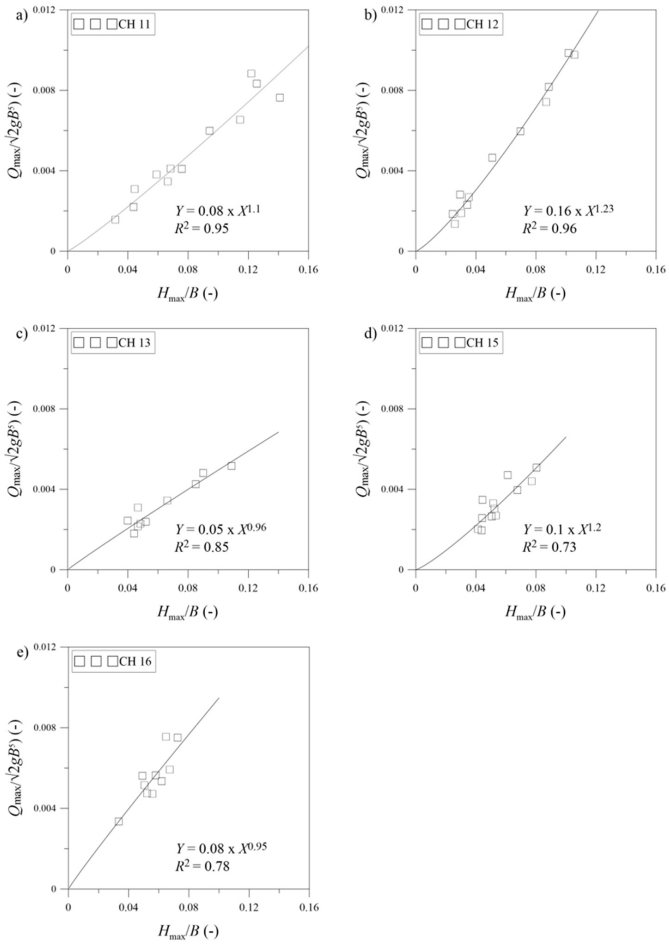

Figure 8. Plot between dimensionless measured maximum overtopping depth and calculated maximum discharge for channel 11, 12, 13, 15, and 16 for an upstream dam slope of 1 to 2.25 for C_d calibration.

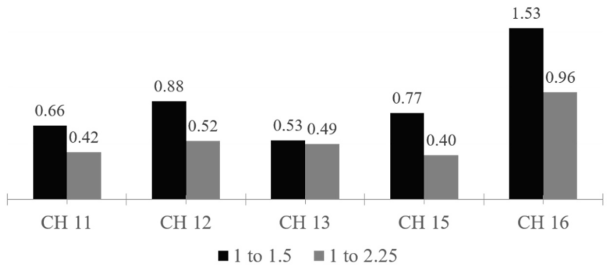

Figure 9. Comparison of C_d values for upstream dam slopes of 1 to 1.5 and 1 to 2.25.

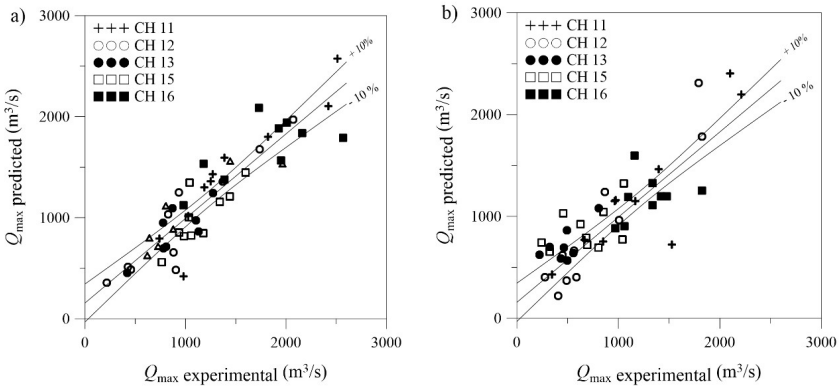

Figure 10. Comparison of calculated and predicted maximum discharge over the dam crest for upstream dam slopes; (**a**) 1 to 1.5 (R^2 = 0.82) and (**b**) 1 to 2.25 (R^2 = 0.72) (full scale), with ± 10% deviation.

Table 5. Coefficients used in the prediction of Q_{max} for each channel using Equation (7). CH, channel.

	1 to 1.5 Dam			1 to 2.25 Dam		
	x	y	R^2	x	y	R^2
CH 11	0.06	0.98	0.83	0.08	1.10	0.95
CH 12	0.07	0.92	0.82	0.16	1.23	0.96
CH 13	0.07	1.07	0.42	0.05	0.96	0.85
CH 15	0.09	1.01	0.75	0.10	1.20	0.73
CH 16	0.08	0.83	0.47	0.08	0.95	0.78

3.3. Maximum Overtopping Depth

One of the key parameters in dam overtopping due to landslide-generated waves is the overtopping depth, d_o, at the dam crest. Referring to Equation (7), the overtopping discharge over the dam crest as a result of these waves is defined primarily based on the overtopping depth, where identifying its value is of great importance. For a creeping slide, once the overtopping depth is predicted from the measured slide, reservoir, and dam parameters, it is easy to calculate Q_{max} values over the dam crest with Equation (7) and the coefficients from Table 5.

Hence, an empirical relation between the relative maximum overtopping depth and the governing parameters—that is, relative slide volume W_s/H^3, the dam front face angle $\beta/90^\circ$, the relative still water depth h/H, and the relative slide release height h_o/H—is derived based on the dimensional analysis as follows:

$$\frac{d_{max}}{H} = \mathrm{a}\left[\left(\frac{W_s}{H^3}\right)^{\mathrm{b}}\left(\frac{\beta}{90^0}\right)^{\mathrm{c}}\left(\frac{\mathrm{h}}{H}\right)^{\mathrm{d}}\left(\frac{h_o}{H}\right)^{\mathrm{e}}\right], \quad (8)$$

where the coefficients are listed in Table 6 for each channel with the following limitations of parameters: $2.2 < W_s/H^3 < 6.87$, $0.27 < \beta/90^\circ < 0.37$, $0.90 < h/H < 0.94$, $1.56 < h_o/H < 6.25$.

On the basis of the analysis, the relative maximum overtopping depth d_{max}/H significantly increases with W_s/H^3 and h/H for all channels. For a constant dam height, h and f provided are related and can be used in an interchangeable manner. Hence, the larger freeboard provided for a dam yields the minimum overtopping depth and further overtopping discharge over the dam crest as a result of slide-generated waves considering the constant B.

Table 6. Coefficients used in the prediction of d_{max} for each channel with Equation (8).

	a	*b*	*c*	*d*	*e*	R^2
CH 11	0.02	0.97	−0.20	0.81	0.31	0.80
CH 12	0.01	1.33	−0.27	1.76	0.32	0.90
CH 13	0.02	0.74	−0.01	0.88	0.24	0.70
CH 15	0.02	0.55	−0.50	0.15	0.13	0.70
CH 16	0.03	0.47	−0.46	5.52	0.38	0.60
Range	0.01 to 0.03	0.47 to 1.33	−0.5 to −0.01	0.15 to 5.52	0.13 to 0.38	

4. Discussion

4.1. General

The present study simplifies a dynamic phenomenon and is based on the assumption that the maximum overtopping discharges of landslide-generated waves can be evaluated with a formulation derived for steady state flow on a weir. However, a rapidly varied flow occurs, and inertial effects exist. Additionally, the front of the slide-generated impulse wave is not parallel to the dam crest and the distribution of the wave is not uniform as it overtops the dam crest. The motivation for the approach presented in this study is to provide a simple means for rough estimation and preliminary information for cases relating to the model setup, that is, relatively narrow mountain reservoirs. Such estimates and preliminary information can be used in risk assessments and in planning the monitoring of the landslide geohazard with due consideration of interrelations to other hazards [40,41]. Direct consideration and physical modelling of a landslide impinging perpendicularly to the reservoirs longitudinal axis are difficult to find in the literature. This setting, however, considers that the shape of a reservoir in a narrow mountain valley is usually longer than its width (see Figure 1), and thus with a potential landslide threat from the mountain slopes along the length of the reservoir. Hence, a potential landslide may fall from these mountain slopes approximately perpendicular to the reservoir's longitudinal axis, and this results in the distribution of the wave not being uniform as it overtops the dam crest. The distribution of the overtopping wave and the variation in overtopping duration is further discussed below, as well as the calculation procedure provided.

4.2. Overtopping Depth and Duration

A general predictive method for maximum discharge (Equation (7)) was presented above based on steady state equation for dams having upstream dam slopes of 1 to 1.5 and 1 to 2.25. Within the framework of the simplified approach, the predictive equation is validated by plotting the experimental discharge with the predicted one, which shows good correlation with 10% deviation (Figure 10). The discharge over a dam as a result of slide-generated waves is expressed based on the maximum overtopping depth. Hence, for the fixed setup (Table 1), which includes a constant slide ramp inclination $\alpha = 50°$, a predictive equation for d_{max} (Equation (8)) is proposed based on slide volume, slide release height, still water depth, upstream dam slope angle, and dam height. The slide velocity, as it impinges the water surface, is indirectly considered through the slide release height and the slide volume, which both influence the slide velocity for the current case. For the fixed setup (Table 1) with the constant slope ramp and a fixed slide volume, increasing the slide release height increases the slide impact velocity. Similarly, considering a constant release height of a slide on the constant slope ramp, a larger volume of slide has a higher impact velocity than the smaller one. The limitation inherent in a setup with a landslide ramp with a constant slope angle must be recognized because the landslide-generated wave height is, among other things, dependent on the slope angle [42]. On the basis of the analysis, both the relative slide volume and relative still water depth were found to have a significant effect on the relative overtopping depth. The d_{max} for all channels relative to CH 11 are illustrated in Figure 11.

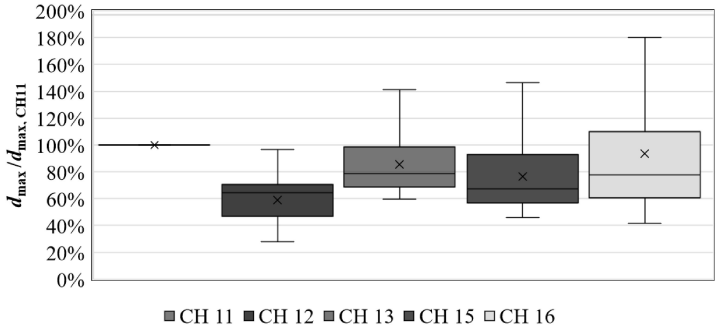

Figure 11. Box plot for the overtopping depth distribution of all channels standardized with overtopping depth measured in channel 11.

Heller et al. [14] discusses the effect of the reservoir shape with two extreme cases. The first case considers a long reservoir and a slide that impacts into this longitudinally, whereas the second case considers that a slide mass can impact at any possible location into the reservoir and the slide width is less than the reservoir. In the second case, the reservoir geometry is such that the impulse wave can propagate radially and freely from the slide impact zone. In 3D settings, the wave parameters depend on the wave propagation angle. This can be seen in the overtopping depth distribution in Figure 11, where a relatively high value is observed at CH 16. On average, a higher overtopping volume is recorded at the edges (CH 11 and CH 16) and a lower overtopping volume is recorded in the middle (CH 12, CH13, and CH 15) of the dam crest sections. Initially, only three channels were installed in other studies using the physical model. However, noting the uneven overtopping over the crest, the number of channels was increased to five to get a somewhat clearer picture of the overtopping distribution.

Overtopping duration is one of the factors for calculating the discharge over a dam for a certain overtopping volume. A higher overtopping volume for short duration of overtopping yields a higher discharge over the crest. Contrary to Figure 11, the duration of overtopping seems to be smaller for the channels at the extreme edges (CH 11 and CH 16) (see Figure 12) for which high overtopping depths are observed. Consequently, higher overtopping discharge values are observed at the edges of the dam crest sections.

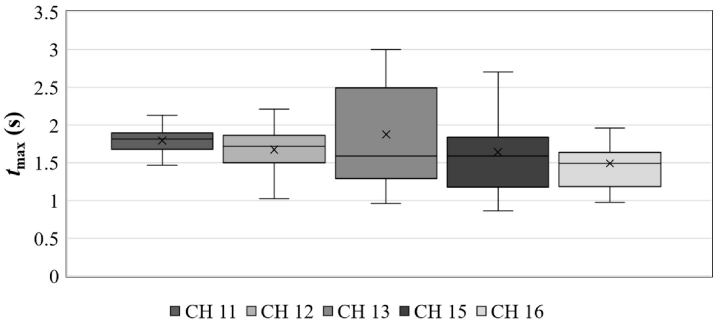

Figure 12. Box plot for the maximum overtopping duration for each channel along the dam crest.

Depending upon the geometry of a particular reservoir, the wave parameters can be computed with a 3D or a 2D approach and fed into 2D run up equations (e.g., the works of [43,44]). For example,

a predictive equations for overtopping volume and duration has been presented for 2D cases without freeboard $f = 0$ [15] and for cases with freeboard $f > 0$ [19].

4.3. Calculation Procedure

A general layout of the calculation procedure proposed in this study is described in Figure 13. For a creeping slide with measured values of slide, dam, and reservoir parameters with the model setup as seen in Figure 1b, one can determine d_{max} for each section of the dam. Then, the maximum overtopping discharge can be calculated with the proposed equation (Equation (7)) with calibrated coefficient values for x and y values listed in Table 5 for each channel. This overcomes the three step procedures (i.e., calculating the overtopping volume and then duration) presented in the literatures for predicting the discharge values. This can be an input parameter for roughly identifying the stone size of riprap to protect the dam against erosion due to slide-generated waves.

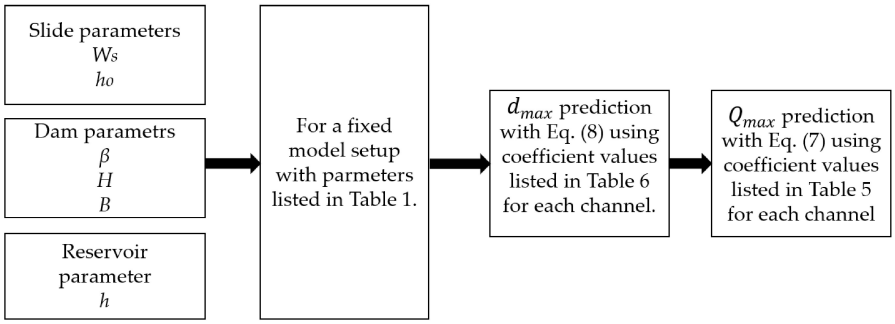

Figure 13. Flow chart showing the proposed calculation procedure for the overtopping discharge.

The calculation procedure presented in Figure 13 is only to be used for a rough prediction of the overtopping discharges for use in hazard and risk assessments as well as preliminary evaluation of potential erosion protection. In any case, the predicted values should be critically evaluated and carefully applied. The application should consider that the dynamic behavior of the overtopping process is not accounted for. Furthermore, limitations of the model setup having the fixed parameters listed in Table 1 must be kept in mind.

5. Conclusions

The present study deals with quantifying the overtopping discharge of waves over dams as a result of landslide-generated waves. An analysis was made to investigate whether a steady state weir equation for predicting discharge can be applied in the case of a landslide-generated wave overtopping a dam. The motivation for this approach was to provide a simple mean for rough estimates of the overtopping discharges to use in preliminary assessments. The predicted overtopping discharges may further bring forth the need for a more detailed study and analysis for a particular dam and a reservoir, considering also dynamic aspects.

The test program involved experiments with a variation of governing parameters including slide release height, slide volume, still water depth, and upstream dam slope. The model simulates a narrow reservoir where the slide impinges from one of the abutments, perpendicular to reservoir's longitudinal axis, whereas the literature mainly describes results from model tests in a wave flume with the landslide waves generated directly opposite to the dam. On the basis of the results from the experiments and data analysis, calibration of the coefficient of discharge c_d values for each dam channel section is obtained from the steady state equation relating the d_{max} and Q_{max}. This value ranges from (0.53 to 1.53) and (0.4 to 0.96) for upstream dam slopes of 1 to 1.5 and 1 to 2.25, respectively (see

Figure 9). The steeper the upstream dam slopes, the higher the value of the observed coefficient of discharge.

A two-step calculation procedure is presented (Figure 13) for the overtopping discharge based on d_{max} values (Equation (7) with coefficients listed in Table 5). Unlike previous studies, the overtopping discharge value can be directly estimated based on the overtopping depth. The results from the proposed equation are compared those calculated (from measured overtopping volume) with a good correlation (R^2 = 0.82 and R^2 = 0.72 for upstream dam slopes of 1 to 1.5 and 1 to 2.25, respectively). However, it should be noted that the limitations in the model setup with fixed model parameters stated in Table 1 should be considered when applying the results from this study, as well as the fact that the dynamic behavior of the overtopping phenomena is not accounted for.

An empirical data analysis was done to arrive at Equation (8) for d_{max} based on slide volume, slide release height, still water depth, dam height, and upstream dam slope, considering a constant slide ramp inclination in all tests. The result highlights the dominant effect of relative slide volume and relative still water depth. Limitations to fit equations are described in the paper.

Author Contributions: Conceptualization, N.N.T., F.G.S., and L.L.; Formal analysis, N.N.T.; Investigation, N.N.T.; Project administration and supervision, F.G.S.; Writing, N.N.T.; Review and editing, F.G.S., Review, L.L. and A.K.J. All authors have read and agreed to the published version of the manuscript.

Funding: This research was funded by Norwegian Water Resources and Energy Directorate (NVE), Project 80051.

Acknowledgments: The support and cooperation of the Norwegian Water Resources and Energy Directorate (NVE) and Grethe Holm Midttømme in associated study and research program at NTNU is gratefully acknowledged. The contribution of Kiflom W. Belete in the early model development and on technical issues is appreciated. The important contribution of Jochen Aberle in the development of the model and Geir Tesaker in the lab is acknowledged. The first author would like to acknowledge the support from Addis Ababa University, School of Civil and Environmental Engineering, as well as from NTNU.

Conflicts of Interest: The authors declare no conflict of interest.

Nomenclature

A (m^2)	area under the curve;
b (m)	slide width;
B (m)	weir length;
b_b (m)	reservoir bottom width;
B_c (m)	crest width;
C_d (-)	coefficient of discharge;
d_{max} (m)	maximum overtopping depth;
f (m)	freeboard;
g (m/s^2)	gravitational acceleration;
h (m)	still water depth;
h_o(m)	landslide release height;
H (m)	dam height;
H_{mo} (m)	the overtopping height;
H_{max} (m)	maximum overtopping height;
l_b (m)	reservoir length;
l_c (m)	crest length;
l_s (m)	slide length;
q (m^3/s/m)	the mean overtopping discharge per meter;
Q_{max} (m^3/s)	maximum discharge;
R^2	Coefficient of determination;
t (s)	overtopping duration;
W_S (m^3)	slide volume;
x and y	calibrated coefficients for each dam section;
V (m^3)	overtopping volume;
α (^{o})	slide ramp inclination;

θ (°) slope of side banks;
β (°) upstream dam slope angle.

References

1. Bosa, S.; Petti, M. Shallow water numerical model of the wave generated by the Vajont landslide. *Environ. Model. Softw.* **2011**, *26*, 406–418. [CrossRef]
2. Manenti, S.; Amicarelli, A.; Todeschini, S. WCSPH with Limiting Viscosity for Modeling Landslide Hazard at the Slopes of Artificial Reservoir. *Water* **2018**, *10*, 515. [CrossRef]
3. Panizzo, A.; de Girolamo, P.; Petaccia, A. Forecasting impulse waves generated by subaerial landslides. *J. Geophys. Res. Oceans* **2005**, *110*, C12025. [CrossRef]
4. Fritz, H.M.; Mohammed, F.; Yoo, J. Lituya Bay Landslide Impact Generated Mega-Tsunami 50th Anniversary. *J. Pure Appl. Geophys.* **2009**, *166*, 153–175. [CrossRef]
5. Wiegel, R.L. Laboratory studies of gravity waves generated by the movement of a submerged body. *Trans. Am. Geophys. Union* **1955**, *36*, 759. [CrossRef]
6. Kamphuis, J.W.; Bowering, R.J. Impulse waves generated by landslides. *Coast. Eng. Proc.* **1970**, *1*. [CrossRef]
7. Watts, P. Tsunami Features of Solid Block Underwater Landslides. *J. Waterw. Port Coast. Ocean Eng.* **2000**, *126*, 144–152. [CrossRef]
8. Heller, V.; Hager, W.H. Wave types of landslide generated impulse waves. *Ocean Eng.* **2011**, *38*, 630–640. [CrossRef]
9. Fritz, H.M.; Hager, W.H.; Minor, H.E. Landslide generated impulse waves. 1. Instantaneous flow fields. *Exp. Fluids* **2003**, *35*, 505–519. [CrossRef]
10. Fritz, H.M.; Hager, W.H.; Minor, H.-E. Landslide generated impulse waves. 2. Hydrodynamic impact craters. *Exp. Fluids* **2003**, *35*, 520–532. [CrossRef]
11. Fritz, H. PIV applied to landslide generated impulse waves. In *Laser Techniques for Fluid Mechanics*; Springer: Berlin/Heidelberg, Germany, 2002; pp. 305–320. ISBN 978-3-662-08263-8.
12. Fritz, H.M.; Hager, W.H.; Minor, H.-E. Near Field Characteristics of Landslide Generated Impulse Waves. *J. Waterw. Port Coast. Ocean Eng.* **2004**, *130*, 287–302. [CrossRef]
13. Huber, A.; Hager, W.H. Forecasting impulse waves in reservoirs. In Proceedings of the Proc. 19th Congrès des Grands Barrages; ICOLD: Paris, France, 1997; pp. 993–1005.
14. Heller, V.; Hager, W.H.; Minor, H.-E. *Landslide Generated Impulse Waves in Reservoirs: Basics and Computation*; ETH Zürich: Zürich, Switzerland, 2009.
15. Müller, D.R. *Auflaufen und Überschwappen von Impulswellen an Talsperren*; ETH Zürich: Zürich, Switzerland, 1995.
16. Xiao, H.; Lin, P. Numerical Simulation of Dam Overtopping Events Caused by the Landslide Generated Impulse Waves in Mountainous Reservoirs. In Proceedings of the 12th International Conference onHydroscience & Engineering, Tainan, Taiwan, 6–10 November 2016.
17. Romano, A.; Di Risio, M.; Bellotti, G.; Molfetta, M.G.; Damiani, L.; De Girolamo, P. Tsunamis generated by landslides at the coast of conical islands: experimental benchmark dataset for mathematical model validation. *Landslides* **2016**, *13*, 1379–1393. [CrossRef]
18. Enet, F.; Grilli, S.T. Experimental Study of Tsunami Generation by Three-Dimensional Rigid Underwater Landslides. *J. Waterw. Port Coast. Ocean Eng.* **2007**. [CrossRef]
19. Kobel, J.; Evers, F.M.; Hager, W.H. Impulse Wave Overtopping at Rigid Dam Structures. *J. Hydraul. Eng.* **2017**, *143*, 04017002. [CrossRef]
20. Huber, L.E.; Evers, F.M.; Hager, W.H. Solitary wave overtopping at granular dams. *J. Hydraul. Res.* **2017**, *55*, 799–812. [CrossRef]
21. Tessema, N.N.; Sigtryggsdóttir, F.G.; Lia, L.; Jabir, A.K. Case Study of Dam Overtopping from Waves Generated by Landslides Impinging Perpendicular to a Reservoir's Longitudinal Axis. *JMSE* **2019**, *7*, 221. [CrossRef]
22. De Girolamo, P.; Di Risio, M.; Romano, A.; Molfetta, M.G. Landslide Tsunami: Physical Modeling for the Implementation of Tsunami Early Warning Systems in the Mediterranean Sea. *Procedia Eng.* **2014**, *70*, 429–438. [CrossRef]

23. Liu, P.L.-F.; Wu, T.-R.; Raichlen, F.; Synolakis, C.E.; Borrero, J.C. Runup and rundown generated by three-dimensional sliding masses. *J. Fluid Mech.* **2005**, *536*, 107–144. [CrossRef]
24. Manenti, S.; Wang, D.; Domínguez, J.M.; Li, S.; Amicarelli, A.; Albano, R. SPH Modeling of Water-Related Natural Hazards. *Water* **2019**, *11*, 1875. [CrossRef]
25. Manenti, S.; Pierobon, E.; Gallati, M.; Sibilla, S.; D'Alpaos, L.; Macchi, E.; Todeschini, S. Vajont Disaster: Smoothed Particle Hydrodynamics Modeling of the Postevent 2D Experiments. *J. Hydraul. Eng.* **2016**, *142*, 05015007. [CrossRef]
26. Li, G.; Chen, G.; Li, P.; Jing, H. Efficient and Accurate 3-D Numerical Modelling of Landslide Tsunami. *Water* **2019**, *11*, 2033. [CrossRef]
27. Vacondio, R.; Mignosa, P.; Pagani, S. 3D SPH numerical simulation of the wave generated by the Vajont rockslide. *Adv. Water Resour.* **2013**, *59*, 146–156. [CrossRef]
28. Løvholt, F.; Glimsdal, S.; Lynett, P.; Pedersen, G. Simulating tsunami propagation in fjords with long-wave models. *Nat. Hazards Earth Syst. Sci.* **2015**, *15*, 657–669. [CrossRef]
29. Mortensen, R.; Lia, L.; Hammeren, R.; Glimsdal, S.; Harbitz, C.B.; Belete, K.W. *Overtopping of Rockfill Dams from Landslide Generated Waves*; Trcold: Antalya, Turkey, 2016.
30. Ponziani, L.; Gardoni, M. Landslide generated waves in dam reservoirs—Experimental investigation on a physical hydraulic model. Master's Thesis, NTNU, Trondheim, Norway, 2017.
31. Biedermann, J. Overtopping of embankment dams from landslide generated waves. Master's Thesis, NTNU, Trondheim, Norway, 2017.
32. Øvregård, E.; Lia, L. *Skred i Magasin—Overtopping av Fyllingsdam Fra Skredgenererte Bølger i Magasin*; NVE: Eden Prairie, MN, USA, 2018.
33. Sigtryggsdottir, F.G. *Landslides into Reservoirs. Overtopping of Embankmnet Dams*; Progress report; NTNU: Trondheim, Norway, 2017.
34. Hiller, P.H.; Lia, L.; Aberle, J. Field and model tests of riprap on steep slopes exposed to overtopping. *J. Appl. Water Eng. Res.* **2018**. [CrossRef]
35. Mehaute, B.L. *An Introduction to Hydrodynamics and Water Waves, Springer Study Edition*; Springer-Verlag: Berlin, Germany, 1976; ISBN 978-3-642-85567-2.
36. Heller, V.; Hager, W.H.; Minor, H.-E. Scale effects in subaerial landslide generated impulse waves. *Exp Fluids* **2008**, *44*, 691–703. [CrossRef]
37. Van der Meer, J.; Pullen, T.; Allsop, W.; Bruce, T.; Schüttrumpf, H.; Kortenhaus, A. Prediction of Overtopping. In *Handbook of Coastal and Ocean Engineering*. 2009, pp. 341–382. Available online: https://www.academia.edu/17255961/Prediction_of_Overtopping (accessed on 5 January 2020).
38. Pullen, T.; Allsop, N.W.H.; Bruce, T.; Kortenhaus, A.; Schüttrumpf, H.; Van der Meer, J.W. EurOtop wave overtopping of sea defences and related structures: Assessment manual. In *Die Küste*; Kuratorium für Forschung im Küsteningenieurwesen: Heide im Holstein, Germany, 2007; Available online: http://www.kennisbank-waterbouw.nl/DesignCodes/EurOtop.pdf (accessed on 5 January 2020).
39. Yarde, A.J.; Banyard, L.S.; AIIsop, N. *Reservoir Dams: Wave Conditions, Wave Overtopping and Slab Protection*; HR Wallingford: Wallingford, UK, 1996; p. 62.
40. Sigtryggsdóttir, F.G.; Snæbjörnsson, J.T.; Grande, L.; Sigbjörnsson, R. Interrelations in multi-source geohazard monitoring for safety management of infrastructure systems. *Struct. Infrastruct. Eng.* **2016**, *12*, 327–355. [CrossRef]
41. Sigtryggsdóttir, F.G.; Snæbjörnsson, J.T. Geological challenges and geohazard monitoring of a mega engineering hydropower project in Iceland. *Eng. Geol.* **2019**, *259*, 105152. [CrossRef]
42. Panizzo, A.; de Girolamo, P.; di Risio, M.; Maistri, A.; Petaccia, A. Great landslide events in Italian artificial reservoirs. *Nat. Hazards Earth Syst. Sci.* **2005**, *5*, 733–740. [CrossRef]

43. Heller, V.; Spinneken, J. On the effect of the water body geometry on landslide–tsunamis: Physical insight from laboratory tests and 2D to 3D wave parameter transformation. *Coast. Eng.* **2015**, *104*, 113–134. [CrossRef]
44. Evers, F. Spatial Propagation of Landslide Generated Impulse Waves. Ph.D. Thesis, ETH Zurich, Zürich, Switzerland, 2017.

Paper III

Landslide Generated Wave Runup over a Rigid Dam for Freeboard Prediction

Netsanet Nigatu, Fjola G. Sigtryggsdottir, Leif Lia, Asie Kemal

Submitted to Journal of Applied Water Engineering and Research

---

Paper IV

The Impact of Freeboard on Embankment Dams

Netsanet Nigatu Tesema, Leif Lia, Asie Kemal Jabir, Fjola G. Sigtryggsdottir

HydroAfrica 2017 - International conferecene on dam safety and hydropower, Marrakash, Morocco

---

The Impact of Freeboard on Embankmnet Dam

Netsanet Nigatu Tesema

School of Civil and Environmental Engineering

Addis Ababa Institute of Technology

King George VI St, Addis Ababa 1000

Ethiopia

Asie Kemal Jabir

School of Civil and Environmental Engineering

Addis Ababa Institute of Technology

King George VI St, Addis Ababa 1000

Ethiopia

Leif Lia

Dep. of civil and environmental engineering

Norwegian University of Science and Technology (NTNU)

NO-7491 Trondheim

Norway

Fjola G. Sigtryggsdottir

Dep. of civil and environmental engineering

Norwegian University of Science and Technology (NTNU)

NO-7491 Trondheim

Norway

Abstract

Embankment dams are the most common dam type worldwide: more than 80% of dams are embankment dams. Throughout history many dam failures have occurred and embankment dams in particular are frequently represented in the statistics. The most common cause of failure of embankment dams is overtopping. The lack of freeboard provided is the main cause of overtopping in embankment dams. Freeboard is the vertical distance of a dam crest above the maximum reservoir water level.

It is clear that the goal of constructing completely stable dams cost effectively is challenging. This is because the parameters used in dam design have variable uncertainties which lead to variations in capacity and safety of the dam. Traditionally, these uncertainties were addressed by deterministic analysis of extreme events. Nowadays, the risk based design procedures for analyzing the role of uncertainties in safety analysis are given increasing importance. This approach considers higher order uncertainty in parameters and models. Risk is a combined measure of the probability and the severity of an adverse effect. It is estimated by the product of the probability of the occurrence of an event and the expected impact. Both of these factors have uncertainties associated with them.

The purpose of this paper is to provide a consistent approach to the analysis and design of safe freeboard. Safe freeboard will protect an embankment dam from overtopping as a result of the simultaneous effects of wind generated wave run up and landslide generated waves. This paper describes the ongoing research on this topic and presents models to be assessed and developed during the PhD-study.

1. Introduction

The construction of safe and cost effective dams is important for the development of sustainable cultures and economies. In areas with scarcity of water, dams are required for water storage during dry periods. However, a dam construction and operation, has some serious consequence potential, for instance, costs, environmental impact and risk of loss of lives and properties in the downstream area. Overtopping is the primary cause in 31% of embankment dam failures, and is a secondary cause in 18 % of failures (ICOLD, 1995) Overtopping may happen for different reasons, such as insufficient spillway capacity, blocked spillways, wind and landslide generated waves, settlement etc. The most important parameter to prevent overtopping is thus the freeboard; the vertical height between the water surface and the dam crest.

The dam crest must be constructed with the consideration of other functions too, such as protection against war action, protection of the core from weathering processes, sufficient width for vehicles etc. All of these influence the design of the freeboard and the dam crest. Although the dam crest and freeboard appears to be a relatively small structure on the top of the dam, incremental changes in the design at the top influences the volume in the bottom section of the embankment dam. One meter of increased height requires a one-meter-thick layer in the full bottom section leading to substantial cost increases for the dam. Due to this effect on construction costs, a desirable aim is for dam freeboard to be minimized despite an increased risk for dam failure. Finding the optimum freeboard is a crucial research topic for dam constructed for different purposes under different conditions. This paper proposes design criteria to be investigated for designing the optimum freeboard, included model tests to study the simultaneous effects of landslide and wind generated waves on the design of freeboard considering different model setups.

Figure 1. Dam crest exposed to overtopping, Photo: Leif Lia

Figure 2. Dam crest exposed to overtopping and failure, Photo: IMPACT

2. Background

Generally the objective of having sufficient freeboard is to provide the necessary assurance against overtopping resulting from: wind setup and wave run up, landslide and seismic motion, settlement, malfunction of structures, other uncertainties in design, construction and operation (USBR, 1981). It states that freeboard will be calculated based on the probability of simultaneous occurrence of those factors. There is a consistent approach proposed by USBR (2012) to the analysis and design of freeboard to protect an embankment dam from overtopping as a result of wind generated waves run up and reservoir setup. It describes methods for determining the minimum, intermediate and normal freeboard based on the reservoir water level. When the reservoir is at the maximum elevation, the minimum freeboard should be greater than 3feet or the sum of the setup and run up that would be generated by the typical winds. When the reservoir is at normal reservoir water level, the normal freeboard will be calculated by adding the level of NRW and run up and setup for a specific determined wind velocity.

2.1 Dam failure mechanisms

When an embankment dam is overtopped the dam breaching process may be triggered by the two main processes:

- stability failure of the slope
- erosion processes in the downstream slope

The switch between these processes is mostly according to the inclination of the slope. The IMPACT project reported by (Løvoll, 2006) reported that with slopes inclined 1:2,5 – 1:3 the failure mechanism changes from stability failure to erosional failure. The IMPACT project did not report any influence from the freeboard on the failure modes. This is obvious since the overtopping itself is the cause of the failure.

For calculating the breaching process induced by overtopping models like BREACH, DAMBRK, HEC-1 can be used and breach characteristics such as the size, shape, time of formation will be predicted. (Hiller et.al 2015) describes of two main flow processes induced by the overtopping of an embankment dam: throughflow in the dam body, and a free surface flow along the dam face (see e.g. Figure 2). Depending on the embankment structure, the duration of overflowing and the magnitude of the overtopping, the relationship between these two types of flow change, resulting in different failure modes.

2.2 Freeboard

The freeboard provided for an embankment dam must be sufficient to prevent the overtopping of the dam that could result from a reasonable combination of number of factors. (Goodarzi et.al, 2012) applied risk and uncertainty analysis to dam overtopping due to various inflows and wind speeds. In this paper the effects of large floods, wind and landslide generated waves are considered as the predominant factors for embankment dam freeboard design.

3. Probability

3.1 Uncertainties

The probability of failure of a system arises from the uncertainties of the load (L) and resistance (R) of the system. Calculation of the probability of failure requires the statistics and distribution, i.e., uncertainties, of each load and resistance variables (Cheng ST, et al., 1982). Depending on the availability of the statistical information on each load and resistance variable and the complexity of the function describing this, various methods have been used to evaluate the risk. The most common ones include Monte Carlo Simulation Method (MCS), Latin Hypercube Sampling (LPS), Mean Value First-Order Second-Moment (MFOSM), and Advanced First-Order Second-Moment (MFOSM), and these are discussed in detail by (Negede A. K., 2009), (Cheng ST et al., 1982), and (Goodarzi E. et al., 2013).

3.2 System failure model

A system's failure can be defined as the system's inability to perform expected tasks. Quantitatively, it is expressed as the load (L) exceeding system resistance or capacity (R) (Goodarzi E. et al., 2013).:

$$\text{Probability of failure} = P(L > R) \quad \ldots\ldots (1)$$

$$= P(Z < 0)$$

Where P() is the probability of failure; Z is a performance function which can be defined as $Z = R - L, Z = R/L - 1, and\ Z = \ln(R/L)$. Load and resistance are terms that have been used in structural engineering. However, they have found wide application in the risk analysis of water resources engineering projects. An example is the failure of a dam due to overtopping. The risk would involve the probability that the water surface elevation in a reservoir exceeds the elevation of the top of the dam. In this case the resistance is the elevation of the top of the dam (freeboard included) and the loading is the maximum elevation of the water surface in the reservoir.

Generally, both the Load and Resistance are expressed as functions of their components

$$L = g_L(X_i) \quad i = 1,2,\ldots.n \qquad \ldots\ldots\ldots\ldots\ldots\ldots\ldots\ldots (2)$$

$$R = g_R(X_j) \quad j = n+1,2,\ldots.m$$

Where X_i, i = 1,2…n, denotes the component variables of the load, and X_j, j = n+1,….m, represents component variables of the resistance.

3.3 Overtopping

A dam is subjected to the occurrence of loading induced by various natural forces during its service life. Overtopping occurs when the water level behind a dam rises above the crest of the dam. Events that contribute to overtopping include failure to make timely and adequate release of flood through the spillway and flood release outlets, waves induced by wind, landslide and other natural forces; and the combined effects of the two.

The probability of overtopping, P[Fv] can be evaluated

$$P[F_V] = P[E_1 U\ E_2\ U \dots \dots \dots U\ E_n] \quad \dots \dots \dots \dots \dots \dots \dots \dots \dots \dots (3)$$

In which E_i represents the failure event of overtoppings due to the i-th natural force. If we denote by h_G the height of the reservoir water raised by an occurrence of a natural force, such as a flood, H_D the height of the dam embankment, and Ho the stage of the reservoir water level before the occurrence of the natural force G, overtopping occurs when (h_G+H_o > H_D). Accordingly, the risk of overtopping, P_G, given an occurrence of G can be expressed as

$$P_G = P[h_G + H_O > H_D] \quad \dots \dots \dots \dots \dots \dots (4)$$

$$= P[h_G > H_D - H_O]$$

3.3.1 Overtopping induced by flood

The embankment should be safe against overtopping during the occurrence of the inflow design flood by the provision of sufficient spillway and outlet capacity. The proper design of a dam's spillway and the flood control capacity of a reservoir can ensure the safety of the dam and avoid any undesirable problems, such as overtopping. Hence, an exact estimate of flood design and extreme inflow hydrograph is required. Traditionally, the approach to dam design emphasizes deterministic analysis on extreme events, such as probable maximum flood (PMF). However, PMF has two problems, first of all the PMF has changed over time. Secondly, the PMF standard does not take into account any risk, costs and economic benefits. Nowadays, due to high uncertainties in the parameters in design, risk based analysis is being used in some places. (Goodarzi et.al., 2013) presented the application of risk and uncertainty analysis to dam overtopping based on univariate and bivariate flood frequency analysis.

Generally, when the spillway and outlets of a dam fail to make timely and adequate release of water that is stored behind the dam, the reservoir level will rise and overtop the crest of the dam. The probability of overtopping due to flood can be defined as

$$P_F = P[h_F > H_D - H_O] \quad \dots \dots \dots \dots \dots \dots \dots \dots \dots (5)$$

In which h_F is the maximum rise of the reservoir level due to flood. The maximum rise of reservoir level could be estimated from the basic equation of reservoir routing.

3.3.2 Overtopping induced by wind generated waves

Wind generated waves on reservoirs are mainly influenced by wind characteristics such as velocity, duration and orientation with respect to the reservoir and by fetch. The fetch is defined as the region in which the wind speed and direction are reasonably constant. The longer the fetch, and the faster the wind speed, the more wind energy is imparted to the water surface and proportionally higher waves will be produced.

In the evaluation of potential overtopping induced by wind generated waves, both wave run up and wind set-up have to be considered.

Wind wave run up h_r is defined as the vertical difference between the highest level attained by the rush of water up the slope and the still water level (SWL). It is governed by the height and steepness of the waves, and by the slope, roughness and porosity of the dam face. Due to the uncertain nature of the incoming waves, each wave will give a different run up level.

Wind set-up is the piling up of water at the leeward end of an enclosed body of water, as a result of the horizontal stress on the water exerted by the wind.

USBR (1992) describe ways to calculate the wave run up height and wind setup. The computation of run up is governed by the angle of the slope, the roughness and permeability of the embankment surface, and the wave characteristics such as the steepness and surf similarity factor (ratio of dam slope to the square root of the wave

steepness) for peak wave heights. Whereas the estimate of wind setup is strongly influenced by the design wind speed, the wind fetch and the average depth of water along the fetch length.

Considering above-mentioned effects that may contribute to overtopping induced by wind: wind setup (h_T) and wave run-up (h_r), the probability of overtopping by wind occurrence can be defined as

$$P_w = P[h_T + h_r > H_D - H_O] \dots\dots\dots\dots\dots\dots\dots\dots (6)$$

A number of formulas have been developed for the computation of the heights of wind setup and wave run-up. The magnitude of wind set up is estimated generally by h_t = f (v, Fe, D) and the vertical run up by h_r = f (Fe, v, β, n, ε), like in USBR (1992).

3.3.3 Overtopping induced by landslide

Waves induced by landslides into bays, fjords, and closed pools, such as reservoirs, have resulted in catastrophic consequences. The case of the landslide-induced wave at Vaiont Reservoir in Italy in 1963, is well known. The wave overtopped an arch dam and inundated the downstream area resulting in 2000 lives lost (Panizzo et al., 2005). This and similar catastrophes drew attention to the importance of considering this phenomenon in the planning and design of dams in landslide prone areas. Consequently, several investigations have been carried out, including into the size of such waves, and their run-up height on a dam face (Ataie-Ashtiani & Yavari-Ramshe, 2011) and (Heller et al., 2009). In some studies, including recent studies at NTNU, discussed later, particular focus is on embankment dams, considering that overtopping may lead to the breaching of such dams, and thus intensifying the threat relating to a landslide-induced wave. Figure 3 from (Heller et al. 2009), explains the three phases of impulse wave development and impact on an embankment dam: (1) a wave is generated as the slide impacts the reservoir, (2) the wave propagates and change and (3) the wave impacts the dam with load transfer and wave run-up potentially overtopping the dam.

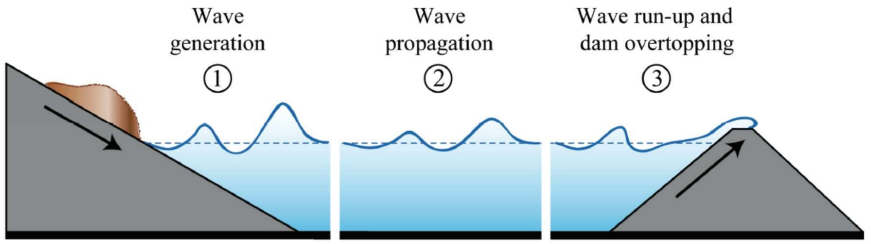

Figure 3. The three phases of a landslide generated impulse wave above a horizontal reservoir bed according to (Heller et al., 2009).

A landslide falling in to the reservoir, if close and large enough, and moving quickly enough, can generate waves large enough to overtop the dam. Sloshing back and forth in the reservoir can result in multiple waves overtopping the dam. The probability of overtopping induced by landslide can be defined as

$$P_L = P[h_L > H_D - H_O] \quad \dots\dots\dots\dots\dots\dots\dots\dots (7)$$

There are several methods available to estimate the height of landslide generated waves, such as in (Heller, 2016), Mortensen et.al, 2016) and (Pugh and Chiang, 1986), and equations such as h_L = f (V, D, v_{slide}, n, T, L) that may express the wave in general terms. h_L is the wave height at the dam, D is the reservoir water depth at the landslide, V is the volume of water displaced by the landslide (usually taken to be the slide volume), and L is the distance from the landslide to the dam, n is the slope of the dam surface and T is the period for the tsunami like wave.

3.3.4 Overtopping induced by concurrence of flood, wind and landslide

(Cheng et al., 1982) noted that the combined load of simultaneous occurrences of different natural forces may be more significant than the load induced by a single natural force. Here the load is the increase in water level above Ho (the stage of the reservoir water level before the occurrence of the natural force). Combination of these loads result in the total magnitude of the increased water level, here expressed as H_T. The magnitude of H_T depends on the duration, magnitude, shape and occurrence time of each component load.

If all the component loads are constant during the coincident occurrence, then H_T is simply equal to

$$H_T = \sum_{i=1}^{n} X_{im} \quad \ldots\ldots\ldots\ldots\ldots\ldots\ldots\ldots\ldots (8)$$

If the intensity of each component load varies with time during the coincident occurrences, then H_T, also varies with time and is given by

$$H_T(t) = \sum_{i=1}^{n} X_i\,(t) \quad \ldots\ldots\ldots\ldots\ldots\ldots\ldots\ldots\ldots\ldots (9)$$

However, the maximum increase in water level, $H_{T,max}$, of the combined load usually is no greater than the sum of the maximum values of the individual loads. This should also represent the critical combination of loads, and thus critical water level increase, defined here as H_C. Considering this, H_C, is given by

$$H_C = H_{T,max} = MAX \sum_{i=1}^{n} X_i\,(t) \quad \ldots\ldots\ldots\ldots\ldots\ldots\ldots\ldots\ldots\ldots (10)$$

In which $X_i(t)$ is the i-th component load at any time t in a coincident occurrence.

For the case of simultaneous occurrences of flood, wind and landslide, the critical water level increase H_c can be calculated as:

$$H_C = MAX\,[h_H(t) + h_Z(t) + h_Y(t)] \ldots\ldots\ldots\ldots (11)$$

In which $h_H(t)$ denotes the height of reservoir level at time t built up by flood, $h_Z(t)$ is the sum of wind setup and wind wave run-up height at time t, and $h_Y(t)$ is the landslide run up wave at time t. The probability of overtopping due to occurrence of flood, wind, and landslide, P_{FWL} can be defined as

$$P_{FWL} = P[L_c > H_C - H_O] \ldots\ldots\ldots\ldots\ldots\ldots\ldots (12)$$

3.3.5 Consequence classes

Different attempts have been made to categorize dams in order to find the optimum focus and use of resources to address dam safety. Fully risk based concepts like risk analysis and probabilistic dam safety analyses have been used in many countries but the popularity for such methodology has varied greatly during the years, see e.g. (Midttømme, Ruud and Lia, 2013).

In the risk analysis approach, the use of acceptance criteria is the usual way to make decisions regarding dam safety, The risk is then either accepted or not. The main reason for abandoning such methods has been the lack of statistical data. More common today is a methodology based on estimating only the consequences from a potential

dam failure. Consequences are listed in groups such as loss of lives, properties or environmental impact. The risks for each group are then assessed by the use of flood wave models like DAMBRK, Hec-Ras, Mike11 etc. From this assessment the dams can be categorized by simple counting approaches. Most such consequence class systems are based on 3 – 5 different classes with a given interval (e.g. class 1 0 – 10 houses, class 2 11 – 100 houses, class 3 101 – 1000 houses and class four > 1000 houses). Other systems are more qualitative by just using a description (class 1 - Minor cons., class 2 - Severe cons. and class 3 - Hazardous cons.). Countries sticking to the consequence class system normally have different design criteria for freeboard and crest width for different classes.

4 Freeboard Design

4.1 Damage and Failures

Freeboard provides a margin of safety against overtopping failure of dams. Its provisions being more critical for embankment dams, as such dams are generally more susceptible to breaching and failure, depending on the materials and configuration and even on environmental conditions.

The lack of sufficient freeboard poses significant flood risks to people and property in the inundation area. A large number of dams fail due to overtopping: Vaiont in Italy in 1963 (overtopping of concrete arch dam by landslide generated wave, not failure), Johnstown Dam in Pennsylvania in 1889 (2200 dead, overtopping of embankment dam), Machu II in India in 1974 (2200 dead, overtopping of embankment dam) and others. Hence understanding and prediction of freeboard are crucial.

There are different factors that should be considered in designing freeboard: flood, wave generated by wind and landslides, reservoir operation and malfunction of spillway and outlet works. Freeboard for embankment dams should also prevent overtopping of the dam by either frequent or infrequent high waves which might interfere with efficient operation of the project, create conditions hazardous to personnel, cause other adverse effects not necessarily associated with the general safety of the structure, or cause a dam breach and failure.

4.2 Sufficient cover of core materials

The dam crest such as in Figure 4 must be constructed with sufficient cover of all core and filter materials. This will influence the current level of the freeboard. The main purposes for this are:

- to ensure sufficient in built quality of all zones
- to minimize the weathering processes
- to keep the filter criteria fulfilled even over the crest
- to avoid frost penetration in sensitive core materials such as clay and moraine (in cold climates)
- The design of the dam crest in different zones shown in Figure 4 will influence the design height of the dam and must be considered together with other criteria for the design of the freeboard

Figure 4. Dam crest during construction, Photo: Priska Hiller

Figure 5. Dam crest with suitable freeboard and cover of core materials, Photo: Leif Lia

4.3 Regulations and guidelines

Dam Safety Guidelines for Eastern Nile Countries present a reference or regional dam safety guideline which addresses the dam safety management issues that may be applicable in the eastern Nile countries. Ethiopia is among the Eastern Nile basin countries, which comprise of Egypt, South Sudan and Sudan. The guideline draws concepts and processes from various international guidelines from within the ICOLD family of Technical and National Committees and also various US Federal Agencies. Due to the limited number of dams designed and constructed from this guideline, little experience is obtained so far.

5. Research and tests to be done

In 2011 the Norwegian Water Resources and Energy Directorate (NVE) initiated, in collaboration with NTNU, a research project focusing on the impact of landslide generated waves in Norwegian hydropower reservoirs, with special emphasis on reservoirs with embankment dams. In relation to this project, several early stage studies have been carried out to this date, mainly conducting model tests with different model setups, referred to in Mortensen et al. (2016). One recent setup is shown in Figure 6. The effects of different parameters relating to both a slide and a dam have been studied, including the following: slide volume, slide width, slide porosity, slide velocity, dam freeboard, upstream dam slope, roughness of the upstream dam face, and inclination of the dam longitudinal axis. In this respect, note that the slide velocity, width, and volume, as well as the depth of the reservoir where the slide impinges, are all included in a so-called impulse product parameter (IPP) defined in (Heller et al., 2009). An increase in any of these parameters also increases the IPP. An exception to this is the porosity. Higher value of the IPP generally results in higher impulse wave, and thus higher run-up wave and overtopping volume. The parameters relating to the dam, other than the freeboard, had insignificant effect. Obviously, a lower freeboard results in a larger volume of water overtopping the dam for the same slide parameters.

This research will be combined with simultaneous running overtopping tests for rockfill dams tests at NTNU, as reported by (Hiller et al., 2015). Further experiments in this PhD study will use both test rigs and optimize the freeboard and dam crest. Different freeboard levels will be recommended based on downstream consequences and cost of construction for the specific rock fill dams.

Figure 6. Model setup for the landslide and reservoir model, Photo: Kiflom Belete

6. Conclusion and remarks

The depth and duration of overtopping and erodibility of the embankment materials are the key parameters to determine the likelihood of dam failure occurring as a result of overtopping. The estimated probability of an embankment dam failure due to overtopping will be site specific and will also be a function of the zoning and details of dam.

The complexity of defining freeboard design criteria for a stable dam has been described in this paper. A method is presented for investigating this further through a failure model, using the concept of reliability from considering load and resistance. The failure model is based on probability, and allows for the potential simultaneous effects of large floods, wind and landslide generated waves. These loading conditions are considered the predominant factors for embankment dam freeboard design. It is planned to investigate further the validity of the main assumptions made in the definition of the model, mainly through model tests.

During the planned study a significant number of tests will be carried out at NTNU corresponding with field investigations on Ethiopian embankment dams. The aim is to set forth a methodology for optimizing freeboard and dam crest. Such a methodology will be of value for numerous new dams to be constructed for different purposes in Ethiopia.

7. References

Ataie-Ashtiani, B., & Yavari-Ramshe, S.," Numerical simulation of wave generated by landslide incidents in dam reservoirs". Landslides,8(4), 417–432. doi:10.1007/s10346-011-0258-8, 2011

Cheng, S.T., Yen, B.C. and Tang, W.H., "Overtopping risk for an existing dam", Civil Engineering Studies, Hydraulic Eng Ser 1982:37.

Goodarzi, E., Mirzaei, M. and Ziaei, M., "Evaluation of dam overtopping risk based on univariate and bivariate flood frequency analysis", Rev Can Genie Civ 39(4):374-387, 2012

Goodarzi, E., Shui, L.T., Ziaei, M., "Dam overtopping risk using probabilistic concepts – Case study: The Meijaran Dam, Iran", 2013

Heller, V et.al, "Landslide generated impulse waves in reservoirs: Basics and Computations", ETH, Zurich, 2009

Hiller, P., Lia, L. and Aberle, J., "Placed riprap as erosion protection on the downstream slope of rockfill dams exposed to overtopping", 25th Congress on Large Dams, ICOLD, Stavanger, 2015

ICOLD Bulletin no 99, "Failure statistical analysis", 1995

ICOLD Bulletin no 124, "Reservoir landslides - investigations and management - Guidelines and case histories", 2000

Løvoll, A., "Breach formation in rockfill dams – results from Norwegian field tests, 22th Congress on Large Dams, ICOLD, Barcelona, 2006 **Midttømme, G.H., Lia, L. and Ruud, A.M.,** "Risk analyses in Norway – rules, recommendations and practical application for dam safety", Symposium on the 81th ICOLD Annual Meeting, Seattle, 2013.Mortensen, R., Hammeren, R., Lia, L., Glimsdal, S., Harbitz, C.B. and Belete, K., "Overtopping of rockfill dams from landslide generated waves", ICOLD European Club Symposium, Antalya, Turkey, 2016

Negede Abate, A. K, "Probabilistic safety analysis of dams: methods and application", University of Dresden, PhD thesis, 2009

Panizzo, A., Girolamo P.D., Di Risio, M., Maistri, A. and Petaccia, A., "Great landslide events in Italian artificial reservoirs", Nat Hazards Earth Syst Sci 5:733–740, 2005

Pugh, C.A. and W.L. Chiang, "Landslide –Generated Wave Studies", ASCE Water Forum, Vol. 1, 1986.

USBR, 1992, "Freeboard criteria and guidelines for computing freeboard allowances for storage dams". Denver (CO): US Dept of the Interior, Bureau of Reclamation, 1992

Appendix A. Calibration

Bucket Calibration

To calibrate the water buckets used for collecting the overtopping volume of water over the dam, a five-step approach is described;

1. Measure the height of empty bucket with the ultrasonic sensor, by placing the sensor at the top of the bucket.
2. Then pour 1 L of water to the bucket and measure the height.

Figure A.1: Measuring the water height in the bucket by pouring 1L of water into it.

3. Repeat this at least ten times by putting an additional 1L of water for each step.
4. Plot the volume of water with the recorded height value for the ten points.
5. Repeat step 1 to 4, at least five times to get the most accurate calibration factor
6. The calibration factor will be the average of the slopes of each line in step 4.
   1L= -5.56V

Wave gauge calibration

The nine wave gauges of type '*DHI wave-meter 102E'* were installed to measure the wave height for each test. All sensors were calibrated before each test, in order to obtain more accurate results.

The procedure for calibrating the wave gauge sensors,

1. After filling up the reservoir to the desired still water depth, leave it for some seconds to still.
2. Fix the zero level by setting each channel at 0V.
3. Then insert a steel bar of 50 mm thickness to elevate the steel bars and set it to -1V value
4. When the calibration process is over, the still bars again put into zero level to start the test.

A calibration factor $\left(\frac{50\ mm}{1\ V}\right)$ is obtained for conversion of the measured voltage into mm.

Ultrasonic sensors calibration

Five ultrasonic sensors were placed above the dam crest to measure the overtopping depth. These sensors have been calibrated by measuring the voltage difference with and without a steel plate of 50 mm thickness.

The following calibration factors is found found for each sensors;

CH 11, 50mm = 4.92V

CH 13, 50mm= 4.93V

CH 15, 50mm= 4.88V

Rotational sensor calibration

The rotational sensor needs to be calibrated for converting the measured voltage into distance. This can be done by pulling out the rope 0.5 m, 1 m, 1.5 m, 2 m, 2.5 m and reading the voltage

recorded, the slope of the line plot between the distance and measured voltage becomes the calibration factor.

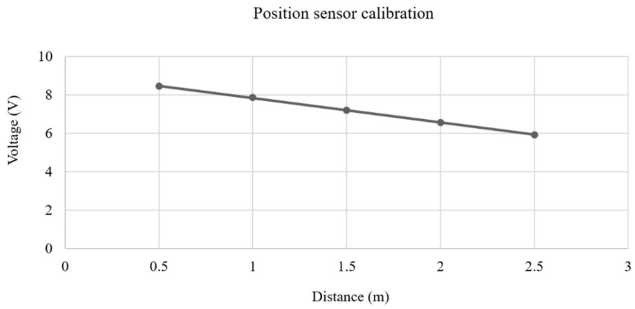

Figure A.2: Distance measured for a rope versus the corresponding voltage reading [37_1.5s_4.5m_2H_200].

Appendix B. Test Procedure

Basically, the test procedure is:

(a) adjustment of the still water level with a point guage;

Figure B.1: Setting up the water level of the reservoir using point guage on the right and piezometer on the left.

(b) loading the slide block on the ramp with the specified release height;

(c) calibration of the wave guage sensors;

(d) calibration of speed sensor;

(e) setting of the agilent measurement software;

(f) release the hook on the slide;

(g) observation of the wave propagation and overtopping process.

Appendix C. Overtopping Volume Calculation

In most of the experiments, three major waves were observed during the impact of landslide generated waves. Figure shows the overtopping height over the dam crest for the three major waves with time of occurrence. Each overtopping wave gives a certain overtopping volume of water with the specified duration. In this section, the volume of water for each wave is determined using a plot between overtopping height with time.

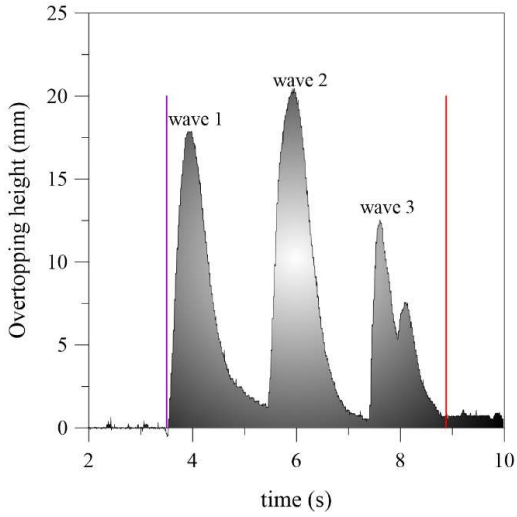

Figure C.1:Plot between maximum overtopping height over the dam crest vs time for the three major waves recorded in channel 11 (Test no. 185_2.25_4.5_2H_200).

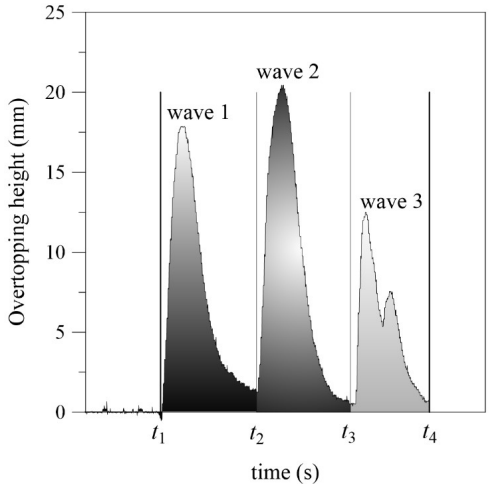

Figure C.2: Overtopping height (mm) vs time (s) plot for maximum discharge calculation considering the three maximum waves recorded in channel 11.

The total volume of water over the dam crest for each section is collected in a bucket and measured for each test. To obtain the volume for each wave: wave 1, wave 2 and wave 3 (Figure C.1), the area under the curve defined by the overtopping height versus time is calculated. In Fig. C.2, wave 1 is defined between times t_1 (initial time) and t_2 (final time), and similarly for the other waves.

Applying the concept of dimensionless quantity based on area and volume, the volume for each wave can be calculated:

$$\frac{\boldsymbol{A_1}}{\boldsymbol{A_t}} = \frac{\boldsymbol{V_1}}{\boldsymbol{V_{total(measured)}}} \tag{1}$$

And recalculating for volume for the first wave (V_1), Eq. (1) can be rearranged as:

$$\boldsymbol{V_1} = \frac{\boldsymbol{A_1 V_{total(measured)}}}{\boldsymbol{A_t}} \tag{2}$$

$$A_t = A_1 + A_2 + A_3$$

where V_1 (m^3) = calculated volume of overtopping water for wave 1; A_1 (m^2) = area under the curve of wave 1; A_t (m^2) = the total area under the curve considering three waves and V_t (m^3) = the total volume of water collected in the bucket.

The overtopping volume calculated in this way for each wave is used to estimate the overtopping discharges.

Appendix D. Parametric Study

Slide impact velocity, slide volume and freeboard related to overtopping volume

Landslide impact velocity is one of the primary parameters to be used for modelling landslide induced waves. Slingerland and Voight (1979) proposed an empirical equation to predict slide velocity as;

$$v_s = v_o + [2g\ s\ (sin\,\beta - tan\,\Phi_s\, cos\,\beta)]^{1/2} \quad (3)$$

where v_s is the slide speed, v_o is the initial slide speed, g is the gravitational acceleration, s is the landslide travel distance from the toe of the landslide mass to the water's edge, β is slope angle of the slide in degrees and Φ_s is angle of internal friction. The initial slide speed is assumed to be 0 m/s.

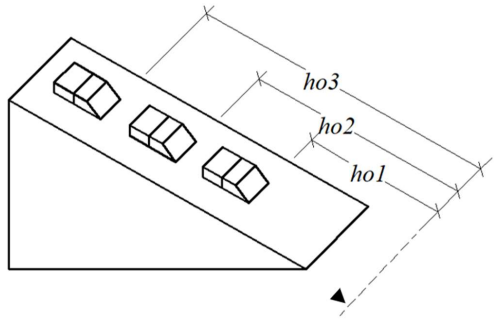

Figure D.1: Definition sketch for the slide impact velocity V_s determination of three identical slides at different slide releasing height (h_{o1}, h_{o2} and h_{o3}).

As seen from Eq. (3), the slide speed is described based on the slide position, the slope angle and angle of internal friction. The results from the experiments of the present study confirm that the initial position of the slide edge relative to the still water level (Fig. D1) is the most dominant parameter which directly influence the speed of the slide (Fig. D2). Increasing the travel distance of the slide to the water increases the value of landslide speed significantly. Slide impact speed in the range of 29 m/s to 60 m/s were observed in this study for different

slide arrangement and position. High speeds have been reported on in the literature, for example the up to 40 m/s backcalulated from the fall of a 100 ton rock boulder (Hungr, 2007).

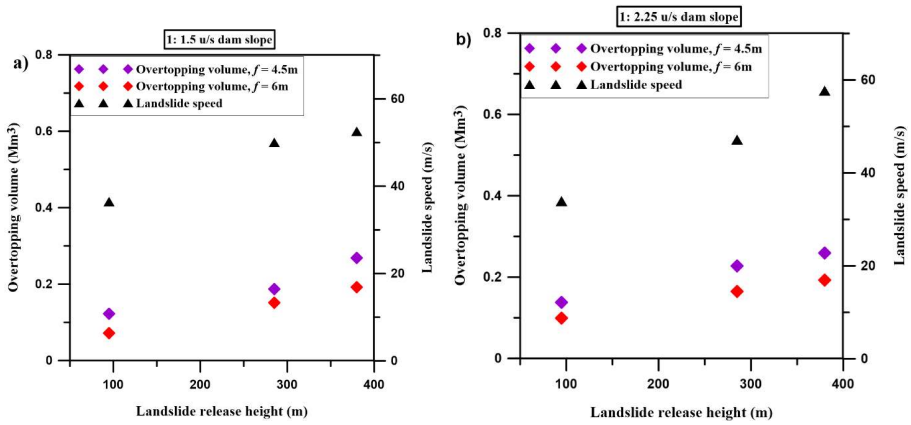

Figure D.2: The impact of landslide release height (m) on landslide speed (m/s) and overtopping volume (Mm^3) for a) 1: 1.5; and b) 1: 2.25 upstream dam slope, where W_s = 0.51 Mm^3 (prototype scale).

The relationship between slide release height, slide speed and overtopping volume for a slide volume of 0.51 Mm^3 is illustrated in Fig. D2 a and b for an upstream dam slope of 1: 1.5 and 1: 2.25 respectively. The maximum distance between the slide bottom edge and the reservoir water level considered in this study is h_{o3}= 380 m in prototype scale. For a specific freeboard value, the amount of water that overtopped the dam as a result of a slide with this release height was about 0.3 Mm^3 which is about 50 % of the slide volume. For a fixed slide release height, slide volume and upstream dam slope, an increase freeboard from f = 4.5 m to 6 m in the reservoir decreases the overtopping volume in a range between 59 % up to 81 % for the experiments conducted in this study.

The effect of slide volume, W_s on overtopping volume, W_w is almost linear for the particular model setup of this study which can be further understood from Fig. D3 a. An increase in slide volume by 33 % increases the overtopping volume by 23 % and 29 %, respectively for freeboard f = 6 m and 4.5 m. In Fig. D3 b present again the relation of the slide release height

and the overtopping volume for a fixed slide volume of W_s = 0.51 Mm^{3}·. The Fig. D3b shows that an increase in the distance between the edge of the slide to the reservoir water level, h_o = *95 m to 380 m*, increases the amount of the overtopping water W_w= 0.12 Mm^3 to 0.3 Mm^3 which is around 47 % of the initial amount. Comparison of the relations in Fig. D3 a and b, demonstrates the dominant effect of the slide volume on the overtopping volume compared to the effect of the slide release height (slide velocity) and freeboard.

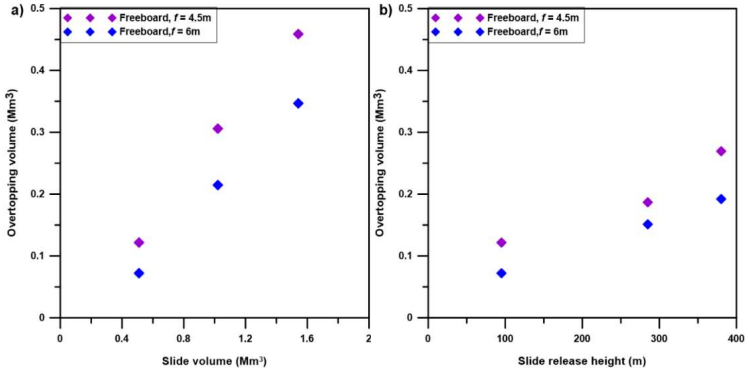

Figure D.3: a) The slide volume versus overtopping volume; and b) slide release height versus overtopping volume for 1: 1.5 upstream dam slope, where W_s = 0.51 Mm^3 (prototype scale).

Appendix E. Summary of Tests

U/s dam Slope	Freeboard, f(m)	Block arrangement	Release Height (h_o) (m)	N° of test	Test number		
1: 1.5	4.5	2H	2	3	37	38	39
			1.5	3	40	41	42
			1	3	43	44	45
1: 1.5	4.5	2V	2	3	46	47	48
			1.5	3	49	50	51
			0.5	3	52	53	54
1: 1.5	4.5	4	1.5	3	55	56	57
			1	3	58	59	60
			0.5	3	61	62	63
1: 1.5	4.5	6	0.5	3	64	65	66
			1	3	67	68	69
1: 1.5	6	6	1	3	70	71	72
			0.5	3	73	74	75
1: 1.5	6	4	1.5	3	76	77	78
			1	3	79	80	81
			0.5	3	82	83	84
1: 1.5	6	2H	2	3	85	86	87
			1.5	3	88	89	90
			1	3	91	92	93
1: 1.5	6	2V	2	3	94	95	96
			1.5	3	97	98	99
			0.5	3	100	101	102
1: 1.5	13	1B	2	3	275	276	277
			1.5	3	278	279	280

			1	3	281	282	283
			0.5	3	284	285	286
1: 2	4.5	2H	2	3	131	132	133
			1.5	3	134	135	136
			1	3	137	138	139
1: 2	4.5	2V	2	3	140	141	142
			1.5	3	143	144	145
			0.5	3	146	147	148
1: 2	4.5	4	1.5	3	115	116	117
			1	3	119	120	121
			0.5	3	149	150	151
1: 2	4.5	6	0.5	3	152	153	154
			1	3	155	156	157
1: 2	6	2H	2	3	158	159	160
			1.5	3	161	162	163
			1	3	164	165	166
1: 2	6	2V	2	3	167	168	169
			1.5	3	170	171	172
			0.5	3	173	174	175
1: 2	6	4	1	3	123	124	125
			1.5	3	127	128	129
			0.5	3	176	177	178
1: 2	6	6	0.5	3	179	180	181
			1	3	182	183	184
1: 2.25	4.5	2H	2	3	185	186	187
			1.5	3	188	189	190
			1	3	191	192	193

1: 2.25	4.5	2V	2	3	194	195	196
			1.5	3	197	198	199
			0.5	3	200	201	202
1: 2.25	4.5	4	1.5	3	203	204	205
			1	3	206	207	208
			0.5	3	209	210	211
1: 2.25	4.5	6	0.5	3	212	213	214
			1	3	215	216	217
1: 2.25	6	6	1	3	218	219	220
			0.5	3	221	222	223
1: 2.25	6	4	1.5	3	224	225	226
			1	3	227	228	229
			0.5	3	230	231	232
1: 2.25	6	2H	2	3	233	234	235
			1.5	3	236	237	238
			1	3	239	240	241
1: 2.25	6	2V	2	3	242	243	244
			1.5	3	245	246	247
			0.5	3	248	249	250
Total				210			

ISBN 978-82-471-9902-2 (printed ver.)
ISBN 978-82-471-9614-4 (electronic ver.)
ISSN 1503-8181 (printed ver.)
ISSN 2703-8084 (online ver.)

NTNU

Norwegian University of
Science and Technology